FINAL REPORT

GUIDELINES FOR INTERPRETATION OF CLOSE INTERVAL SURVEYS FOR EXTERNAL CORROSION DIRECT ASSESSMENT

CONTRACT NO. DTPH56-06-T-0011

PREPARED FOR

PIPELINE AND HAZARDOUS MATERIALS SAFETY ADMINISTRATION

US DEPARTMENT OF TRANSPORTATION

WASHINGTON, DC

PREPARED BY

CC TECHNOLOGIES, INC., A DNV COMPANY

MARK YUNOVICH, MS, MBA, NACE CORROSION SPECIALIST

COLIN SCOTT, PHD, PE

WILLIAM HARPER, PHD, PE

TONY ALFANO, MS

NOVEMBER 2007

TABLE OF CONTENTS

TABLE OF CONTENTS ii
LIST OF FIGURES iv
LIST OF TABLES vii
INTRODUCTION 1
BACKGROUND 2
OBJECTIVES AND DELIVERABLES 3
WORK PLAN 4
Task 1 – Laboratory Analysis of Factors Affecting Potential Distribution 5
Task 1.1 – Literature survey and state-of-the-art 5
Task 1.2 – Experimental and computational modeling 5
Task 2 – Field-based data collection and analysis 5
Task 2.1 – Collection of preliminary ECDA information 6
Task 2.2. – CIS data analysis 6
Task 2.3. – Direct examination of selected anomaly sites 7
Task 3 – Computational modeling using field data 8
Task 4 – Guidelines for interpretation of CIS for ECDA 9
Task 5 – Reporting and public submission of results 9
RESULTS AND DISCUSSION 9
Task 1 – Laboratory Analysis of Factors Affecting Potential Distribution 9
State-Of-The-Art 9
Conclusions 13
References 13
Experimental and computational modeling 15
Laboratory-based modeling 15
Conclusions 21
Computation modeling 22
Finite Element Modeling and Regression Analysis 22

Description of Preliminary 2D Model 23
Regression analysis of 3D model work 38
Discussion of Results 48
Forward (FEA) vs. reverse model (CP3D) 54
Numerical simulation conclusions.....57
Task 2 – Field-based data collection and analysis.....59
Sourced data: type, limitations and assumptions 59
Methodology of Shape selection 60
Acquiring Data 61
Data Alignment.....62
Shape Selection 62
Task 3 – Computational modeling using field data 64
Correlation between CIS shapes and corrosion 64
Correlation between metal loss and CIS shape parameters 81
Regression analysis correlating metal loss to CIS and soil characteristics.....86
Conclusions 91
Correlation between numeric analysis and field data 92
Task 4 – Guidelines for interpretation of CIS for ECDA 93
GENERAL CONCLUSIONS 94

APPENDIX A: GUIDELINES

LIST OF FIGURES

Figure 1 Simplified schematic of a CIS profile. 2

Figure 2: Example data from pipeline survey showing ON and OFF potentials (from Reference 5). 12

Figure 3. Schematic of the test configuration.....15

Figure 4. Pipe segments showing the external coating and electric lead.....16

Figure 5. The pipe assembly inside the cell; the reference electrode is fed through the hole in the lid. 17

Figure 6. General view of the experimental cell and the pipe assembly. 18

Figure 7. Small cell filled with clay and sand.....19

Figure 8. ON and OFF-potentials with both Defects electrically connected for OFF-potential measurements.....20

Figure 9. A potential distribution from the 2D model for a coating defect located at the 12 o'clock position (shown at the top of the graph). The anode can be seen lower right. 25

Figure 10. Calculated ON potential distributions with varying depth of anode. 26

Figure 11. Calculated ON potential distributions with varying defect size.....27

Figure 12. Calculated ON potential distributions with varying defect orientation.....29

Figure 13. Calculated ON potential distributions with varying soil resistivity. Soil resistivity units are Ω-inches.....30

Figure 14. Calculated ON potential distributions with varying depth of cover. 31

Figure 15. A contour plot of the potentials calculated for the basic test (test ID #1). 34

Figure 16. A contour plot of the potentials calculated for the basic test (test ID #1) (close-up). 35

Figure 17. A contour plot of the potentials calculated for test “AA”. 37

Figure 18. A contour plot of the potentials calculated for test “AA” (close-up). 38

Figure 19. A comparison of finite element analysis calculated, and regression analysis estimated ON-potentials. 47

Figure 20. A plot of ON and OFF potentials as a function of soil resistivity.....48

Figure 21. A plot of ON and OFF potentials as a function of pipe diameter 49

Figure 22. A plot of ON and OFF potentials as a function of depth of pipeline centerline. 50

Figure 23. A plot of ON and OFF potentials as a function of coating potential.....51

Figure 24. A plot of ON and OFF potentials as a function of defect orientation. 51

Figure 25. Plot of defect size vs. varying OFF and fixed ON potentials (at different soil resistivities). Two ON potentials (-1.1V and -1.0V) are used in the calculation. Inset shows the relationship between the ON and OFF potentials (circles and squares, respectively).....52

Figure 26. Plot of defect size vs. varying ON and fixed OFF potentials (at different soil resistivities). Two OFF potentials are used in the calculation (-500 mV and -600 mV). Inset shows the relationship between the ON and OFF potentials (circles and squares, respectively). 53

Figure 27. Overlaid CIS potentials and ILI metal loss data 62

Figure 28. Example of two shapes belonging to the same catalogue number (CN 5). 64

Figure 29. Shape CN1. Lower graph shows expanded view of the encircled area in the upper graph. 65

Figure 30. Shape CN2. Lower graph shows expanded view of the encircled area in the upper graph. 66

Figure 31. Shape CN3. Lower graph shows expanded view of the encircled area in the upper graph. 67

Figure 32. Shape CN4. Lower graph shows expanded view of the encircled area in the upper graph. 68

Figure 33. Shape CN5. Lower graph shows expanded view of the encircled area in the upper graph. 69

Figure 34. Shape CN6. Lower graph shows expanded view of the encircled area in the upper graph. 70

Figure 35. Shape CN7. Lower graph shows expanded view of the encircled area in the upper graph. 71

Figure 36. Shape CN8. Lower graph shows expanded view of the encircled area in the upper graph. 72

Figure 37. Shape CN9. Lower graph shows expanded view of the encircled area in the upper graph. 73

Figure 38. Two shapes belonging to the same catalogue number (CN5), but falling into two different potential ‘zones’ with respect to the -850mV CP protection criterion. 74

Figure 39. Occurrence of CIS shapes with and without metal loss. Catalogue shapes are shown on the top of the graph. 79

Figure 40. Average external damage area and standard deviation for each CN shape.....80

Figure 41. Average external damage area for each CN shape – separated by compliance with the -850mV CP criterion. 81

Figure 42. Example of calculating Scaled Metal Loss variable for shape CN5. 82

Figure 43. Scaled Metal Loss Histogram. 83

Figure 44. Natural logarithm-transformed Scaled Metal Loss Histogram. 83

LIST OF TABLES

Table 1. Possible CIS Shapes 6

Table 2. The test matrix for the initial 3D model verification work. 34

Table 3. Descriptions and results of FEA model runs. 40

Table 4. The results of the regression analysis. 45

Table 5. Possible CIS Shapes 63

Table 6. List of variables identified in the investigation 75

Table 7. Soil variables characterizing conditions in the vicinity of metal loss anomalies. 78

Table 8. One-way ANOVA: LNScaledML versus Catalogue Number (full data set, n = 252) 84

Table 9. One-way ANOVA: LNScaledML versus Catalogue Number (only data not meeting -850mV criterion, n = 116) 85

Table 10. Variables and their coefficients for regression equation. 87

Table 11. Statistical analysis of regression model. 88

Table 12. Regression variables in order of importance. 88

Table 13. Sensitivity analysis of regression variables. 89

INTRODUCTION

Close interval surveys (CIS) are the most common tool employed during external corrosion direct assessment processes (ECDA) implemented in accordance with the NACE RP0502-02 Standard Recommended Practice “Pipeline External Corrosion Direct Assessment Methodology”. The technique is well established, relatively simple to perform, and provides a significant amount of information with respect to the corrosion condition of a pipeline. CIS is typically one of the two indirect assessment techniques which a pipeline operator would select per ECDA directives.

CIS is usually performed by taking potential measurements 1) with the cathodic protection (CP) system connected to the pipe (i.e., ‘on’) and 2) with cyclic interruption of the CP system to remove so-called IR-drop effects (i.e., ‘off’). CIS has historically been performed with the goal of comparing the potential to a criterion for CP effectiveness. This polarized potential should be free from IR-drop effects that result from current passing through the resistive layer of soil between the CP anode and pipe. Field experience shows that even when on-potential excursions are in excess of -3V (vs. copper/copper sulfate reference electrode (CSE)), the off potentials can be less negative than -0.5V (CSE), which makes the IR drop error component more than 85% of the measured value.

An ideal off-potential plot should be free from all errors, including those contributed by stray currents (SC) and other uninterruptible sources. Error corrections are necessary, which include filtering and averaging techniques. The off-potentials, which are a measure for CP effectiveness, are then compared to the acceptance criterion (e.g., minimal polarization potential of -850 mV (CSE)) to determine compliance with NACE RP0169-02 Standard Recommended Practice “Control of External Corrosion on Underground or Submerged Metallic Piping Systems”.

For the purpose of prioritizing susceptibility to external corrosion (i.e., the goal of ECDA), CIS contains additional information beyond comparison to a CP effectiveness criterion. This information includes the profile of the ‘on’ and ‘off’ potentials (e.g., the presence of peaks and valleys) and the difference between the ‘on’ and ‘off’ potentials caused by IR-drop effects. These secondary factors were not commonly considered historically, but they contain information relevant to the CP and corrosion condition of the pipeline under assessment

BACKGROUND

Using the RP0169 compliance criterion, pipeline operators rely on CIS to select locations which may be at risk to corrosion. In some instances, the selection is obvious – the few sites with the most positive off-potential would be the prime candidates. However, on many occasions, there would be a large number of locations with the off-potentials failing to meet the acceptance criterion, which exhibit similar potential magnitude. For example, consider the simplified schematic of a CIS profile shown in Figure 1 (assuming that there are no SC present).

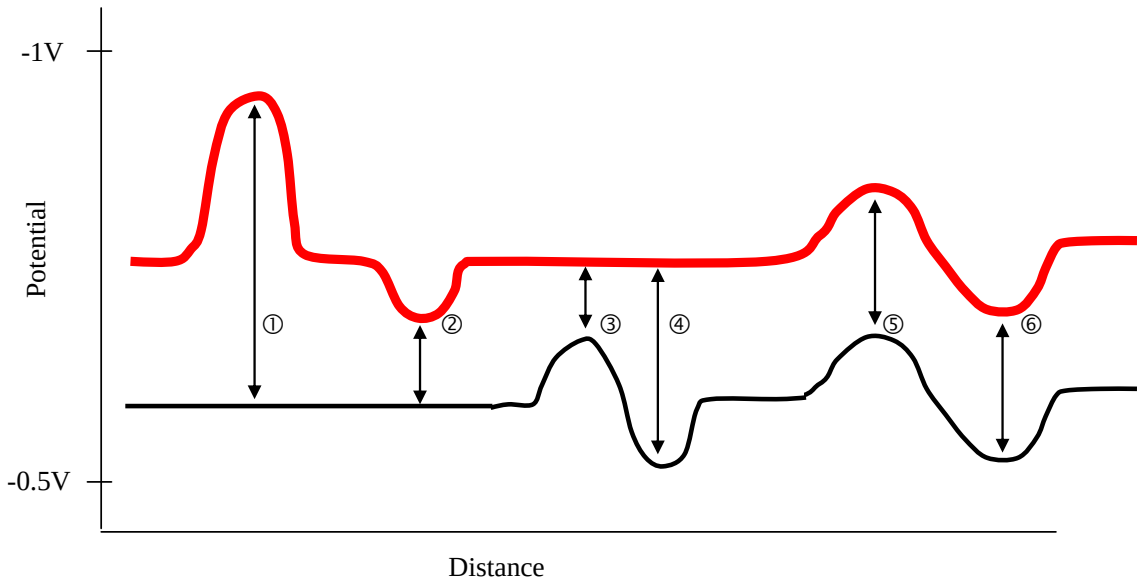

Figure 1. Simplified schematic of a CIS profile.

The red line shows the on-potential plot; the black line shows the off-potential plot. Let's assume that the off-potentials are out of compliance with the CP protection criterion. There are six possible scenarios of the on-potential vs. off-potential behavior, as illustrated in the chart. The primary question is, which of the six locations labeled on the plot would receive the priority status at the 'defect sentencing' step? In the example, Location 1 has the highest IR drop, and Locations 2 and 3 have the lowest. What is the significance of the difference?

Similarly, is Locations 3 ‘better’ or ‘worse’ than 1 and 2? What about Location 3 vs. Location 5 and Location 4 vs. Location 6? [1]

The IR drop magnitude depends on both the current and the resistance at a given location. The current distribution may also have time dependence, especially if influenced by dynamic SC. The resistance value R represents the soil (bulk) resistance and the impedance of the pipeline coating and coating defects. The soil resistance values are likely to be relatively stable (may exhibit seasonal variations due to drying/wetting of the soil and show long-term trends due to degradation of the external coating). One can conclude that at Location 1, the local resistance (“R”) is higher than at Location 2. However, if this is correct, because the local current pick up would be lower at the higher resistance spot, the magnitude of “I” will be lower at Location 1 than at Location 2. The next logical conclusion is that the off-potential at Location 1 should be more positive than at Location 2, but, as shown in the example, it is not.

To be more precise, the off-potential value is the function of current density (thus the area of the exposed metal is also important) and the environment at steel interface. The amount of current driven to the location is dependent on the local resistance (impedance), which, in part, is determined by polarization resistance, the measure of corrosion rate at that location. To further complicate the issue, the impedance of a defect in the external coating is a inversely proportional to its size.

Interpretation of CIS data is often subjective and without a consensus view of how to prioritize indications. The presented work aimed to develop guidelines on CIS interpretation so that ECDA indications are prioritized in a more accurate and consistent manner.

OBJECTIVES AND DELIVERABLES

The primary objective of the project was to develop guidelines that 1) improve prioritization of CIS indications, and 2) create more uniform CIS data interpretation. This is particularly true where the off-potentials do not meet the CP protection criterion and yet exhibit similar values. The off-potentials are the only direct measure of the effectiveness with which the underground pipeline is

[1] The illustration omits several other possible ON/OFF potential combinations. See Task 2.2 scope in Work Plan for further discussion.

protected from corrosion; therefore, the proper interpretation of the CIS results is a critical component of the ECDA process.

In some conditions, the supplementary above-ground techniques, such as AC/DCVG, could serve as a 'tie-breaker' by indicating a larger or a smaller coating flaw (holiday) at the site with comparable off-potentials. In many instances, the resolution of the supplemental method is insufficient to make the distinction.

The guidelines, the primary deliverable of the project, outline the observed trends and provide decision flow charts and narrative for making decisions regarding interpretation of the CIS profiles and prioritizing anomalies regarding the threats to pipeline integrity. The guidelines are expected to enable the end users to further differentiate between the sites selected for direct examinations following the indirect assessment step of the ECDA process, thus contributing to the process of prioritization of the excavation of the anomalies.

WORK PLAN

The original research work plan included laboratory (Task 1, Task 3) and field work (Task 2). The laboratory efforts initially focused on the critical parameters affecting the on and off-potentials on a buried pipe. It was anticipated that the field-based activities would provide input by generating the empirical data from close interval surveys and, most importantly, direct examination of actual pipelines. The empirical data would then be analyzed to determine the existence of trends correlating the *conditions at the pipeline surface* (coating holiday geometry and distribution, soil resistivity, corrosion behavior of exposed steel) to the *at-grade CIS profiles*. However, in the early stages of Task 2, it was realized that the data that combined both CIS profiles and direct examination results was extremely scarce, despite the search which extended beyond the co-funding agency. In order to meet the objectives, a modified approach to analysis was required; it was decided to use inline inspection (ILI) data, superimposed on the CIS profiles collected from the same pipeline.

Following the acquisition and analysis of the field data, the trend analysis results were processed through computational "forward" model(s) to confirm and verify the consistency and universality of the trends. Each Task and included sub-Tasks are described below. Task 4 consists of preparing the guidelines for the CIS interpretation. Task 5 activities consist of reporting (quarterly reports) and presenting of the results (interim and final Peer Reviews).

Task 1 – Laboratory Analysis of Factors Affecting Potential Distribution

Task 1 included literature survey to establish the state-of-the art with respect to the understanding of the parameters of the pipeline surface and soil characteristics affecting the at-grade potentials measured during CIS. Following the search, the laboratory-based work commenced in order to define quantitative relationships between these parameters and the CIS profile, using small-scale experimental cells with controlled conditions. Computational "reverse" modeling was then conducted, which aim was to contribute to defining the functions linking critical pipeline and soil characteristics and on- and off-potentials.

Task 1.1 – Literature survey and state-of-the-art

Limited literature review was performed to establish the state-of-the-art with regard to the advances in understanding of the electrochemical/physical factors determining the at-grade on- and off-potentials on buried steel structures. Existing modern computational models were broadly evaluated to determine which ones were available and held the most promise.

Task 1.2 – Experimental and computational modeling

Some critical dependencies between the pipeline surface conditions (pipeline diameter, size of coating defect and its circumferential position, defect clustering, corrosion/polarization behavior, extent of polarization, coating resistance), soil parameters (soil resistivity, depth of cover) and at-grade potentials (both on and off) were evaluated.

In addition to the "forward" models based on the finite element analysis (FEA), Task 1 included limited computational simulations using a University of Florida "reverse" CP3D model to assess the correlation between the results provided by the two different approaches.

The extensive forward-model simulations were run concurrently with a small-scale laboratory-based assessment of the trends by simulating the pipeline, coating, soil, and polarization characteristics to produce 'seed values' which could be used in the quantitative relationships established by the model.

Task 2 – Field-based data collection and analysis

Task 2 originally included collection of CIS and direct examination data on actual pipelines on SoCal transmission system. Approximately 250 miles of underground natural gas transmission pipelines were scheduled for ECDA during 2005-2006. The Task was further divided in several sub-Tasks.

Task 2.1 – Collection of preliminary ECDA information

The sub-Task consisted of collecting and summarizing the information about the prospective ECDA regions. This information was collected early in the project as it was required for the Task 1 activities (sub-Task 1.2). As noted earlier, early in Task 2, it became apparent that the amount of data from direct examinations was not going to be sufficient not only to achieve statistically significant conclusions, but it also lacked the variety to cover all possible combinations of CIS profile shapes.

This was despite the copious amount of information submitted by SoCal, the files accumulated in the CC Technologies archives, and data provided by various other pipeline operators. Considering the challenges associated with accumulating the necessary real-life data for analysis, in order to maximize the use of the available funds allocated to Task 2, it was decided that it would be preferable to change the type of data used for the analysis rather than visit new excavation sites at SoCal and other pipeline systems.

Therefore, the chosen approach was to use inline inspection data from actual pipelines. The ILI data indicated the external corrosion damage, which was superimposed on the CIS profiles obtained from the inspected pipelines.

Task 2.2. – CIS data analysis

The sub-Task consisted of analysis of the CIS profiles collected by SoCal (and other pipeline operators) during ECDA surveys to select locations falling within nine possible categories of on/off potential cases, some of which are illustrated in Figure 1. All possible permutations of profile shapes are summarized in Table 1.

Table 1. Possible CIS Shapes

Catalogue Number	1	2	3	4	5	6	7	8	9
On Potentials Off Potentials **Shape**									

1. Flat ‘on’, valley in ‘off’ potentials
2. Flat ‘on’, peak in ‘off’ potentials
3. Valley in ‘on,’ flat ‘off’ potentials
4. Peak in ‘on,’ flat ‘off’ potentials

5. Valley in ‘on’ and ‘off’ potentials
6. Peak in ‘on’ and ‘off’ potentials
7. Flat ‘on’ and ‘off’ potentials
8. Peak in ‘on’, valley in ‘off’ potentials
9. Valley in ‘on’, peak in ‘off’ potentials.

Naturally, some of the shapes are more frequently encountered in practice than others (compare, e.g., catalogue number (CN) 5 to CN 8).

Task 2.3. – Direct examination of selected anomaly sites

Originally, the sub-Task was planned to include in-situ characterization of the uncovered anomalies from the sites selected upon completion of Task 2.2. The evaluations were expected to include:

- soil resistivity survey (using Wenner 4-pin method and soil-box testing of the soil samples collected in the excavation);
- measurements of anomaly geometric characteristics (depth of cover, circumferential location, size, remaining wall thickness;
- anomaly distribution (in case of multiple anomalies) – circumferential positions and axial spacing;
- in-situ measurements of corrosion behavior of steel at the uncovered anomaly (linear polarization resistance (LRP) to determine instantaneous corrosion rate and Tafel analysis to determine polarization characteristics of the exposed steel substrate).

Given the reasons explained earlier, the in-situ, direct examination data was supplanted with information gleaned from ILI runs. The ILI data included the *estimated* size of corrosion anomalies, their orientation, and proximity to each other, i.e., providing the most of the values for the originally planned corrosion-related variables. While the extent of the overall corrosion damage (remaining wall thickness) was known, the actual corrosion rate, however, was not.

Considering that the soil data was expected to have significant bearing on the CIS profiles, the soil characteristics were obtained using National Resource Conservation Service (NRCS) soil database.

This database contains soil information which is grouped into soil polygons. Each polygon contains up to six separate components, where the dominant

component is identified. A component is a portion or area of the soil polygon; there can be up to six distinct areas reported for the same soil polygon. The data extracted from the database included parameters that went beyond the original planned number of variables and included:

- Electrical conductivity (Number of cations absorbed)
- Salinity (Milliohms per centimeter)
- pH
- Amount of organic mater found in the soil (%)
- Amount of sand comprising the soil (%)
- Amount of silt comprising the soil (%)
- Amount of clay comprising the soil (%)

The data was used to establish the correlation between the site characteristics and the potential values gathered during CIS (in effect serving as an 'empirical inverse' model). The data was also used to establish whether any of the potential behavior cases is associated with elevated corrosion risks by linking potential values and corrosion behavior at the anomaly site. In this manner, the field data provided the basis for connecting the CIS profile and pipe surface conditions so that an informed determination can be made as to whether any specific cases of on/off potential behavior are associated with higher or lower threats to pipeline integrity from external corrosion. Particular attention was paid to the levels of cathodic protection polarization (i.e., the data will be analyzed not only with respect to the on/off potential *behavior*, but also with regard to the *magnitude* of the on/off potential values).

For further specifics of data treatment, please refer to the appropriate section in the Results and Discussion part of the report on page 59.

Task 3 – Computational modeling using field data

Task 3 activities included computational modeling (using a statistical analysis) of at-grade potential distribution obtained during CIS on the actual pipelines. The forward models will be constructed using soil resistivity, depth of cover, and polarization characteristics for a 'typical' pipeline. The models were used to simulate various potential distributions on a section of buried pipe and to establish trends linking the pipe and soil variables to the above-ground shape of closer interval survey profile.

Task 4 – Guidelines for interpretation of CIS for ECDA

Upon completion of the laboratory and field components of the proposed research effort, the findings were summarized into a set of guidelines for the pipeline operators. The guidelines, the primary deliverable of the project, outline the observed trends and provide decision flow charts and narrative for making decisions regarding interpretation of the CIS profiles and prioritizing anomalies regarding the threats to pipeline integrity. The guidelines were prepared in the format suitable for inclusion in the NACE International RP0502.

Task 5 – Reporting and public submission of results

Task 5 consisted of generating and submitting quarterly update reports, discussing the results and the Peer Review meeting, and presenting the project results at a public forum (presentation at the 2008 NACE International convention is planned).

RESULTS AND DISCUSSION

Task 1 – Laboratory Analysis of Factors Affecting Potential Distribution

State-Of-The-Art

There are several known completed and ongoing research projects that are relevant to the research topic. An earlier work sponsored by PRCI and conducted by CC Technologies[1] evaluated several aspects of the CIS on bare and coated buried pipeline, with a particular focus on establishing the area of the pipe sampled during a pipe-to-soil potential measurement. The work included surveys on sections of underground pipelines with known defect configurations and finite element analysis (FEA) modeling. The research made several important conclusions.

> For a bare pipe, it was established that the area of the pipe sampled during CIS (which was found to be the same for both on- and off-potentials) is independent of soil resistivity, but is dependent on the depth of soil cover over the pipe. Further, it appeared that the anomalies at the bottom half of the pipe was not sampled by the at-grade CIS and that the sampled circumferential area is a function of pipe diameter-to-pipe depth ratio.
>
> The conclusions with regard to the coated pipe were less definitive due to the complexity of the corrosion conditions and the need to consider coating quality, holiday size and location, and pipe diameter vs. depth.

Although the research offered only qualitative relationships, the observations pointed out several critical trends – in particular, that a critical parameter affecting the CIS resolution on coated pipe is the ratio between the coating and soil resistivity. Another conclusion was that FEA modeling seemed to point that only relatively large area (over 20 in^2) defects are likely to be detected by the at-grade CIS. All conclusions were drawn only with regard to the off-potentials; on-potentials were not treated.

Several reports and papers[2-10] were reviewed in an attempt to determine what has previously been accomplished with regard to utilizing possible ECDA methods to prioritize locations for risks to pipeline integrity. The work reviewed generally was focused on using CIS, DCVG, or ACVG in an attempt to determine the overall condition of the pipeline and the condition of the protective coating or to verify that sufficient cathodic protection (in terms of potential) was in place. In the course of the review, special emphasis was given to identifying cases where the ON potential data was compared to OFF potential and/or depolarization data in an effort to correlate the results and to interpret the overall condition and risk of corrosion.

Because differences and variations in the ON and OFF potentials can result from not only possible differences in the applied level of CP and coating integrity but also on soil properties, interpretation is sometimes difficult. Of the works reviewed, only a few included both the ON and OFF potential data or utilized the on potential to make integrity decisions.

The prevailing approach, as defined in NACE RP0169-2002[11] is to obtain the true OFF potential as an indication of effective cathodic protection. If the OFF potential is more negative than -850 mV vs. the copper/copper sulfate scale, the pipe is generally considered to be sufficiently protected and the locations found to be in compliance with the criterion are not typically investigated further. The ON potential measurement, though used to help determine the IR drop in the potential data, is usually not considered indicative of the level of cathodic protection at the pipe due to interference problems arising from IR drop in the soil, stray currents, sacrificial anodes, and other factors. However, despite the built-in uncertainty it is still sometimes used.

Whited[5], for example, described the use of directional drilling to insert reference electrode access piping underneath above ground storage tanks. He illustrated that if the potential measurements could be made in close proximity to the location of interest (i.e., underneath the storage tank bottom) that the on potential

data could be used as a reliable indication of the level of effective cathodic protection being offered. However, when measured from the perimeter (i.e., a distance away from the location of interest underneath the tank bottom), the values were considerably different with the error introduced likely originating from IR drop in the soil.

Two studies[6,9] included both on and off potential survey data. These data exhibited fluctuations in the potential readings for both the ON and OFF potentials (see for example, Figure 2). In some cases, there were fluctuations in the ON potential with no concomitant fluctuations in the OFF potential. The complimentary case of fluctuations in the OFF potential with no change in the ON potential was also observed in some cases. Lastly, in some cases fluctuations that were observed in the OFF potential were associated with fluctuations in the ON potential as well. The question, however, from these studies that remains unanswered is if there is any significance or indication of a possible integrity threat (e.g., coating disbondment, etc.) based on the observed magnitude of the differences in the ON and OFF potentials. That is, are the cases where the difference between the ON and OFF potentials is small of greater risk than those where the difference is large? Based on the information and literature reviewed thus far, it is unclear if this is true. Intuitively, it would be expected that locations that exhibit small differences between the ON and OFF potentials should perhaps be less protected than areas that have larger differences (neglecting for this consideration the possible effects of overprotection), because of the lower CP current and thus lower IR drop. However, due to possible differences in the magnitude of interferences, this may not always hold.

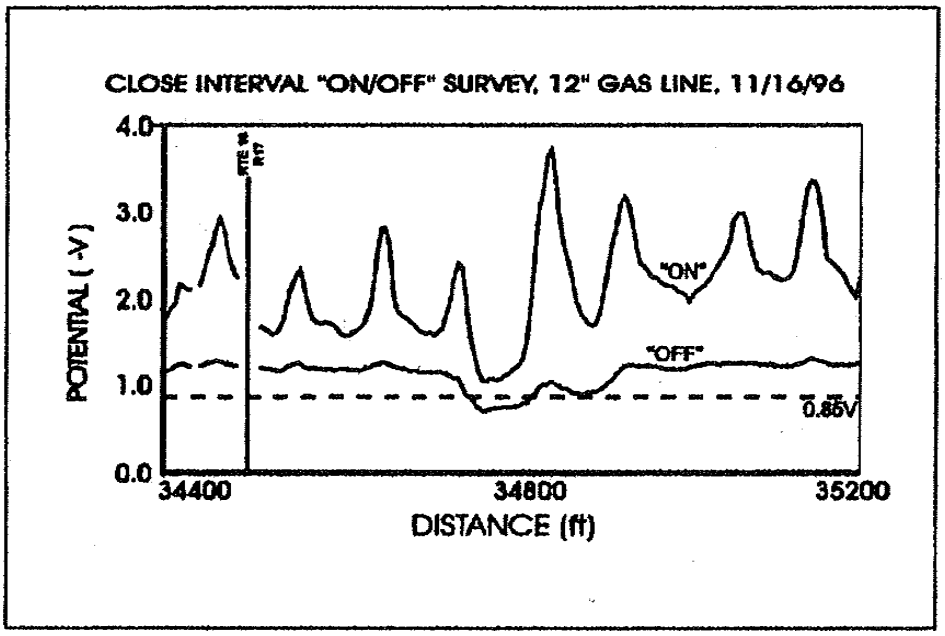

Figure 2: Example data from pipeline survey showing ON and OFF potentials (from Reference 5).

The meaning and possible interpretation of ON potential data with respect to overall integrity and effective cathodic protection becomes even more important when it is realized that ON potential information is in many cases the only "reliable" data that can be obtained. In such cases, the OFF potential data may be corrupt due to various factors (e.g., stray current, sacrificial anodes) that prevent the true OFF potential to be obtained. Thus the work proposed in the present project is critically important and necessary to address this issue.

In the realm of the modeling, a number of recent publications have explored both "forward" and "inverse" models to interpret pipeline survey data. A forward model strives to predict the at-grade potential distribution for a given set of geometric and corrosion characteristics of the pipe; there is an extensive history of forward models, which include both analytical and numeric. Numeric models, which are more versatile, use either FEA or boundary element method (BEM) or a combination of FEA and BEM. On the basis of previous work, Riemer and Orazem[12,13] developed the CP3D model, which accounts for localized defects (in axial and circumferential directions) but is applicable for long pipelines. An inverse model, as the name implies, attempts to establish the conditions on the pipe surface through numeric analysis, using the at-grade potential measurements as the basis.

In a more recent work, Qiu and Orazem[14] evaluated an approach that combined a BEM forward model with a non-linear regression algorithm to find pipe surface properties from pipe-to-soil potentials measured at grade level. The authors concluded that, depending on the quality of the input, the model was promising. Another observation was that the presence of even modest noise may render the potential survey data insufficiently sensitive to the pipe surface condition to achieve the desired resolution of the coating defects.

Recent research, sponsored by NGA and conducted by CC Technologies in cooperation with University of Florida (O. Moghissi and M. Orazem) investigated the impact of pipe-related parameters (size, CP level, coating condition, polarization resistance, etc) and soil-related parameters (soil resistivity, depth of cover) on the above-ground measurements by External Corrosion Direct Assessment (ECDA) techniques, including CIS. The approach was to employ the CP3D model to calculate the inverse solution (e.g., predict the pipe conditions based on the ECDA results) so that ECDA criteria may be developed.

Conclusions

The literature search results are consistent with the expectations in that even among the publications that address the issue of the CIS profile interpretation (the ones selected for the review), there is no discussion about the implications of the differences in the CIS profile shapes. There seems to be no consideration given to whether any of the CIS shapes can be further interpreted to address such issues as coating defect size or the likelihood of corrosion – at least not beyond the commonly recognized concurrent drop (to more positive values) in potential on ON and OFF potential charts in the vicinity of the coating holiday on a buried pipe.

In this context, the primary focus of the efforts of this project - to determine whether certain correlations between the CIS profile shapes and corrosion conditions at the pipe/soil interface can be possible - receives an additional 'boost' with regard to its relevance and originality.

References

1. N.G. Thompson, K.M. Lawson, "Improved Pipe-to-Soil Potential Survey Methods", Final Report, PRCI Catalog No. L51640e, April 1991
2. P.H. Vieth and J.F. Kiefner, Methods for Prioritizing Pipeline Maintenance and Rehabilitation, PRCI Report #PR-3-919 (1990).

3. S.M. Segall, R.G. Reid, and R.A. Gummow, Use of an Integrated CIPS/DCVG Survey in the ECDA Process, Paper No. 06193, Corrosion2006, NACE International (2006).

4. J.P. McKinney, M.E. Orazem, O.C. Moghissi, and D. D'Zurko, Development of ECDA Criteria for Prioritization of Indications, Paper no. 06188, Corrosion2006, NACE International (2006).

5. T. Whited, Techniques for Accurate Evaluation of Aboveground Storage Tank Cathodic Protection System Effectiveness, Paper no. 00829, Corrosion2000, NACE International (2000).

6. R.L. Pawson and R.E. McWilliams, Bare Pipelines, The 100 mV Criterion & CIS. A Field Solution To Practical Problems, Paper no. 01587, Corrosion2001, NACE International (2001).

7. J.L. Didas, Applying the 100 Millivolt Polarization Criterion to Older and Bare Ore Ineffectively Coating Transmission Pipelines, Paper no. 01584, Corrosion2001, NACE International (2001).

8. K.G. Leewis, Pipeline Integrity & Direct Assessment, Paper no. 03191, Corrosion2003, NACE International (2003).

9. N.G. Thompson and K.M. Lawson, Development of Coupons for Monitoring Cathodic Protection Systems, PRCI Report PR-186-9220 (2001).

10. N.G. Thompson and K.M. Lawson, External Corrosion Control Monitoring Practices – Volumes I and II, PRCI Report PR-186-9610 (1998).

11. NACE RP0169-2002, Standard Recommended Practice "Control of External of External Corrosion on Underground or Submerged Metallic Piping Systems, NACE International, 2002.

12. D. Riemer and M. E. Orazem, "Development of Mathematical Models for Cathodic Protection of Multiple Pipelines in a Right-of-Way," Proceedings of the 1998 International Gas Research Conference, San Diego, November 8-11, 1998

13. D. P. Riemer and M. E. Orazem, "Models for Cathodic Protection of Multiple Pipelines with Coating Holidays," Cathodic Protection: Theory and Applications, M. E. Orazem, editor, NACEInternational, Houston, Texas, 1999

14. C. Qiu and M.E. Orazem, “A weighted non-linear regression-based inverse model for interpretation of pipeline survey data”, Electrochimica Acta, Vol. 49, 3965-3975 (2004)

Experimental and computational modeling

Laboratory-based modeling

The preliminary analysis indicated that the primary factors affecting the potential profile as measured with ECDA methods at grade level are (1) the size of the pipe, (2) the circumferential position of the defect, and (3) the depth of burial. Other important factors that affect the measurements include the spacing of the defects and soil resistivity. Given the relatively small size of the laboratory cell and the attendant scaling issues (depth of cover vs. defect size), the effect of the defect size was not expected to be accurately modeled and was given a lower priority. The experimental modeling efforts were run concurrently with the early efforts to develop 2D and 3D numerical models.

Laboratory-based modeling used a small (sized approximately 20 by 12 by 12 inches) cell. The cell accommodated an assembly made of several segments of 2 inch diameter steel pipe coated with liquid epoxy coating. The total length of the assembly was approximately 16 inches. The assembly includes three sections with an intentionally introduced defect (6 mm diameter). Each section was electrically isolated from another with a gasket. To achieve axial separation, a ‘dummy’ section was inserted between the first and the third section. The schematic of the assembly is shown in Figure 3; the construction of the segments is illustrated in Figure 4.

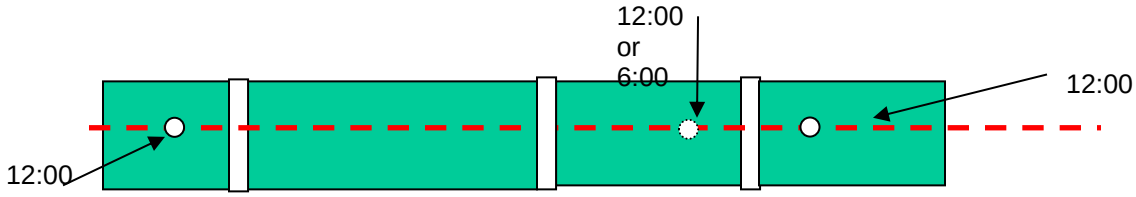

Figure 3. Schematic of the test configuration

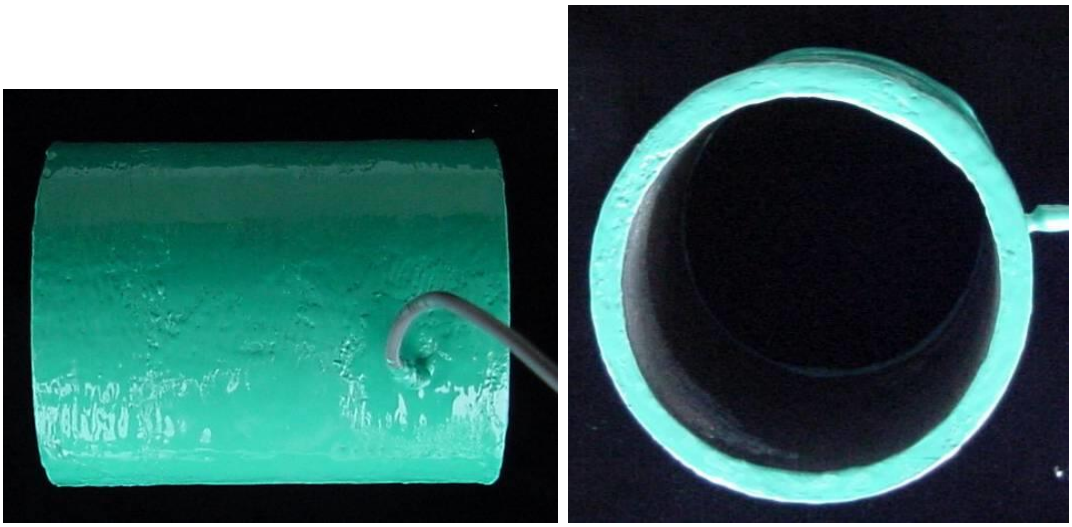

Figure 4. Pipe segments showing the external coating and electric lead.

Defect 1 was located at approximately 7 inches from the left edge of the cell at 12:00 o'clock position; Defect 2 was located approximately 15 inches from the left edge at either 12:00 o'clock or 6 o'clock position; Defect 3 was located approximately 2 inches further to the right at 12:00 o'clock position.

The photographs of the pipe segments, the actual cell with the pipeline assembly are shown in Figure 5 and Figure 6.

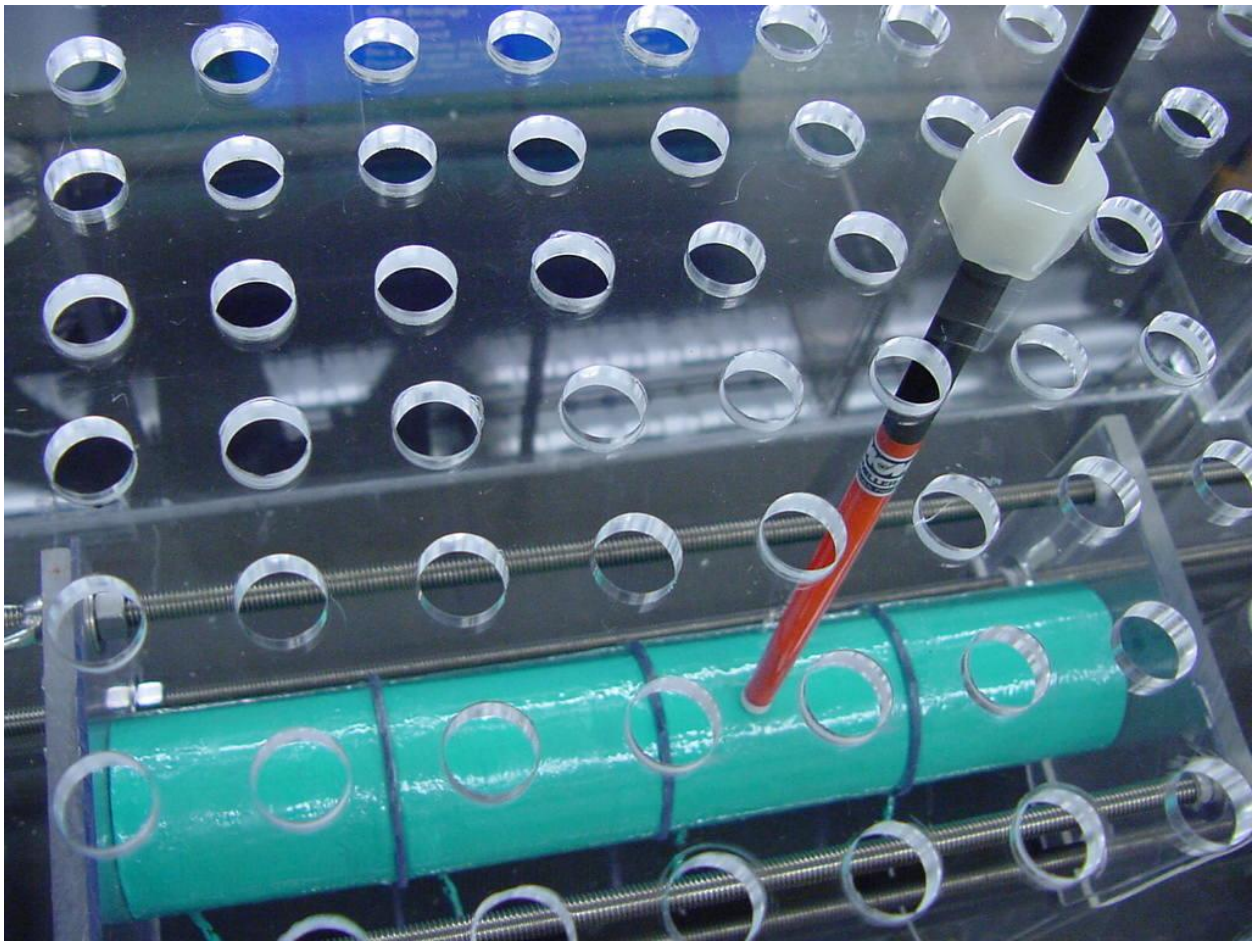

Figure 5. The pipe assembly inside the cell; the reference electrode is fed through the hole in the lid.

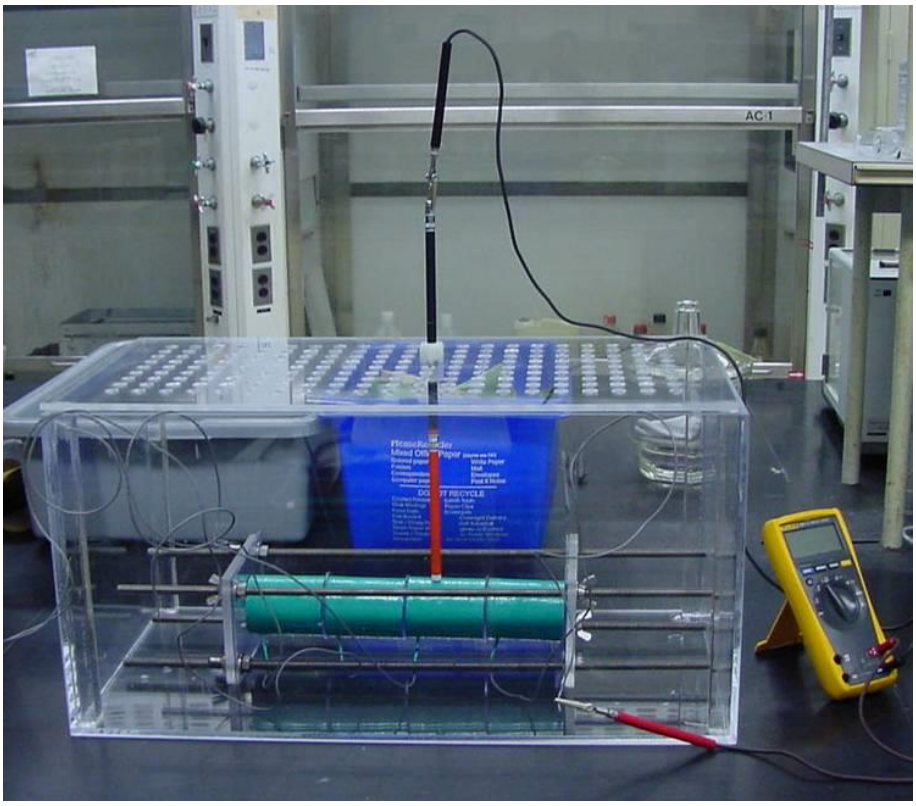

Figure 6. General view of the experimental cell and the pipe assembly.

The cell was covered with a lid with a network of approximately 280 equally spaced holes, such that a reference electrode position can be consistent. In addition to the pencil-shaped copper/copper sulfate reference electrodes, the potentials of the defects could be measured with the help of platinized niobium wires placed in close proximity to the defect surface. The platinized wire maintains a relatively stable potential and thus can be used a pseudo-reference electrode. The potential of the wire can be then measured against the standard CSE and convert the potential values measured with regard to Pt to the CSE scale.

This configuration of the cell and the pipe assembly also permits flexibility in the approach to polarizing the pipeline segments to different potentials in order to simulate the conditions occurring on actual pipelines on a smaller scale, but with realistic parameters. The polarization was accomplished via the use of a potentiostat and variable resistors to adjust the currents to each of the sections.

The experimental work started with preliminary runs in the cell filled with tap water. After the water-based tests, the cell was filled with sand and clay, such that each type of soil occupied approximately half of the volume. Defect 1 was

located in clay, and Defects 2 and 3 (at the 6:00 and 12:00 position, respectively) were backfilled with sand. Both sand and clay were moistened with water. The depth of cover for the pipe assembly was approximately 2 inches. The photograph in Figure 7 depicts the setup.

The resistivity of sand was considerably higher than that of clay (approximately 74,000 ohm-cm for sand and 90 ohm-cm for clay). The CP anode was located closer to Defect 1, in the sand portion of the cell.

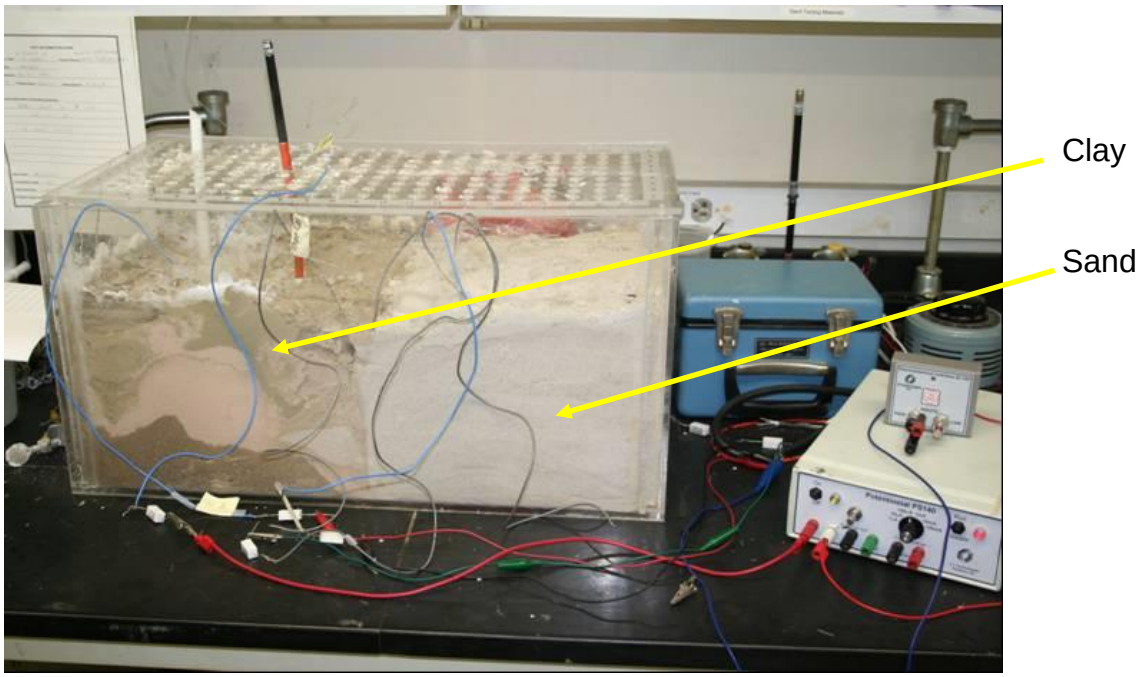

Figure 7. Small cell filled with clay and sand.

All three defects were switched in (i.e. were connected electrically for some of the measurements). Given the differences in the specific resistance between sand and clay, the distribution of CP current to the Defects varied, with Defect 2 (6 o'clock position, closer to the clay/sand border, receiving most of the current.

The plot in Figure 8 shows the distribution of ON and OFF-potentials. Measurements were taken in two different ways: (Set 1) with all the Defects forming a common network during OFF-potential measurements (labeled "Combined" in Figure 8); (Set 2) with ONLY individual Defect's OFF-potential collected (labeled Defect 1, 2, or 3 OFF). Certainly, in real life it would be impossible to collect the CIS data the way it was taken for Set 2, as the defects on a continuous pipeline are all electrically connected. Also, while it is the OFF potential of each Defect that is of the primary interest (i.e., potential value taken

at a single specific location), the data for Set 2 was taken similarly to the CIS profile for the Combined set (Set 1).

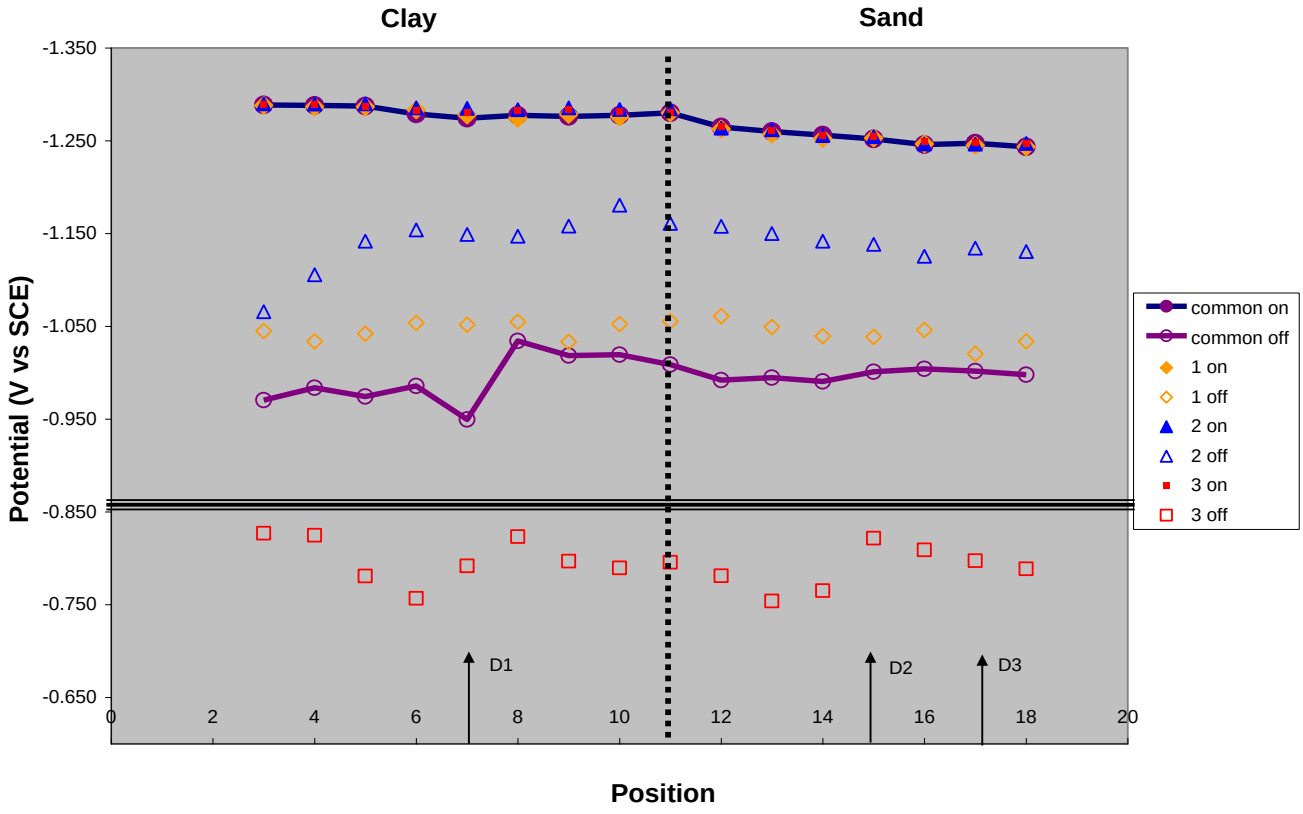

Figure 8. ON and OFF-potentials with both Defects electrically connected for OFF-potential measurements. All ON potential lines duplicate each other.

The primary finding is that, depending on how the measurements are taken, the results are quite different. Thus, the "Combined OFF" profile shows that the pipeline appears to be within the compliance with RP0169 criterion of -850mV (CSE), shown in the plot as the red horizontal line. However, when the OFF potentials are measured for each individual Defect, it becomes apparent that the Combined OFF value is in fact a composite number, comprising the weighted average of all three Defect OFF potentials (as it would be on a real pipeline).

Generally, any single potential value (E) collected during close interval survey (CIS) could be represented as:

$$E = \frac{\sum E_i g_i}{\sum g_i}$$

where E_i and g_i are the potentials of each individual defect in the coating and conductivity of the measurement path between the reference electrode and the defect, respectively.

Therefore, the defect with the least resistive path (Defect 2 in this case, which has the most negative CP potential) will be weighed the most heavily (i.e., its contribution to the measured E value will be the largest).

As shown in the graph, the CIS profiles for Defects 1 and 2 actually have OFF potentials more negative than the Combined OFF values. On the other hand, the CIS profile for Defect 3 has OFF potentials that are more positive than the RP0169 criterion.

These findings are consistent with the equation above. Defect 3 receives the least amount of protection due to the highest impedance of the three Defects. For the same reason, the Common OFF CIS is skewed towards the Defects that have lower impedance and also receive more protection.

This observation points out the danger of relying on CIS profiles exclusively when making determination with regard to the CP effectiveness. Additional information must be obtained, such as soil resistivity data. If a pipeline traverses soils with drastically different properties, or if there is reason to believe that the coating condition (or coating type) changes at some point, further investigations are indicated. The locations with higher impedance (due to soil properties or defect geometry) may not be reflected in the collected CIS data.

Conclusions

The primary conclusion of the experimental work in the small-scale cell is that, as also indicated by the numerical simulations, the resistance-based factors are the major drivers that determine the relationship between the ON and OFF potentials. This observation perhaps follows the conventional wisdom, if not the definition of the difference between ON and OFF potentials – which is the IR drop, with the R being the composite term encompassing the geometry and soil-related impedances. However, this particular step in the modeling process was important in that, in addition to verifying certain numerical model-based observations, it provided the assessment of the range of potential (CIS)

responses to the changes in soil resistivity, which assisted in the selections made for the parametric values for further efforts on numeric modeling.

The experimental modeling also highlighted one particular aspect of CIS measurements – that, in fact, most OFF potential measurements are, in all likelihood, not completely free from IR drop. The latter is caused by interaction between defects in close proximity. Further, this observation underscored the often underappreciated inherent difficulty of interpreting CIS profiles; every point on the CIS shape (typically) represents not a single defect, but an array of adjacent coating holidays of various sizes. Therefore, numerical modeling, which focuses on individual defects, can not be expected to fully reflect the complexity of real-life conditions on a buried pipeline. In this regard, the numerical modeling results would be best understood in terms of trend analysis, rather than the means of providing absolute, precise correlations between at-grade potential measurements and coating holidays.

Computation modeling

Finite Element Modeling and Regression Analysis

The distribution of potentials on and around a cathodically protected underground pipeline was modeled using finite element analysis (FEA). FEA is a numerical technique for solving complex problems when no analytical methods are available. It involves subdividing a complex geometry into a number of simpler elements and nodes, which are referred to as a “mesh”. Physical properties are related to the elements and nodes by established mathematical equations. The equations governing each element are combined for all of the elements in the model to produce a series of simultaneous equations that is solved by a computer. FEA allows the potential and current distributions under a wide variety of conditions to be calculated quickly, despite the cumbersome mathematics involved.

In the case of analysis of a cathodic protection (CP) system on an underground pipeline, the parameters of interest to be solved for are potentials and currents. These will be determined by pipeline geometry, anode location, anode applied current or voltage, soil resistivity, defect size and location, and polarization behavior of the pipeline steel. Either the anodic current or anodic potential is specified. The polarization behavior of bare steel at defects in the pipeline coating can be accounted for, and this determines the overall potential distribution around the pipe. The model inputs are varied and solved, and the calculated potential distributions provide insight into system design and

inspection. In particular, one can solve for the on-potentials at the ground surface of the model and off-potentials at defects in the pipe coating.

FEA can be used to quickly and efficiently calculate the expected ON and OFF potentials for a given combination of pipe dimensions, soil resistivity, defect size and location, and polarization behavior. By defining a matrix of parameters that are typical of conditions seen in the field, one can efficiently simulate a wide range of situations. The data produced can be analyzed statistically to identify the sensitivity of the various parameters to the measured ON and OFF potentials. If the mathematical relationships amongst the parameters can be described by an equation then there is a better understanding of cathodic protection. The mathematical relationships can be determined by regression analysis. If the regression analysis is well-correlated, then the equation can be used to infer defect sizes and coating conditions from the measurable parameters. In effect, one can develop a useful mathematical tool to assist field crews in prioritizing dig sites.

The software used for the analysis was COSMOS/M from the Structural Research and Analysis Corporation (Version 2.8). This software does not include a solver which specifically manages electrochemical problems, so the heat transfer solver was used. It can be demonstrated that heat flux and charge flux are analogous. Heat, temperature and thermal conductivity are analogous to current, potential and electrical conductivity. Modeling results will be offered later that are automatically labeled “Temp” by the software’s temperature distribution plotting module. For the purposes of this work the “Temp” must be considered as an electrical potential. Polarization behavior of bare steel was modeled using the convective heat transfer features of the COSMOS software. The software is able to simulate a surface in which the potential and current density follow a prescribed relationship.

The ultimate goal of the finite element and regression analysis work was to develop a mathematical understanding of potential distributions that can assist in further understanding of the factors determining the resultant potential profile measured by CIS.

Description of Preliminary 2D Model

A simple 2D model was constructed and run several times to demonstrate the applicability of the modeling technique and confirm some expected trends. The assumptions inherent in a 2D model produce some numbers that are inconsistent with the 3D “real world“, so results are offered for demonstration purposes only.

A model was constructed using 2D planar elements and nodes as shown in Figure 9. This model is a cross-section of a 12 inch diameter pipeline and the surrounding soil, and is used to study the potential distributions around the pipe. The resistivity of soil was prescribed to all of the elements. The pipe was not included, but instead modeled as a hole in the soil mesh. Effectively, this assumes the pipe is coated with a perfectly insulating material. The nodes mark the locations at which currents and potentials are either prescribed or calculated. In this work, current or potentials were prescribed at the anode. Defects were modeled by treating surfaces of elements adjacent to the hole as convective heat transfer surfaces, with a temperature dependent convection coefficient used to simulate polarization behavior of bare steel. Note that this technique relies on the electrical-thermal analogy discussed above.

The model was run repeatedly with a variety of inputs. Anode location, coating defect size, coating defect position, soil resistivity, pipeline depth of cover and the applied anodic current or potential were all changed at various times during the study.

Some simulations were run to determine the most appropriate location of the anode with respect to the 12 inch diameter pipeline. Initially, it was placed at a location with approximately the same depth of cover as the pipeline, which was at 3.5 feet. The goal was to achieve a more uniform potential distribution. A more uniform potential distribution would signify that the pipeline is being protected evenly by the cathodic protection. The results show that as the anode is moved to a greater depth in the soil, the surface potential becomes more uniform. This is also expected to improve if the anode is moved to a position that is closer to being directly underneath the pipeline.

One of the output potential distributions is offered below as Figure 9. The red shaded area at the top of the plot represents the high potential at the pipeline coating defect. The blue shaded area in the lower right of the plot represents the lower potential of the anode. In this simulation the anode potential was prescribed as -1.000V. Note the legend is labeled as “Temp”, though this is considered as a potential.

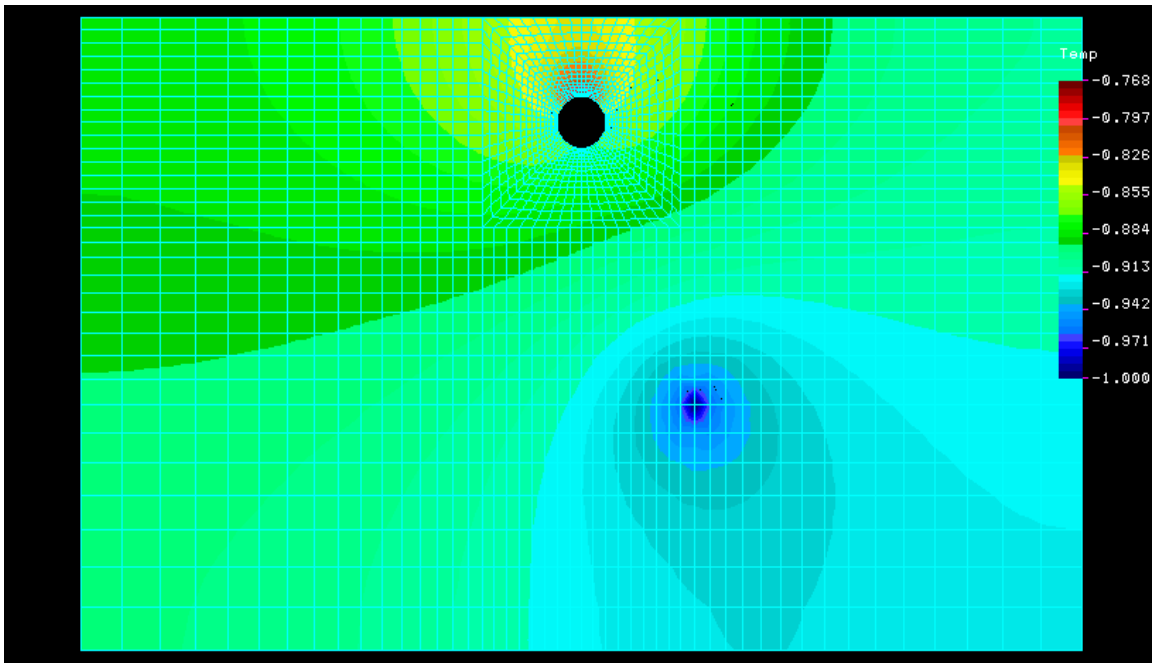

Figure 9. A potential distribution from the 2D model for a coating defect located at the 12 o'clock position (shown at the top of the graph). The anode can be seen lower right.

Results of Preliminary 2D Model

The preliminary 2D model was used to demonstrate the applicability of finite element analysis for the given problem. The calculated potentials were plotted and various trends observed. These trends are consistent with those expected based on field experience. In each case the plots are the potentials calculated along the top of the model, across the transverse section of the pipe.

Figure 10 is a plot of the ON potential distribution across the surface for various anode depths. The anode was kept at constant horizontal distance from the pipe, but the depth was changed from 4 to 8 to 15 feet beneath the soil surface. The effect of anode depth is seen in the figure. The effect is very small, with potential varying by only a few millivolts across eight feet of soil surface. Note that the distributions are non-symmetrical, as the anode was not placed directly below the pipeline. The distribution becomes more uniform as the anode is place deeper. This implies the pipeline is protected more uniformly.

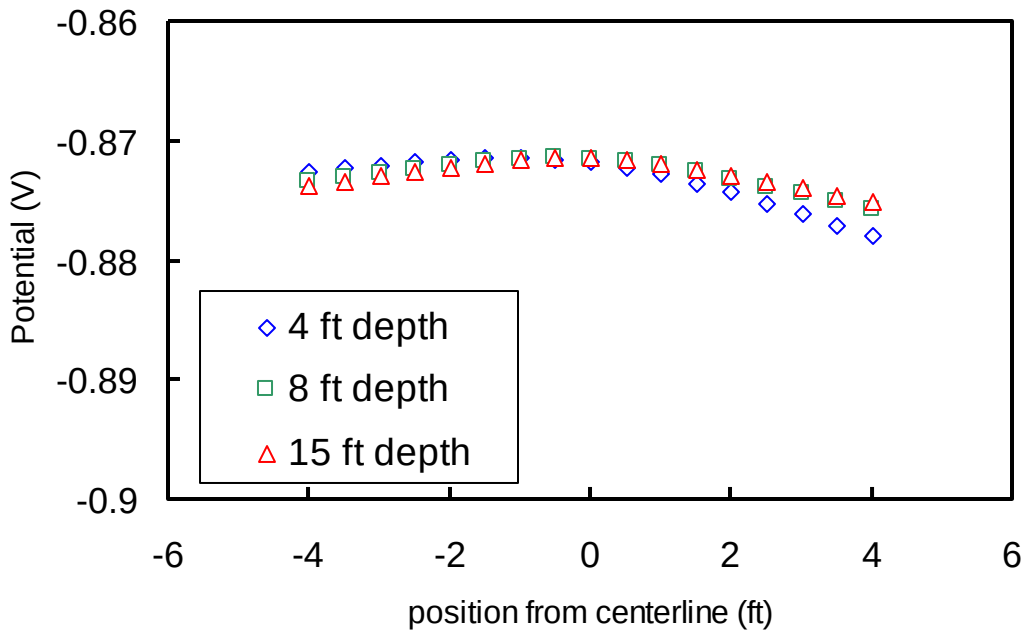

Figure 10. Calculated ON potential distributions with varying depth of anode.

This model is a cross-section of a pipeline and the surrounding soil, and is used to study the potential distributions around the pipe. The resistivity of soil was prescribed to all of the elements. The nodes mark the locations at which currents and potentials are either prescribed or calculated. The pipe was not included, but instead modeled as a hole in the soil mesh. Effectively, this assumes the pipe is coated with a perfectly insulating material. Defects were modeled by treating surfaces of elements adjacent to the hole as convective heat transfer surfaces, with a temperature dependent convection coefficient used to simulate Tafel behavior of bare steel.

Shown in Figure 11 is a plot of the ON potential distribution across the surface for various defect sizes. Defect size was changed by treating more than one element surface as a polarization surface. The effect of defect size is seen in the Figure. This range of defect sizes leads to a change in ON potential of approximately 150 millivolts. Potential becomes more positive as the defect size increases. Potential gradient across the surfaces also increases.

There is a change in potentials calculated by the model as coating defect size changes. One of these observed changes is that as holiday size increases, the

potentials become more positive. This result is expected due to the increased difficulty in protecting a larger size defect, as is the case in actual cathodic protection practice.

Another observed trend is that the change in the shape of each curve in Figure 11 is also a function of holiday size. As the coating holiday size increases, curvature of the corresponding plot also increases. This is also expected because a larger defect or holiday will consume a greater amount of CP current. This increase in CP current entering the pipeline at the holiday leads to a greater change in potentials along the soil surface directly above the pipeline. In other words, a larger defect should lead to a steeper change in the potential distribution as measured on top of the grade.

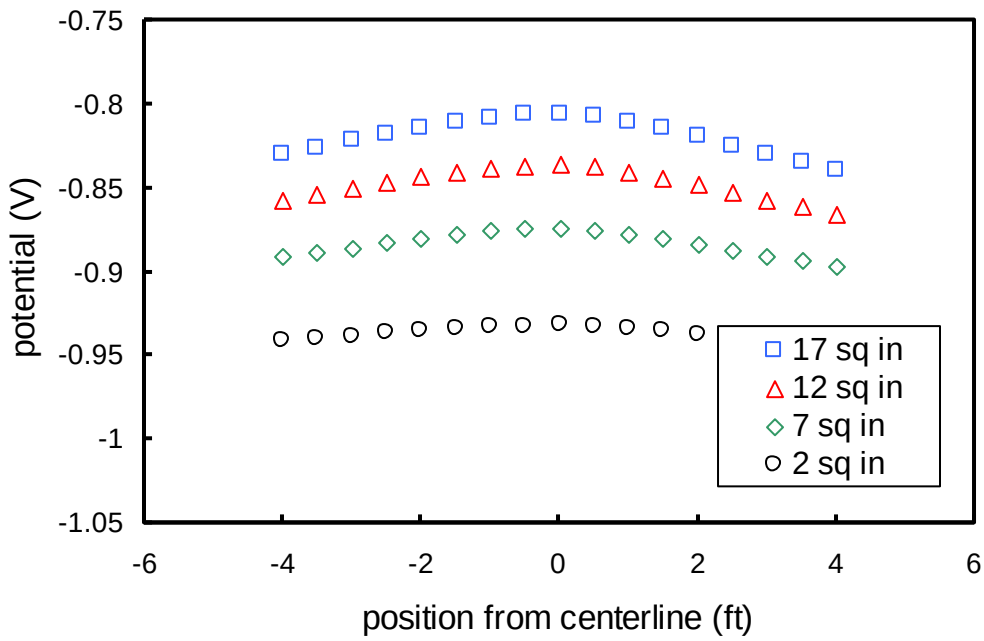

Figure 11. Calculated ON potential distributions with varying defect size.

Figure 12 is a plot of the ON potential distribution across the surface for various defect orientations. Defect orientation was changed by changing which element surface in the model was defined as a polarization surface. The defect orientation was changed from 12 to 3 to 6 to 9 o'clock on the pipe's end-face. The effect is seen in the Figure. The defect orientation leads to a change in ON potential of approximately 30 millivolts. Potential becomes more positive if the defect is located nearer the top of the pipe. Potential gradient across the surfaces also increases. Note that potential distributions are not symmetrical, particularly for

the 3 and 9 o'clock orientation defects. Such a skewed distribution could be used to infer defect orientation from ON–potential measurements.

A distribution of ON-potentials is expected with change in defect orientation, as the depth of soil cover changes with orientation. The difference between the ON- and OFF-potentials is expected to be a function of the "IR" drop. The depth of soil between the surface and defect will contribute to the resistance. Given the anodic current was kept constant for this series of models, one would expect this behavior. Note the potential distribution for the 12 o'clock defect shows a sharper curvature than the 6 o'clock defect. This indicates that the influence of the defect on the potential distribution is highly localized. In addition, the pipe is between the defect and surface and is blocking the steep gradients.

The curves for position 3 and position 9 also are skewed due to the range, in which simulated results were included. If a wider range of measurement distances (relative to the top of the pipeline) had been included, the potential distribution would expected to be more uniform. The peaks of these coating holidays at position 3 and position 9 also look a little bit flatter and more positive than the peak at the 12 position. This is expected due to the locations of positions 3 and 9 being at a larger depth from the grade level. Potential measurements are expected to be much more sensitive for defects that have the shortest distance between the measurement point and the defect site. This is also shown by the defect at position 6 which corresponds to the bottom of the pipeline. Its potential profile has the flattest peak. This can be caused due a much larger IR-drop through the soil.

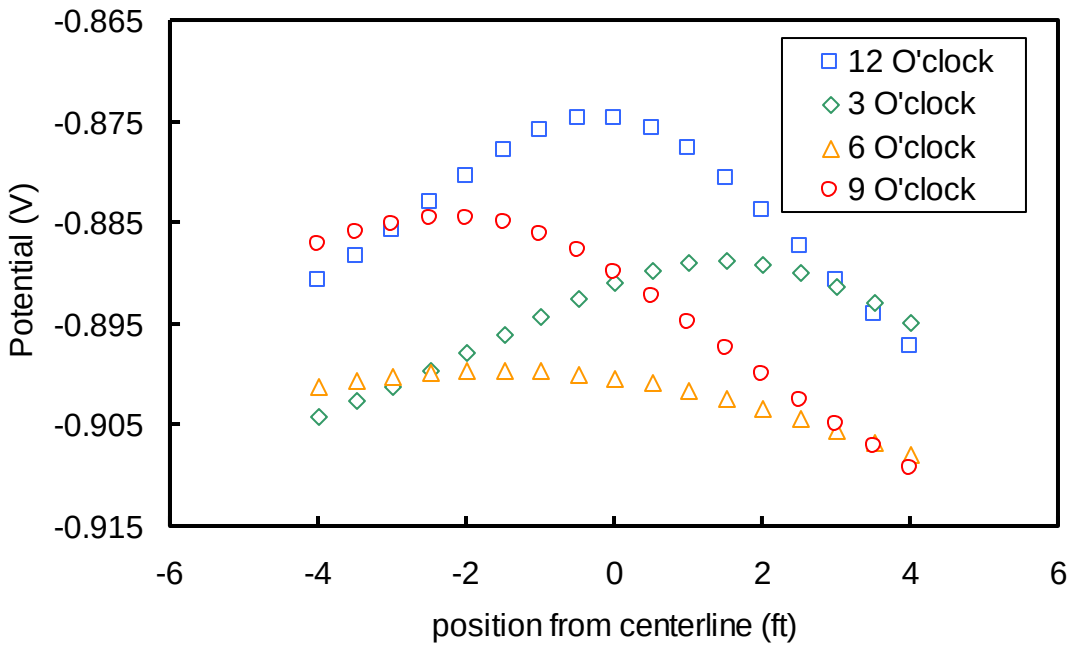

Figure 12. Calculated ON potential distributions with varying defect orientation.

Figure 13 is a plot of the ON potential distribution across the surface for various soil resistivities. Soil resistivity was changed as the material property assigned to the elements used to construct the model. Resistivity was changed from 500 to 50,000 Ω-inches. The effect is seen in the figure. The change in soil resistivity leads to a change in ON-potential of approximately 200 millivolts. As soil resistivity increases, the soil surface potential profiles become more positive. This could suggest that the larger soil resistivity impedes the ability to polarize the pipeline's defect causing more unprotected (more positive) soil surface potentials. Results also show that the peak of a given profile is larger at a greater soil resistivity. However, this result is unexpected and could be considered inconclusive due to the very small peaks in the profiles that are present.

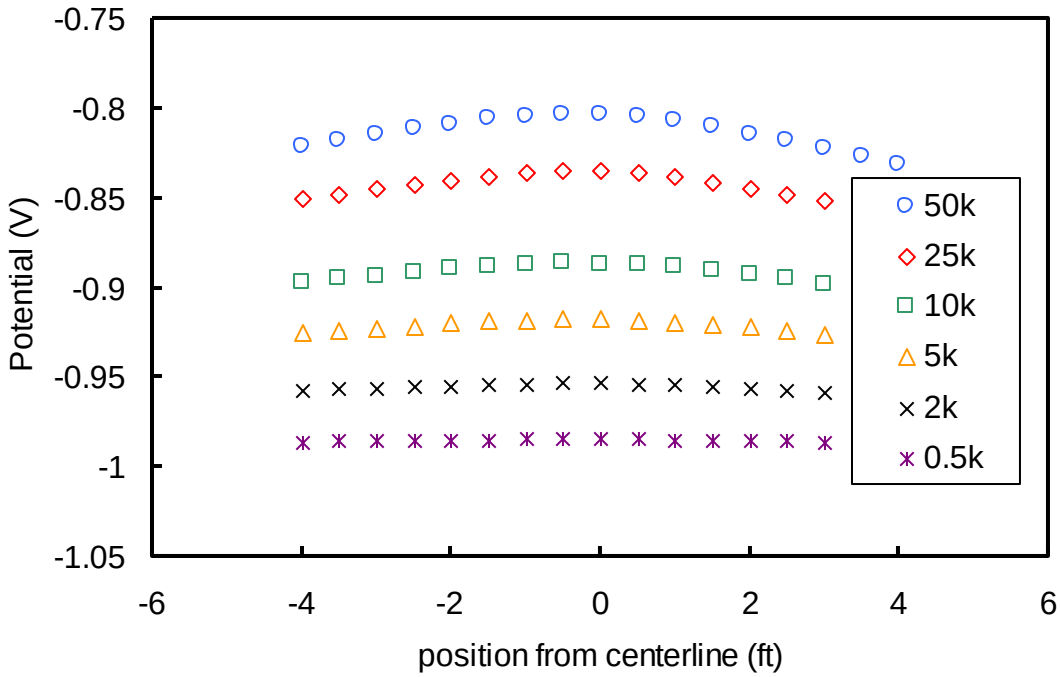

Figure 13. Calculated ON potential distributions with varying soil resistivity. Soil resistivity units are Ω-inches.

Figure 14 is a plot of the ON potential distribution across the surface for various depth of cover. Depth of cover was changed by adjusting inputs while the geometry of the model was constructed. Depth of cover was changed from 3 to 3.75 feet. The effect is seen in the figure. The change in depth of cover leads to a change in ON-potentials of approximately 200 millivolts. A smaller depth of cover leads to the peaks that are larger for defects that are closer to the ground surface. The soil surface potential profiles are also found to be more positive for pipelines with smaller depths of cover. This result is expected because as the distance between a potential measurement and a coating holiday increases, the resistance in the measurement path increases and, as such, the IR-drop component in the grade-level potential measurements rises as well.

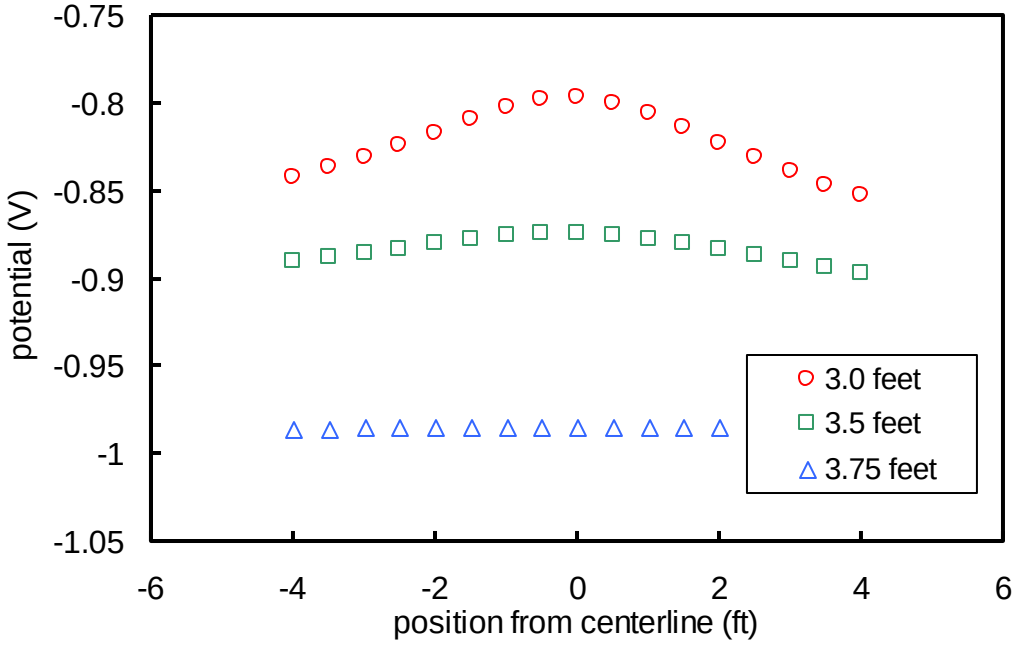

Figure 14. Calculated ON potential distributions with varying depth of cover.

The initial simulations using the 2D model were considered successful in that the results appeared to follow expected trends. This indicates that the finite element analysis technique is a valid approach to understanding the problem and that assumptions made during the development of the model are reasonable.

Description of the 3D Model

A more complex 3D model was developed for the bulk of the simulations. This model was used to study both the potential distributions around the pipe and *along* the pipe, both of which may be used to infer the location and orientation of defects on the pipe surface. Again, the parameters were varied and the calculated potential distributions studied.

Note that the initial 2D model represents a transverse cross-section through the pipeline. A 2D model representing a longitudinal cross-section through the pipeline would not have captured its cylindrical nature, nor the trends demonstrated previously. The 2D model was developed to explore the modeling capabilities and demonstrate the validity of the FEA method. A close interval survey is done along the pipeline, and for these potential distributions a 3D model is necessary. The continuing efforts were aimed at developing a working 3D model.

The 3D model was developed from the initial 2D model. The cross-section remained the same, but elements were “extruded” in the longitudinal direction to simulate a 40 foot length of pipe. The anode was kept at a constant distance away from and beside the pipe. As the anode was located at the end of the model there is an effective symmetry plane through the transverse section of the pipe.

It was decided to modify the way that the defect current-potential relationship is modeled. In the 2D model, the polarization behavior of the defect was modeled using the software’s convective heat transfer solver with *a Tafel-type* curve as input. The defect is effectively the surface area of an element. This approach is valid, but allows less control over the defect potential studied if a *constant anodic current* is specified. It is in the interests of this study to have more control over these parameters. In addition, the exponential nature of the Tafel-type curves used as inputs in the 2D model lead to some numerical difficulties when the anodic current was specified. It was decided, therefore, to prescribe the defect potential at individual nodes and the current at the anode in the continuing modeling efforts. The defects become point defects. Defect size can be simulated by prescribing a desired potential on multiple nearby nodes.

As with the 2D model, several combinations of inputs were studied to verify that the model was working correctly.

Figure 15 and Figure 16 show contour plots of the potential distributions calculated for the basic test. The basic test (Test ID #1) simulates an 8 inch diameter pipe, soil resistivity of 5000 Ω-in, and a defect (OFF-) potential of -800mV. Note that the potential gradient at the simulated point defect is very high and the range can only be seen in close-up.

The results of the initial 3D model were successful, as the results of the 2D model were. Several expected trends were identified from the results. However, consideration of the results and the model geometry suggested some improvements. Continuing efforts were aimed at modifying the 3D model for the bulk of the analyses. The following changes were implemented:

1. The length of pipe was shortened from 40 feet to just 10 feet. Preliminary results demonstrated that potential distributions near defects were concentrated within about five feet axially. By reducing the model length to 10 feet and refining the element size, the accuracy of the solutions are improved without any loss of information.

2. The anode was placed directly below the pipe, and was simulated using a string of nodes below and along the pipeline. This better simulates a deeply located anode by providing a more uniform distribution of current.
3. The model was redefined using double symmetry. That is, one symmetry plane divides the pipe transversely and one symmetry plane divides the pipe longitudinally. This allowed for mesh refinement within the capabilities of the software, and improved solution accuracy. In addition, contour plotting of the calculated potentials was possible along this cross-section. This provides a better visual understanding of the potential distribution, and can offer insight for the continued modeling efforts.
4. A formal test matrix was developed as the modeling proceeded and the results were analyzed. This allowed for modifications to be made to input parameters to ensure that realistic values were being produced. It is difficult to account for differences in model versus field potentials arising from scale differences a priori. By modifying the test matrix continually, parameters were studied more efficiently, and the appropriate range of ON potentials was ensured.

Table 2. The test matrix for the initial 3D model verification work.

Test ID #	Pipe Dia. (in)	Soil Res. (Ω-in)	Anodic Current (A)	Defect Pot. (mV)	Defect Size (nodes)	Defect Orientation (O'clock)	Calculated ON Pot. (V)	Calculated Anodic Pot. (V)
1	8	5000	0.01	-800	1	12	-4.651	-5.340
2	24	5000	0.01	-800	1	12	-3.617	-4.549
3	8	100	0.01	-800	1	12	-0.877	-0.891
4	8	50000	0.01	-800	1	12	-39.307	-46.196
5	8	5000	0.1	-800	1	12	-39.307	-46.196
6	8	5000	0.01	-1000	1	12	-4.851	-5.540
7	8	5000	0.01	-800	2	12	-1.783	-2.466
8	8	5000	0.01	-800	4	12	-1.646	-2.330
9	8	5000	0.01	-800	1	3	-4.665	-5.329
10	8	5000	0.01	-800	1	6	-4.683	-5.332
11	8	5000	0.01	-800	1	9	-4.671	-5.341
12	8	5000	0.01	-800	1+1	12+12	-2.101	-2.723
13	8	5000	0.01	-800	1+1+1	12+12+12	-1.590	-2.200
14	8	5000	0.03	-800	2	12	-3.749	-5.799
15	8	5000	0.05	-800	4	12	-5.031	-8.449
16	8	5000	0.01	-800	2	3	-1.796	-2.457
17	8	5000	0.01	-800	4	3	-1.658	-2.320
18	8	5000	0.01	-800	2	6	-1.812	-2.459
19	8	5000	0.01	-800	4	6	-1.675	-2.323
20	8	5000	0.01	-800	2	9	-1.801	-2.468
21	8	5000	0.01	-800	4	9	-1.664	-2.332

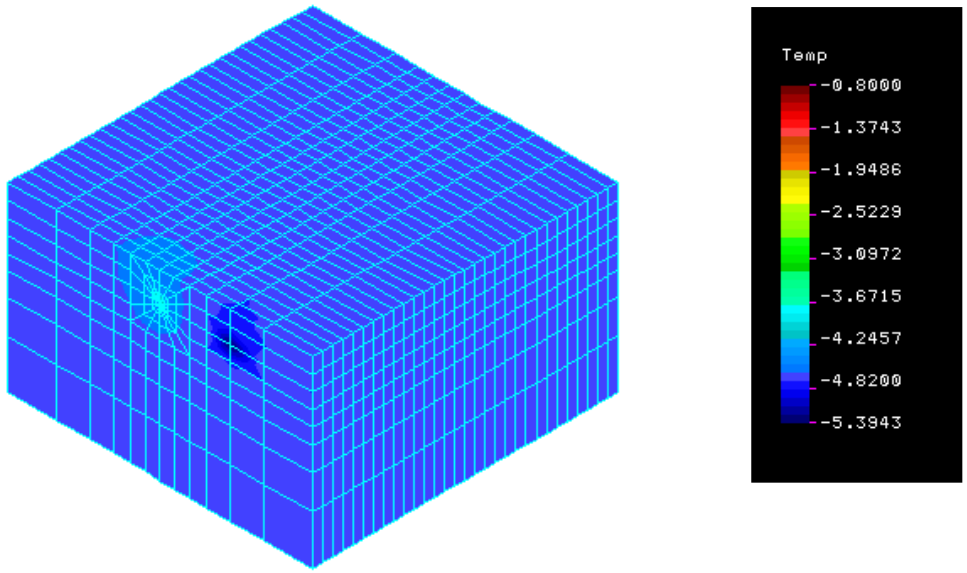

Figure 15. A contour plot of the potentials calculated for the basic test (test ID #1).

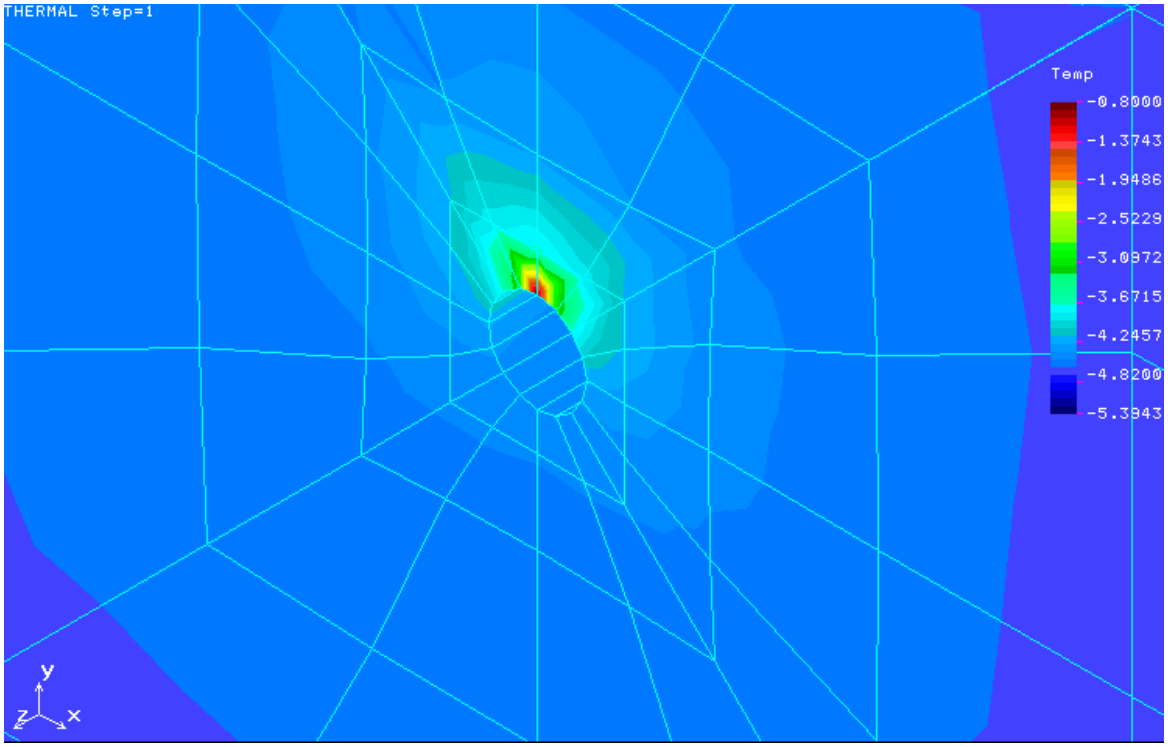

Figure 16. A contour plot of the potentials calculated for the basic test (test ID #1) (close-up).

A *constant current* was prescribed at the nodes at the base of the model. The current selected was based on trials that calculated a surface potential similar to that which would be expected in the from field measurements. Potentials were prescribed to the nodes along the simulated pipeline. The majority of the nodes were prescribed a potential appropriate for a well-protected pipeline, and one or a few nodes were prescribed a potential appropriate for a defect. Several models were run, and the preliminary results analyzed to ensure the validity of the model and confirm expected trends, as earlier. The parameters and calculated values of interest were recorded from each model and tabulated in a working spreadsheet.

Several parameters were varied during the course of the analyses. These included:

a) Pipe diameter was varied 8, 16 or 24 inches.

b) Depth of pipe centerline was varied 24, 36, 48 inches. This, in combination with the pipe diameter, leads to a variation in depth of cover from 20 inches for the top of the pipe to 60 inches to the bottom of the pipe.

c) Soil resistivity was varied from 10^2 to 10^5 Ω-inches. This is expected to have a significant effect on calculated ON potentials.

d) Defect potential was varied from -600 to -1000mV.

e) Coating potential was varied from -800 to -1400mV. This difference between defect and coating potentials was limited to either 200 or 400 mV. In each case the coating potential was more negative than the defect potential.

f) The orientation of the defect was prescribed as the 6 o'clock, the 9 o'clock or 12 o'clock position. These, in combination with the pipe diameter and depth of pipe centerline, lead to a variation in depth of cover.

g) Defect size was varied by prescribing a potential to 1, 3 or 4 nodes. Note that the effective area of the defect does not scale linearly with number of nodes due to the symmetry in the model. The "3" or "4" size defects represent an area of approximately 5x that of the "1" node defect. The choice of 3 or 4 depends on the model symmetry and defect location. The anodic current was kept constant for (almost) all simulations. No attempts were made to account for the varying current densities and / or symmetry effects that may have been caused. In a few select cases, multiple defects were simulated by applying potentials to more than one node.

Several combinations of the above parameters were defined and used to construct input files for the finite element analyses. Trends of the resulting calculated ON potentials were used to confirm the validity of the model and guide further testing. Some of the values used may be considered inappropriate, or not applicable to typical field conditions. These values were selected in order to study extreme conditions and demonstrate the sensitivity of the calculated ON potentials to the various parameters.

Initially, fifty-five (55) models were run with a variety of input parameters. Preliminary results were analyzed. Statistical analysis was then used to determine what combinations of input parameters were necessary to more fully develop the test matrix. Further forty-five (45) models were run. The results of the one hundred (100) total models were analyzed statistically to determine if a regression equation could be developed that accurately describes the mathematical relation between the input parameters and outputs. If such a regression equation exists, it could be used to predict the size and orientation of defects based on field measurements. If such a regression equation does not exist, it may demonstrate that field measurements cannot consistently predict pipeline coating conditions.

Below are the results of finite element analysis Test “AA” (see Table 3 and Figure 17 and Figure 18). This model was run as a model with a defined pipeline diameter of 8 inches and depth of centerline of 48 inches. The soil resistivity was defined as 2000 Ω·in. A defect of potential -800 mV was prescribed on the 12 o’clock orientation of the pipe, and the remaining nodes on the pipe were prescribed with -1000 mV. These results are used to demonstrate a typical potential distribution. The red shaded area around the pipe represents the high potential at the pipeline coating and defect. The blue shaded area in the lower right of the plot represents the lower potential of the anode.

The figures below show contour plots of the calculated potentials. Note that the model is defined using double symmetry. The defect is defined on the front edge of the model. The model could be mirrored on its right side plane to produce the 12 o’clock to 3 o’clock to 6 o’clock half of the pipe, i.e. the plane defines the pipe’s longitudinal symmetry. It could also be mirrored on its left side plane to produce another ten foot length of pipe, i.e. the plane defines the pipe’s axial symmetry. The symmetry planes have two advantages; (1) it saves on computation time by reducing the geometry fourfold, and (2) it allows the “internal” potential gradients to be inspected visually. The symmetry planes should be considered in any visual interpretation of the contours.

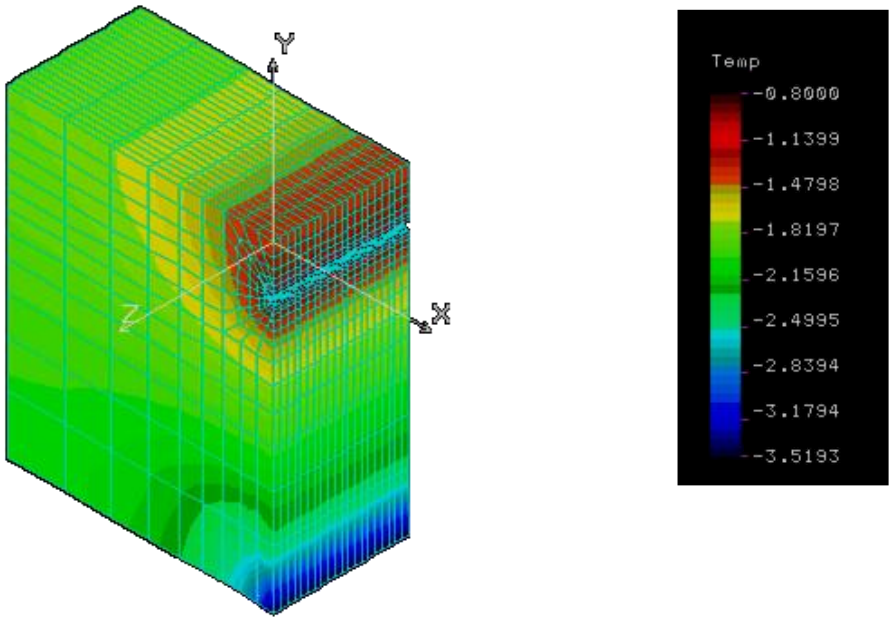

Figure 17. A contour plot of the potentials calculated for test “AA”.

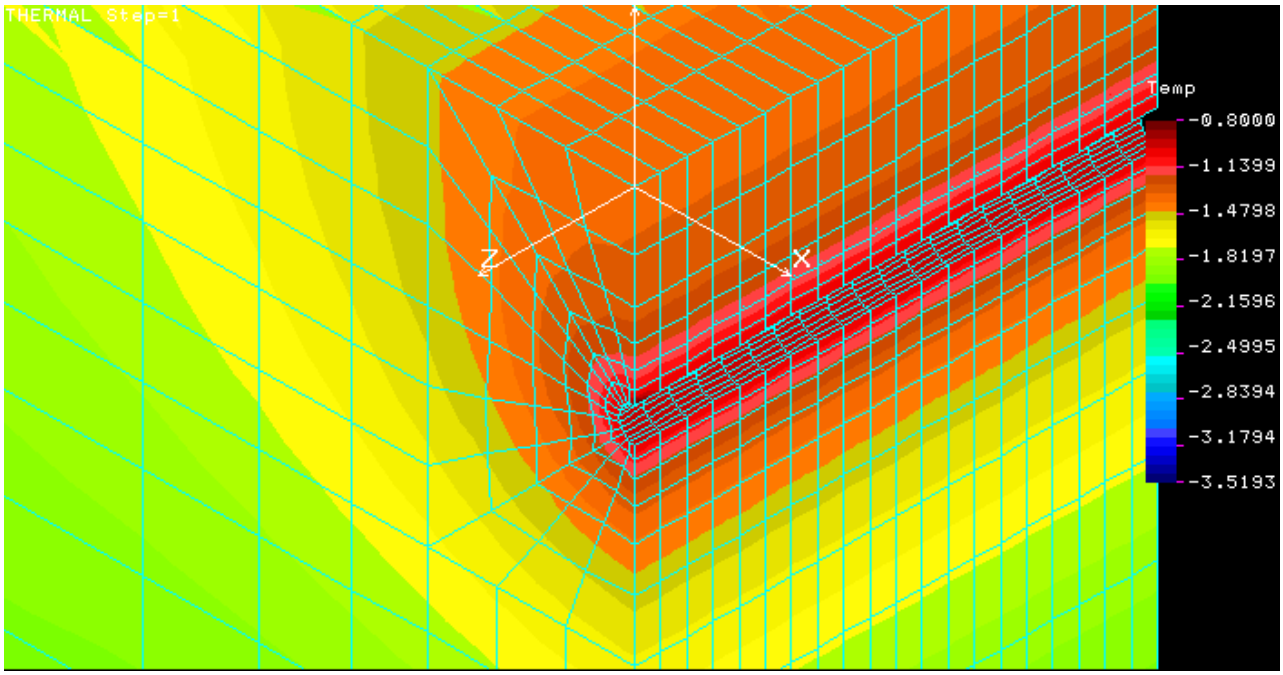

Figure 18. A contour plot of the potentials calculated for test "AA" (close-up).

Regression analysis of 3D model work

The results of the 3D finite element modeling work are reported in Table 3. Each line in the table lists the sample identification, model geometry, prescribed potentials and defect size and location. These parameters are *inputs* to the models. The columns at the right side of the table list the calculated surface (ON) potentials and the calculated anodic potential. These are the *outputs* of the model. Variations in the parameters and results were used to develop a regression equation.

The statistical analysis was preformed using Minitab software. Minitab has the capability of performing regression analysis on data, and identifying the statistical significance of the various regression coefficients. This helps to identify which of the measured parameters has a greatest effect on the potential distributions. From this, one can infer how accurate measurements have to be to resolve the size and location of defects.

Statistical analysis requires several steps to complete. The first step in the development of the regression equation is normalization of the data. The various parameters (soil resistivity, depth of cover, OFF potentials, etc) have different ranges of their typical values, largely because of the different units used to measure each. These ranges influence the regression analysis, and can

mathematically bias the solution towards certain parameters. A normalization scheme is used to effectively “level the playing field”, and prevent the range of a given parameter from artificially biasing the analysis.

In general terms, the normalization is done by assigning the value “zero” to the average of a parameter range and the values “-1” and “+1” to the lower and upper values in the range, respectively. For example, the pipe diameter was varied between 8 and 24 inches. The average for this range is 16, so any models run with a 16 inch diameter pipeline were assigned a “normalized diameter” of zero. Models run with an 8 inch diameter were assigned a normalized diameter of “-1”, the lower limit of the range. Models run with a 24 inch diameter were assigned a normalized diameter of “+1”. Other diameters within the range are assigned values calculated by linear interpolation.

Table 3. Descriptions and results of FEA model runs.

Test #	Pipe Diameter (in)	Depth of Centerline (in)	Soil Resistivity (Ω–in)	Soil Conductivity (1/Ω-in)	Defect Potential (mV)	Coating Potential (mV)	Difference in Potentials (mV)	Defect Size (nodes)	Defect Orientation (O'Clock)	Calculated Surface Potential (V)	Calculated Anodic Potential (V)
AA	8	48	2000	0.0005	-800	-1000	200	1	12	-1.355	-3.519
BB	24	48	2000	0.0005	-800	-1000	200	1	12	-1.142	-3.292
CC	8	48	4000	0.00025	-800	-1000	200	1	12	-1.711	-6.039
DD	8	48	1333	0.00075	-800	-1000	200	1	12	-1.094	-2.528
EE*	8	48	2000	0.0005	-800	-1000	200	1	12	-1.711	-6.039
FF	8	48	2000	0.0005	-600	-1000	400	1	12	-1.355	-3.519
GG	8	48	2000	0.0005	-1000	-1200	200	1	12	-1.555	-3.719
HH	8	48	2000	0.0005	-800	-1000	200	1	6	-1.355	-3.519
II	8	48	2000	0.0005	-800	-1000	200	1	9	-1.355	-3.519
JJ	8	48	2000	0.0005	-600	-800	200	1	12	-1.155	-3.319
KK	8	48	2000	0.0005	-800	-1000	200	3	12	-1.353	-3.519
LL	8	48	2000	0.0005	-800	-1000	200	3	6	-1.355	-3.518
MM	8	48	2000	0.0005	-800	-1000	200	2	12+12	-1.355	-3.519
NN	8	48	2000	0.0005	-800	-1000	200	2	6+6	-1.355	-3.519
OO	8	24	2000	0.0005	-800	-1000	200	1	12	-1.226	-3.606
PP	24	24	2000	0.0005	-800	-1000	200	1	12	-1.028	-3.366
QQ	8	48	2000	0.0005	-800	-1000	200	2	12+6	-1.355	-3.519
RR	8	48	2000	0.0005	-800	-1000	200	2	12+9	-1.354	-3.519
SS	8	48	2000	0.0005	-800	-1000	200	2	6+9	-1.355	-3.519
TT	8	48	2000	0.0005	-800	-1000	200	5	random	-1.353	-3.516
UU	8	48	2000	0.0005	-800	-1000	200	10	random	-1.348	-3.513
VV	8	48	2000	0.0005	-800	-1200	400	1	12	-1.555	-3.719
WW	8	48	2000	0.0005	-600	-800	200	1	6	-1.155	-3.319
XX	8	48	2000	0.0005	-1000	-1200	200	1	6	-1.555	-3.719
YY	8	48	2000	0.0005	-600	-800	200	1	9	-1.155	-3.319
ZZ	8	48	2000	0.0005	-1000	-1200	200	1	9	-1.555	-3.719

Test #	Pipe Diameter (in)	Depth of Centerline (in)	Soil Resistivity (Ω–in)	Soil Conductivity (1/Ω-in)	Defect Potential (mV)	Coating Potential (mV)	Difference in Potentials (mV)	Defect Size (nodes)	Defect Orientation (O'Clock)	Calculated Surface Potential (V)	Calculated Anodic Potential (V)
3A	24	48	10000	0.0001	-800	-1000	200	1	12	-1.715	-12.461
3B	24	48	100000	0.00001	-800	-1000	200	1	12	-8.162	-115.615
3C	24	48	1000	0.001	-800	-1000	200	1	12	-1.070	-2.146
3D	24	48	100	0.01	-800	-1000	200	1	12	-1.006	-1.114
3E	8	48	4000	0.00025	-800	-1000	200	3	12	-1.709	-6.038
3F	8	48	4000	0.00025	-800	-1000	200	3	6	-1.710	-6.038
3G	8	48	1333	0.00075	-800	-1000	200	3	12	-1.235	-2.679
3H	8	48	1333	0.00075	-800	-1000	200	3	6	-1.236	-2.678
3I	16	48	2000	0.0005	-800	-1000	200	1	12	-1.220	-3.378
3J	8	36	2000	0.0005	-800	-1000	200	1	12	-1.303	-3.553
3K	24	36	2000	0.0005	-800	-1000	200	1	12	-1.093	-3.321
3L	8	48	10000	0.0001	-800	-1000	200	1	12	-2.778	-13.597
3M	8	48	100000	0.00001	-800	-1000	200	1	12	-18.782	-126.972
3N	8	48	1000	0.001	-800	-1000	200	1	12	-1.177	-2.260
3O	8	48	100	0.01	-800	-1000	200	1	12	-1.017	-1.126
3P	8	48	4000	0.00025	-600	-1000	400	1	12	-1.710	-6.039
3Q	8	48	1333	0.00075	-600	-1000	400	1	12	-1.236	-2.679
3R	8	48	4000	0.00025	-600	-800	200	1	6	-1.511	-5.839
3S	8	48	1333	0.00075	-600	-800	200	1	6	-1.037	-2.479
3T	8	48	4000	0.00025	-1000	-1200	200	1	12	-1.911	-6.239
3U	8	48	1333	0.00075	-1000	-1200	200	1	12	-1.437	-2.879
3V	8	48	4000	0.00025	-1000	-1200	200	1	6	-1.911	-6.239
3W	8	48	1333	0.00075	-1000	-1200	200	1	6	-1.437	-2.879
3X	8	48	4000	0.00025	-600	-800	200	1	12	-1.511	-5.839
3Y	8	48	1333	0.00075	-600	-800	200	1	12	-1.037	-2.479
3Z	8	48	4000	0.00025	-600	-1000	400	3	12	-1.706	-6.037
4B	8	48	1333	0.00075	-600	-1000	400	3	12	-1.232	-2.678
4C	8	48	4000	0.00025	-600	-1000	400	3	6	-1.709	-6.037

Test #	Pipe Diameter (in)	Depth of Centerline (in)	Soil Resistivity (Ω–in)	Soil Conductivity (1/Ω-in)	Defect Potential (mV)	Coating Potential (mV)	Difference in Potentials (mV)	Defect Size (nodes)	Defect Orientation (O'Clock)	Calculated Surface Potential (V)	Calculated Anodic Potential (V)
4D	8	48	1333	0.00075	-600	-1000	400	3	6	-1.235	-2.677
BH1	8	36	2000	0.0005	-800	-1000	200	4	9	-1.300	-3.551
BH2	8	24	1000	0.001	-1000	-1400	400	1	6	-1.513	-2.703
BH3	8	24	1000	0.001	-1000	-1200	200	1	12	-1.312	-2.503
BH4	8	24	1000	0.001	-600	-1000	400	1	12	-1.111	-2.303
BH5	8	24	1000	0.001	-600	-800	200	3	6	-0.913	-2.102
BH6	8	24	10000	0.0001	-1000	-1400	400	1	12	-2.534	-14.432
BH7	8	24	10000	0.0001	-1000	-1200	200	1	6	-2.336	-14.232
BH8	8	24	10000	0.0001	-600	-1000	400	1	6	-2.136	-14.032
BH9	8	24	10000	0.0001	-600	-800	200	3	12	-1.929	-13.832
BH10	8	48	1000	0.001	-1000	-1400	400	1	12	-1.577	-2.659
BH11	8	48	1000	0.001	-1000	-1200	200	1	6	-1.378	-2.459
BH12	8	48	1000	0.001	-600	-1000	400	1	6	-1.177	-2.259
BH13	8	48	1000	0.001	-600	-800	200	3	12	-0.975	-2.059
BH14	8	48	10000	0.0001	-1000	-1400	400	1	6	-3.178	-13.997
BH15	8	48	10000	0.0001	-1000	-1200	200	1	12	-2.978	-13.797
BH16	8	48	10000	0.0001	-600	-1000	400	1	12	-2.777	-13.597
BH17	8	48	10000	0.0001	-600	-800	200	3	6	-2.577	-13.396
BH18	16	24	2000	0.0005	-800	-1200	400	4	9	-1.288	-3.654
BH19	16	36	1000	0.001	-800	-1000	200	4	9	-1.080	-2.203
BH20	16	36	2000	0.0005	-1000	-1400	400	4	9	-1.561	-3.805
BH21	16	36	2000	0.0005	-800	-1000	200	1	9	-1.168	-3.409
BH22	16	36	2000	0.0005	-800	-1200	400	3	6	-1.368	-3.607
BH23	16	36	2000	0.0005	-800	-1000	200	4	9	-1.165	-3.407
BH24	16	36	2000	0.0005	-800	-1200	400	3	12	-1.355	-3.608
BH25	16	36	2000	0.0005	-800	-1000	200	1	9	-1.168	-3.409
BH26	16	36	2000	0.0005	-600	-1000	400	4	9	-1.161	-3.405
BH27	16	36	10000	0.0001	-800	-1000	200	4	9	-1.841	-13.046

Test #	Pipe Diameter (in)	Depth of Centerline (in)	Soil Resistivity (Ω–in)	Soil Conductivity (1/Ω-in)	Defect Potential (mV)	Coating Potential (mV)	Difference in Potentials (mV)	Defect Size (nodes)	Defect Orientation (O'Clock)	Calculated Surface Potential (V)	Calculated Anodic Potential (V)
BH28	16	48	2000	0.0005	-800	-1200	400	4	9	-1.414	-3.574
BH29	24	24	1000	0.001	-1000	-1200	200	1	12	-1.210	-2.383
BH30	24	24	1000	0.001	-1000	-1400	400	3	6	-1.418	-2.580
BH31	24	24	1000	0.001	-600	-800	200	1	6	-0.818	-1.983
BH32	24	24	1000	0.001	-600	-1000	400	1	12	-1.002	-2.183
BH33	24	24	10000	0.0001	-1000	-1200	200	1	6	-1.379	-13.028
BH34	24	24	10000	0.0001	-1000	-1400	400	3	12	-1.511	-13.228
BH35	24	24	10000	0.0001	-600	-800	200	1	12	-0.972	-12.628
BH36	24	24	10000	0.0001	-600	-1000	400	1	6	-1.179	-12.828
BH37	24	48	1000	0.001	-1000	-1200	200	1	6	-1.272	-2.346
BH38	24	48	1000	0.001	-1000	-1400	400	3	12	-1.460	-2.545
BH39	24	48	1000	0.001	-600	-800	200	1	12	-0.870	-1.946
BH40	24	48	1000	0.001	-600	-1000	400	1	6	-1.071	-2.146
BH41	24	48	10000	0.0001	-1000	-1200	200	1	12	-1.915	-12.661
BH42	24	48	10000	0.0001	-1000	-1400	400	3	6	-2.115	-12.859
BH43	24	48	10000	0.0001	-600	-800	200	1	6	-1.516	-12.261
BH44	24	48	10000	0.0001	-600	-1000	400	1	12	-1.714	-12.461
BH45	24	36	2000	0.0005	-800	-1000	200	4	9	-1.092	-3.319

EE* - this model was run with 2x the current the other models were run.

The regression analysis performed was a multi-variable linear regression of the various parameters, to the calculated surface potential. No effort was made to derive a formal physically based equation. However, it was considered that there may be parameters correlated with each other. Some terms were multiplied together to produce combined terms, and these were also included in the analysis. The normalization scheme was also applied to the combined terms. The goal of the preliminary analysis was to identify which terms had a statistically significant effect on the regression equation.

Once the data were normalized, a preliminary regression analysis was performed. The correlation of each regression coefficient was calculated using established methods which are built-in functions of the Minitab software used for the analysis. The correlation statistics were used to determine which of the parameters are statistically significant, that is, which of the parameters can be mathematically shown to be relevant. These parameters were also ranked based on their significance.

Once the key parameters were identified using the regression of the normalized parameters, a second regression was performed using the non-normalized data. In effect, the first regression is used to determine which parameters are relevant for the second regression. By normalizing, the second regression is not biased by the unequal ranges in the parameters.

The result of the second regression analysis was that six different terms were identified as being statistically significant;

1. Depth to Center x Resistivity. This is a combined term that includes the depth from the surface level to the centerline of the pipe times the resistivity of the soil.
2. Diameter x Resistivity. This is a combined term that includes the diameter of the pipe times the soil resistivity.
3. Defect Potential. This is the defect potential that is prescribed, effectively the OFF-potential.
4. Soil Resistivity. This is expected to have a significant effect on all of the calculated values.
5. Potential Difference. This is the difference between the prescribed defect (OFF-) potential and the prescribed coating potential.

6. Defect Size. This term was simply based on the number of nodes used to define the defect. As discussed above it does not scale linearly with defect area, due to current density and symmetry effects.

In addition, there was a constant identified in the regression.

The coefficients for the linear regression analysis are given as Table 4. Note that the units used in the regression files must be consistent with those described in Table 3. During the bulk of the modeling, the input parameters were listed in millivolts, whereas the outputs were listed as volts. The regression coefficients can be easily adjusted to account for any change in units.

Table 4. The results of the regression analysis.

Parameter	Coefficient
Constant	-0.02137
DepCenter_Res	-0.0000025
Dia_Res	0.00000636
Defect Potential	0.0009925
Soil Resist	-0.00010639
Pot_Diff	-0.00098133
Defect Size	0.008711

The absolute values of the coefficients show how much the ON potential value is affected by the change in the parameter.

The signs in the table indicate the direction of each parameter's influence on the ON potential values. Thus, for example, the larger the defect size, the more positive the ON potential is likely to be (lower geometry-related resistivity, and, consequently, lower IR). Similarly, the term linked to the parameters which values increase as the pipe is buried deeper (depth of cover multiplied by soil resistivity) leads to more negative ON potentials as well. Naturally, OFF potentials (defect potential), which is entered as a negative value, factors considerably in the ON potential value (the more negative OFF is, the more negative the ON will be, everything else being equal). The positive sign of the parameter combining

pipeline diameter and resistivity suggests that the influence of the pipeline diameter dominates – the larger the pipe, the lower the depth of cover under the model assumptions (the depth to centerline is kept the same). However, the influence of this particular parameter is fairly small, based on its absolute value.

Several terms were identified as being *not* statistically significant, and these require some discussion.

1. Depth to defect. It is surprising that the depth of soil cover did not feature in the regression as statistically significant, even when multiplied by the soil resistivity to create a combined term. Both depth to centerline and pipe diameter became significant when combined with soil resistivity. These other terms are similar parameters, and their effects may have overshadowed the depth to defect term by chance.
2. Coating potential. It is reasonable that the coating potential prescribed to the intact coating did not feature, given that both the prescribed defect (OFF-) potential and difference between defect and coating potentials did feature significantly. These three terms are really two terms and a difference between them. They would not all expected to be featured.
3. Defect orientation. This term was included to account for potential differences arising due to orientation of the defect at the 6 or 9 or 12 o'clock position. As above (1), it is surprising that the term did not feature significantly in the regression equation. Again, it may be that several terms of similar nature overshadowed each other.

The result of the regression analysis is a basic equation used to mathematically relate the various input parameters with the calculated surface potential. That is:

$$ON-potential \approx -0.02137 - 2.5\times10^{-6}\times(DepCenter\times \mathrm{Res}) + 6.36\times10^{-6}\times(Dia\times \mathrm{Res})$$

$$+9.925\times10^{-4}\times(DefectPotential) - 1.0639\times10^{-4}\times(Soil\ \mathrm{Res}istivity)$$

$$-9.8133\times10^{-4}\times(Pot_Diff) + 8.711\times10^{-3}\times(DefectSize)$$

The quality of the regression analysis is demonstrated by Figure 19. The plot shows a comparison of ON-potentials calculated by finite element analysis and those calculated using the regression equation. The great majority of the data points fall along the diagonal line, which indicates good correlation. There are a few outliers in which the finite element and regression values vary by up to 350 mV. The average residual is 4 mV, indicating that the regression equation is a

very good technique for predicting the ON-potential that would have been calculated by finite element analysis.

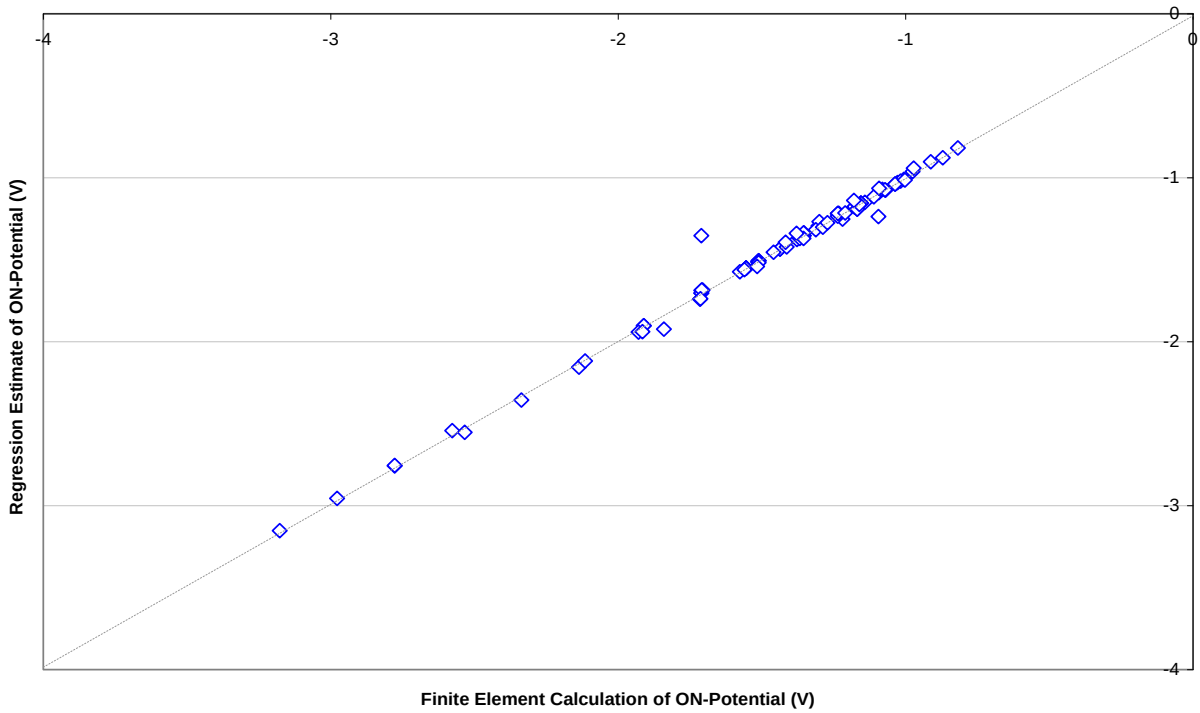

Figure 19. A comparison of finite element analysis calculated, and regression analysis estimated ON-potentials.

In order to use this to equation to estimate the size of the defect, one must re-cast the regression equation to allow calculation of the defect size.

$$DefectSize \approx [0.02137 + 2.5\times10^{-6}\times(DepCenter\times \mathrm{Res}) - 6.36\times10^{-6}\times(Dia\times \mathrm{Res})$$

$$-9.925\times10^{-4}\times(DefectPotential) + 1.0639\times10^{-4}\times(Soil\ \mathrm{Resistivity})$$

$$+9.8133\times10^{-4}\times(Pot_Diff) + (ON - Potential)]/(8.711\times10^{-3})$$

This equation can be used to infer the defect size from all of the other parameters, which are known or measurable. Note that, as described above, the defect size value does not scale linearly with defect area, due to current density and symmetry effects. However, it does provide a semi-quantitative way to prioritize dig sites. In addition, the changes in defect size and the various potentials seen during the modeling follow expected trends.

Note that the regression equation was developed using data for a limited range of input parameters. The regression equation is only valid for combinations of

parameters that are within these ranges. Any extrapolation should be done with caution.

One may find that there are combinations of parameters that result in negative defect sizes. This is clearly not physically realistic. However, it must be reiterated that the defect size is based on the number of nodes used to define the defect in the finite element models and it is only semi-quantitative. A negative defect size does not indicate a superior coating, but does indicate a defect size smaller relative to other defects. Although the calculated defect sizes are only semi-quantitative, is still does allow for relative ranking of defect sizes, thus providing additional insight for prioritization of dig sites.

Discussion of Results

Trends in the ON and OFF potentials are expected to infer the condition of pipeline coatings, and therefore help pipeline operators in the corrosion assessment process. The results of the finite element analyses and associated trends in ON and OFF potentials are discussed below in an attempt to understand how this information can be used.

Figure 20 is a plot of the ON and OFF potentials for several of the test cases. In these cases the *soil resistivity* was changed, but all other parameters were kept the same. Note that the soil resistivity scale is logarithmic. The plot indicates that the effect of the soil resistivity is to increase the difference between the two measured potentials. This is expected based on the IR-drop arguments, as discussed above. The more resistive soil will support a higher potential difference for a given current.

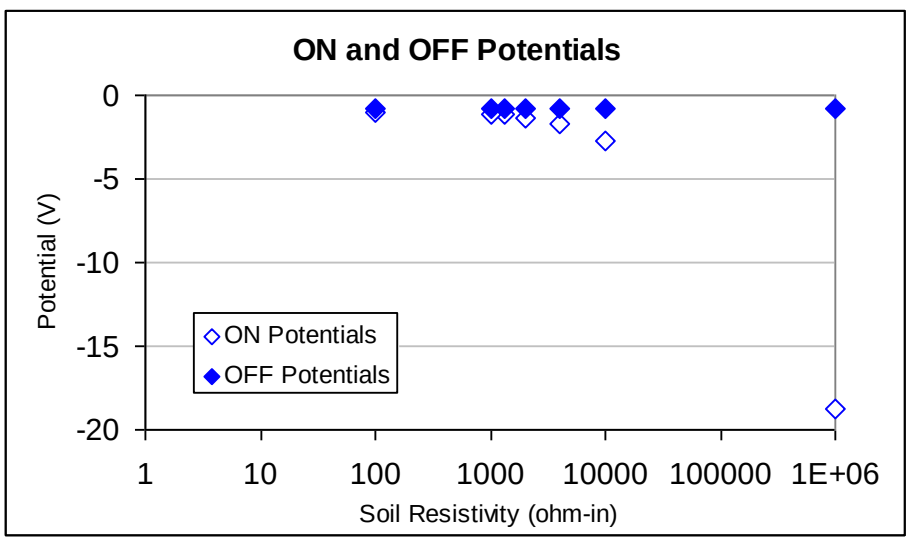

Figure 20. A plot of ON and OFF potentials as a function of soil resistivity

Figure 21 is a plot of the ON and OFF potentials for several of the test cases, in which the *pipe diameter* was changed. All other parameters were kept the same. The plot indicates that a *smaller* pipe diameter will tend to a *greater* difference between the two measured potentials. The difference is not as pronounced as the effect of soil resistivity, which was varied logarithmically and therefore led to a greater difference in potentials. It is important to note that the *depth to centerline* of these models was kept the same and so the *depth of cover* between grade and pipe surface varies. As above, the soil depth increases the resistance for a given current and leads to a higher potential difference.

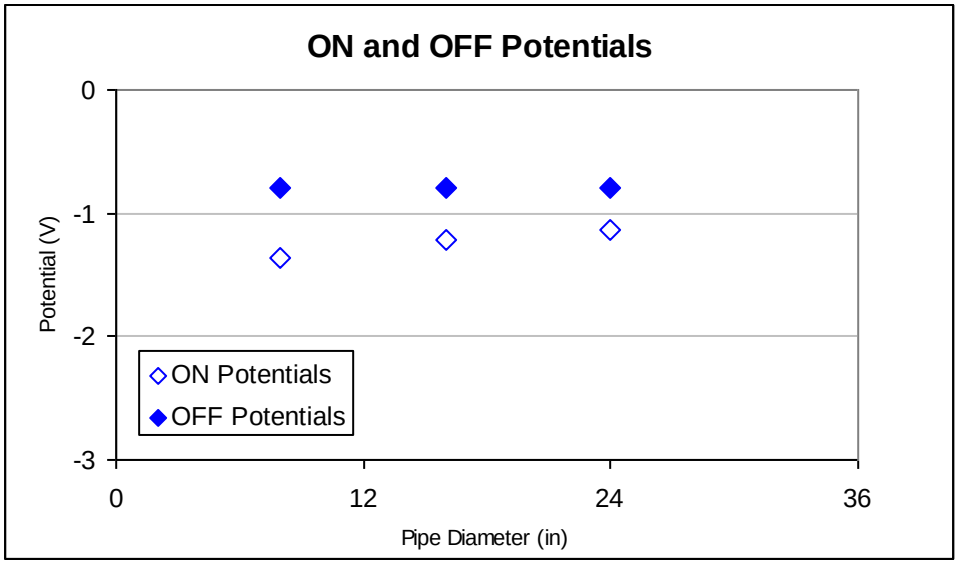

Figure 21. A plot of ON and OFF potentials as a function of pipe diameter

Figure 22 is a plot of the ON and OFF potentials as the depth of pipe centerline is changed. The plot indicates that a deeper buried pipe will tend to increase the difference between the two measured potentials. Note that the *pipeline diameter* was kept the *same* and so the *depth of cover* between grade and pipe surface *varies*. As above, the soil depth increases the resistance for a given current and support a higher potential difference. Figure 21 and Figure 22 demonstrate the same phenomenon, but by varying different geometric features. The result of both is a change in soil depth.

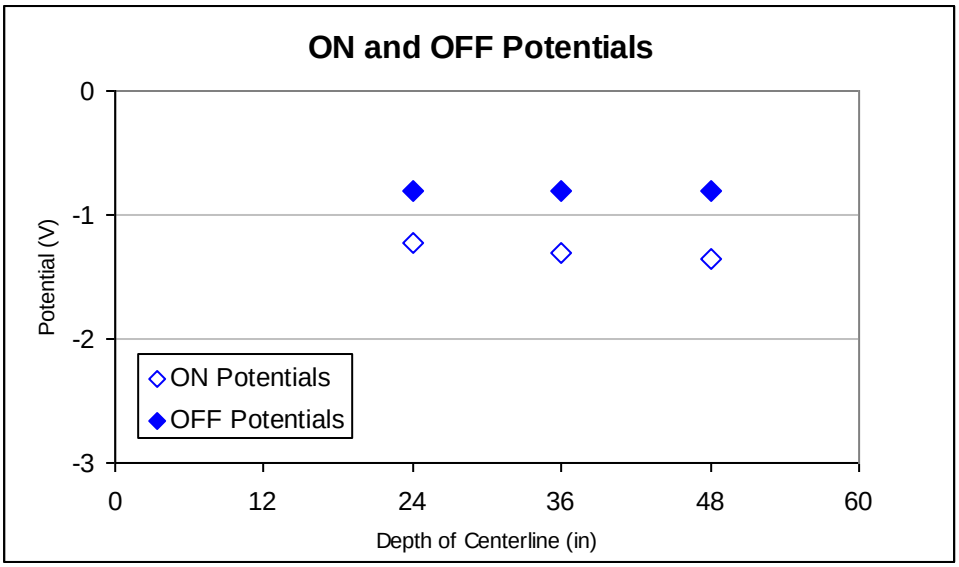

Figure 22. A plot of ON and OFF potentials as a function of depth of pipeline centerline.

Figure 23 is a plot of the ON and OFF potentials for two different coating potentials (treated in the model as the *potential of the coated pipe* outside of the anomaly). This plot represents a situation in which three measurable potentials are plotted. This plot is included to demonstrate that the ON potential, which was calculated by the finite element analysis from prescribed OFF and coating potentials, shows no variation with coating potential. This indicates that the ON potential is not necessarily influenced by the condition of the coating away from the defect. This particular observation correlates well with the prior art and the field observations – depending on the resistance (soil and defect geometry), the presence of an anomaly manifests itself in the CIS survey fairly when the surveyor is fairly close to the coating holiday.

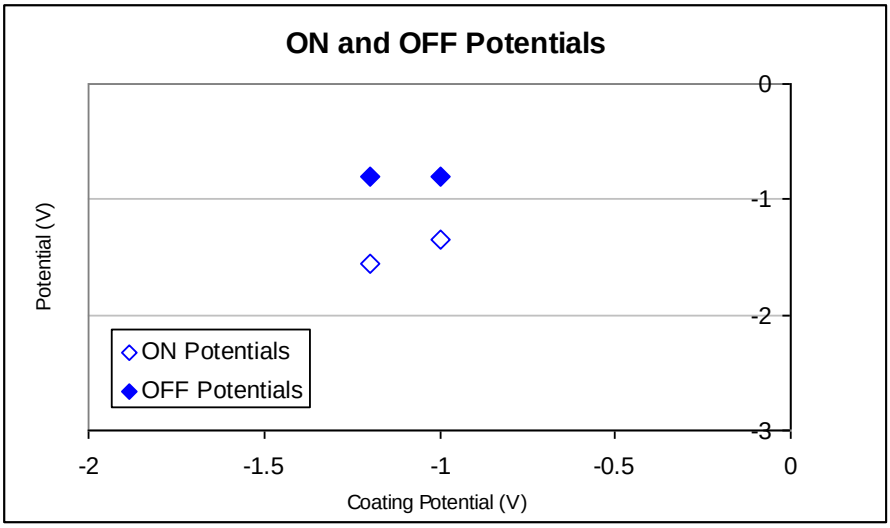

Figure 23. A plot of ON and OFF potentials as a function of coating potential.

Figure 24 is a plot of the ON and OFF potentials vs. the *defect orientation*. There is a negligible difference in the ON and OFF potentials as the defect location varies from 12 to 3 to 6 to 9 o'clock on the pipeline. This result is counter-intuitive. Given the IR drop arguments as described above, and the variability in soil depth of cover for defects at different locations, one would expect a difference in potentials to be seen. If there were a difference in potentials in this case, one would be able to locate the defects on the pipe circumferentially prior to digging. However, no difference is seen in the potentials that would allow this type of inference.

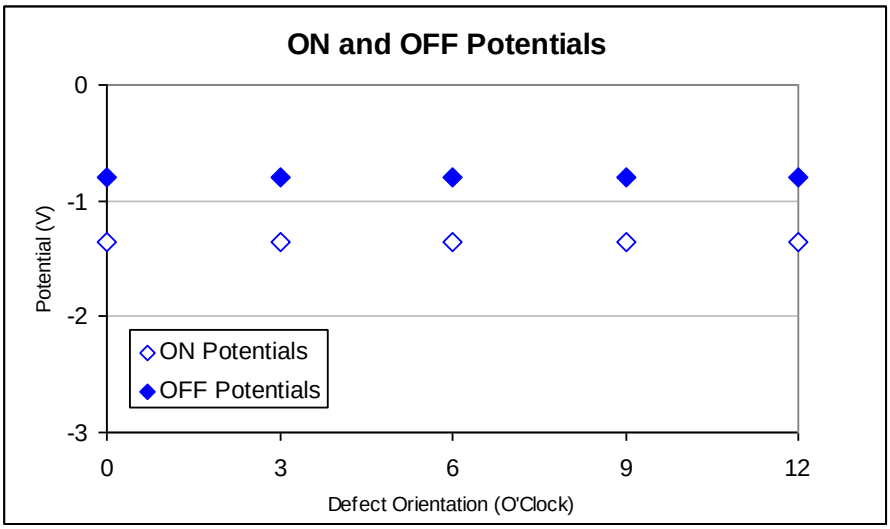

Figure 24. A plot of ON and OFF potentials as a function of defect orientation.

Effects of ON and OFF potential variations

Using the regression analysis formula, further semi-quantitative trend analysis is possible, particularly with regard to the effect of the holiday size on the combination of various ON and OFF potentials, which is the primary goal of the project.

Figure 25 summarizes the defect size as a function of varying OFF potential values and soil resistivity and a constant ON potential (also fixed are the pipeline diameter, depth of centerline, and coating potential, which is what one would expect for a CIS on a given pipeline segment). The CIS profile of this type is simulated by a sketch in the upper right corner (shape CN 3 or CN 4 from Table 1 on page 6).

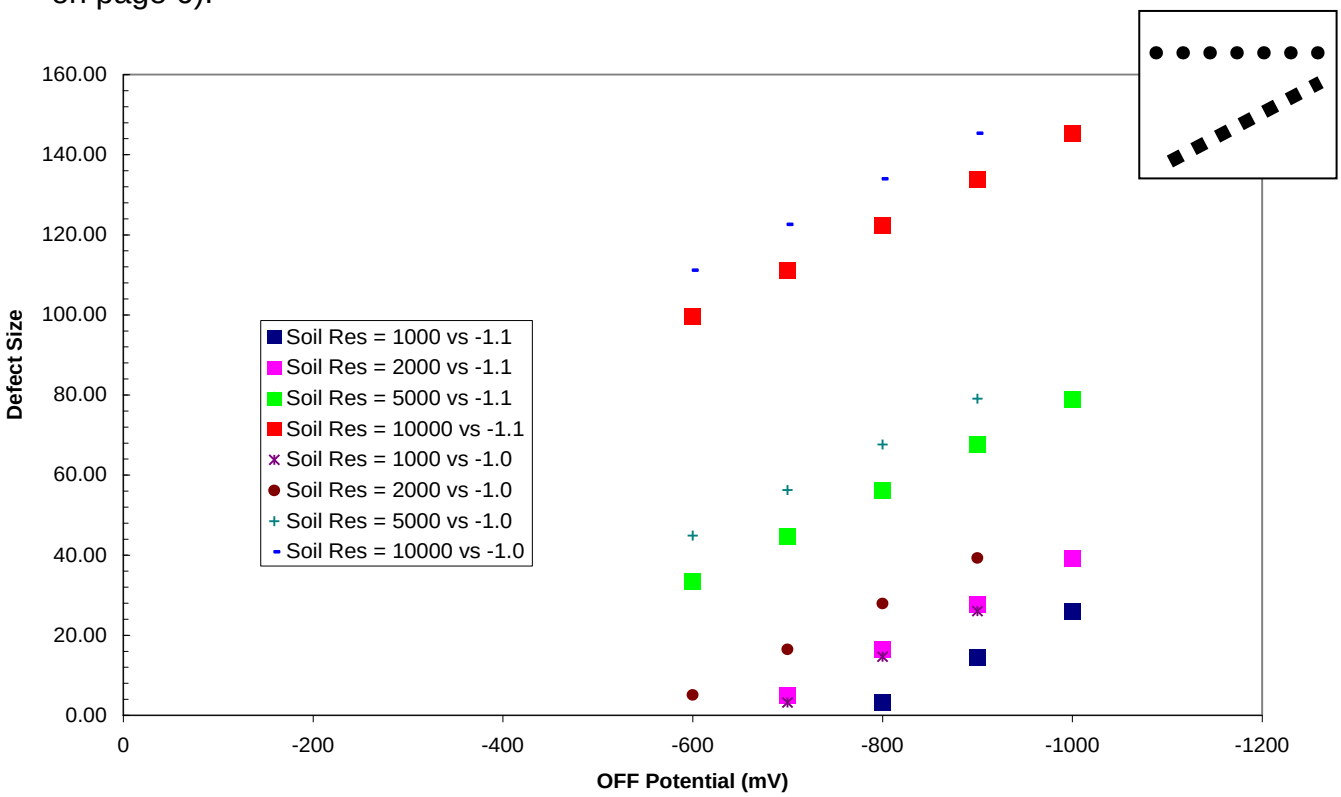

Figure 25. Plot of defect size vs. varying OFF and fixed ON potentials (at different soil resistivities). Two ON potentials (-1.1V and -1.0V) are used in the calculation. Inset shows the relationship between the ON and OFF potentials (circles and squares, respectively).

The analysis shows that as the gap between ON and OFF potentials closes (IR decreases), the defect size increases. This is consistent with the notion that the resistance associated with the defect geometry is inversely proportionate to the defect size (the larger the defect, the lower the geometry-related resistance).

Therefore, the data for the ON potential of -1V shows larger defect sizes than the data for the ON potential of -1.1V for the same OFF potential (even smaller IR drop). As the soil resistivity increases, for the same IR drop, the holiday size increases (to compensate for the same value of R, which is a composite number encompassing both the soil resistance and the resistance associated with the defect size).

The "inverse" of the above case – changing ON potentials while OFF potentials remain steady (shape CN 1 or CN 2) – is illustrated in Figure 26.

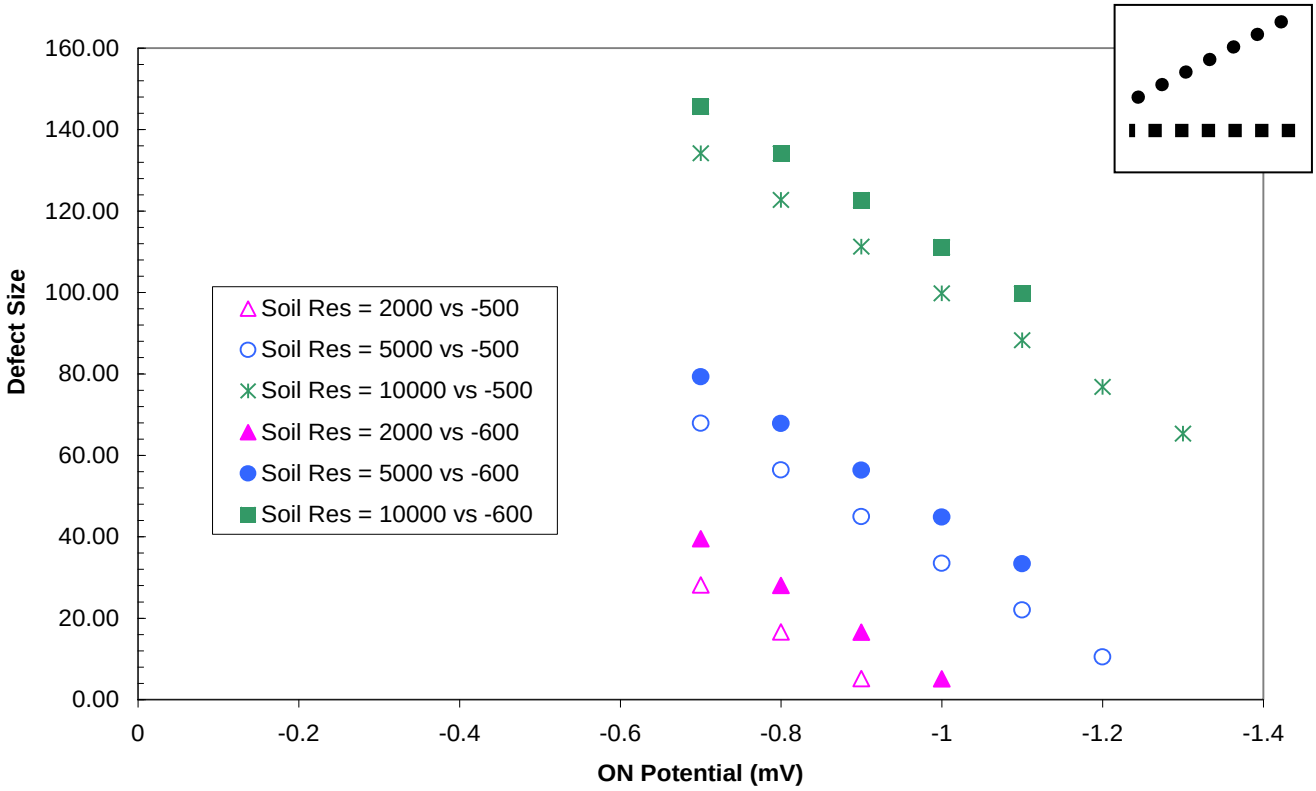

Figure 26. Plot of defect size vs. varying ON and fixed OFF potentials (at different soil resistivities). Two OFF potentials are used in the calculation (-500 mV and -600 mV). Inset shows the relationship between the ON and OFF potentials (circles and squares, respectively).

Similarly, the analysis shows that as the gap between ON and OFF potentials increases (and, consequently, IR increases as well), the defect size decreases. For the same soil resistivity, the data for the OFF potential of -600 mV shows larger defect sizes than the data for the OFF potential of -500 mV for the same ON potential (smaller IR drop). As in Figure 25, when the soil resistivity increases, for the same IR drop, the holiday size increases (to compensate for the

same value of R, which is a composite number encompassing both the soil resistance and the resistance associated with the defect size).

Forward (FEA) vs. reverse model (CP3D)

The reverse model that was selected for the purposes comparing the results to the forward model used in this research was developed by Orazem (see References 12 and 14 in the literature review on page 15). The CP3D model predicts a defect size as a function of soil resistivity, depth of cover, dips in ON- and OFF-potentials, and the total IR drop away from the indication.

A comparison of data provided by the finite-element-regression model developed throughout the course of this work and the CP3D model is shown in Figure 27.

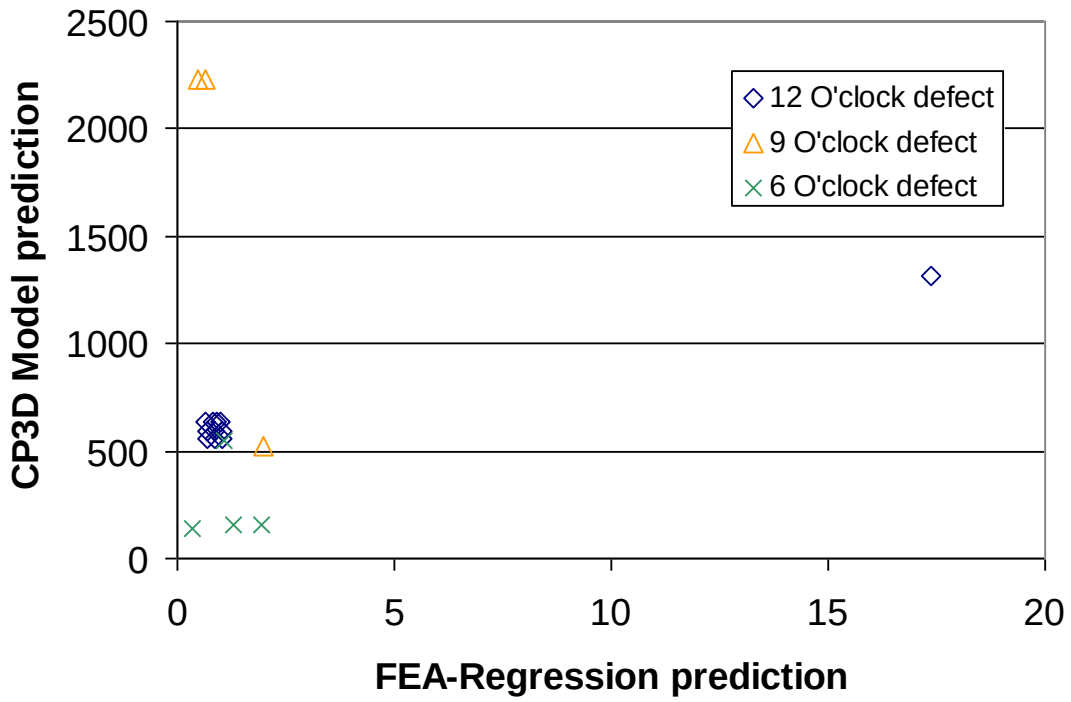

Figure 27. Comparison of results provided by the forward and reverse models.

The data from the preliminary series of 18 tests was selected for the comparison. These data cover a range of soil conductivities, depths of cover and ON- and OFF-potentials. These parameters were input to the CP3D model and predicted defect areas using the two techniques were plotted. Note that the CP3D model predicts defect size in square inches, whereas the finite-element-regression model is semi-quantitative and predicts defect size in equivalent number of nodes in the model. Although these measurement techniques are different, they should provide an indication as to whether or not the models are consistent.

Certain broad trends between the two model predictions are similar. Several examples of such trends are presented in Figure 28.

The trends show that for the same depth of cover and potential distribution, the holiday size scales linearly with soil resistivity (the greater the soil resistivity, the greater the defect to maintain the same IR drop). However, the soil resistivity effect, according to the model, is modest.

Likewise, as the depth of cover increases (as so does the overall impedance – keeping the soil resistivity the same), so does the defect size. In keeping with the same logic, the greater the IR drop, the smaller the defect size with all the other parameters remaining the same.

However, inspection of Figure 27 shows that there are some inconsistencies in the two models. There is a clustering of several data points, but there are also several outliers that imply fundamental differences in the two techniques. The two points on the upper left of the figure represent conditions in which the CP3D model predicts a very large defect, but the finite-element-regression model predicts a flaw size comparable to the others in the test matrix. These two data points are based on a larger ON/OFF potential difference (IR drop) than the other test cases.

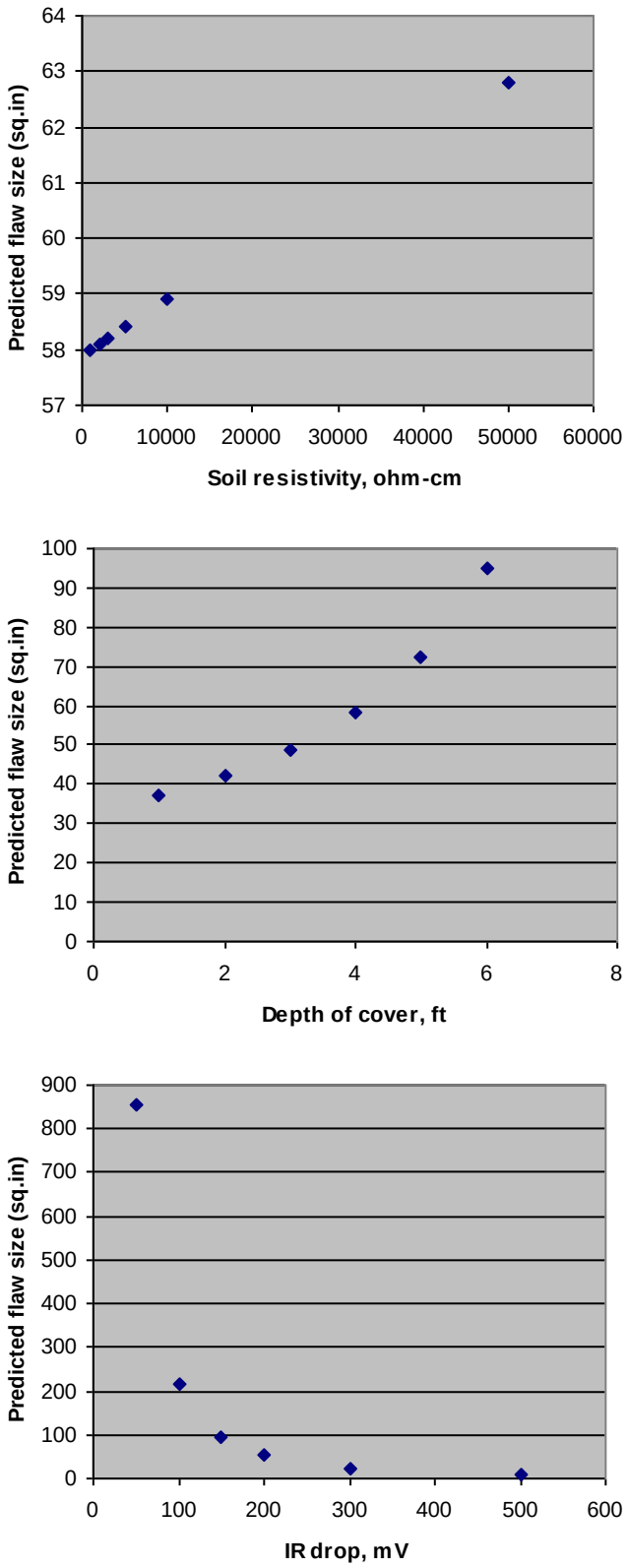

Figure 28.Predicted flaw size vs: soil resistivity (top), depth of cover (middle), IR drop away from the anomaly (bottom).

One point to the right of the figure represents conditions in which the finite-element-regression model predicts a defect that's larger than any of the others in the test matrix. This data point has higher soil conductivity than the other test cases. Three data points in the lower left of the figure represent conditions in which the Orazem model predicts a smaller defect size. These data points are based on test cases with either shallower depths of cover or lower conductivities.

It is clear from inspection of the data in the figure that there are differences in the defect size predictions provided by the two models. There does not appear to be a qualitative trend that might explain the differences. The work described above demonstrated that the trends in finite element results with the change in the various parameters followed physical expectations. This indicates the approach is generally sound.

One possible source of error is in the polarization behavior of the bare steel. Preliminary modeling took this into account. However, there were numerical difficulties associated with these models which could not be resolved. Specifying the ON- and OFF-potentials and disregarding the exponential nature of polarization behavior may have artificially influenced the calculated current density and potential gradient near the defect and skewed the calculated results. Unfortunately this cannot be easily verified, or corrected for, given the numerical difficulties encountered.

Numerical simulation conclusions

The results suggest that numerical model adequately described most of the first order effects between defect geometry, soil related parameters, and CP potentials. On the basis of the model-generated values, a regression analysis-derived relationship of the pipe/soil characteristics and ON potentials was established. The regression equation indicates that the impedance (soil resistivity and defect geometry) dominates the relationship, with the defect size being an important factor in determining the ON potential value for a given OFF potential.

However, the relationship between the at-grade potential measurements and the actual at-pipeline depth conditions is complex. On a real-life "macro" system, such as a buried pipeline, the modeling assumption that the holidays represent isolated breaches in an otherwise perfect external coating is not going to be universally applicable. There are variations of soil chemistries and soil particle sizes, which can be considerable even over a short distance along the pipe; these differences can affect not only the impedance characteristics of soil, but polarization behavior of the steel exposed through holidays.

Early attempts to include polarization behavior in the modeling were discontinued due to numerical difficulties encountered during modeling with constant current scenarios, and to achieve better control over the known or measurable potentials.

Further, the presence of multiple adjacent holidays or electrically conductive areas of the (aging) coating, as demonstrated by the experimental modeling, may produce a 'composite' ON/OFF CIS potential value, which, under certain circumstances, can obscure the actual CP potential of the least polarized holiday.

Given the complexity of such a relationship and the inevitably simplifying assumptions necessarily employed by any model, it is not entirely surprising that the results of the analysis are inconsistent in some aspects. Depth of cover and soil resistivity both affect the difference in ON and OFF potentials, and this can be explained in terms of the IR drop. The orientation of the defect does not seem to have an effect. One must consider further the nature of the IR drop between grade and pipe surface.

Figure 16 and Figure 18 demonstrated that the high potential gradient associated with the defect is highly localized. Inspection of the finite element output files indicates potential gradients near the defects in the order of 100's of mV per inch near the simulated defects.

The effect is greater in the high resistance soils. Given that the potential gradients are so highly localized near the defects, it is not reasonable to assume a simple mathematical relationship amongst depth of cover, soil resistivity and potential difference. In effect, the IR-drop calculations cannot assume a linear relation, and any conclusions drawn from a simple inspection of the data must be made with caution. The IR-drop arguments are inherently valid, but do not describe the *complete relationship* of the various parameters that affect the ON and OFF potentials.

With regard to the CIS shapes, the regression analysis shows that for some of the less-explainable shapes, such as CN1-2 or CN3-4, the change in the OFF potential to more negative values with the ON potential remaining the same may be indicative of coating condition equivalent to a series of defects of increasing sizes. Conversely, if the OFF potentials remain the same and the ON potentials increase, the worst of the coating conditions occur at the most positive of the ON potentials. In that sense, the results are in agreement with the intuitively expected – the lower the IR drop (the separation between ON and OFF lines), the larger the defect, and the more positive the combined ON and OFF potential values (it is after all, more difficult to protect larger holidays). In other words, it is very likely

that, if other conditions are fixed, the coating holiday is located at the spot of the most positive local potentials making up the CIS shape – which is traditionally assumed when analyzing CIS profiles.

The regression equation could be used to further refine the field data, as CIS will provide ON, OFF and coating potentials. The OFF and coating (pipe outside of the anomaly regions) potentials would have to be determined by recognizing variation in the OFF potentials. The OFF potential associated with a defect is expected to be more positive than the OFF potential associated with intact coating. The coating potential used for the above calculations would be taken as the "baseline", the more negative of the OFF potentials measured along a given length of pipe. The OFF potential associated with a defect would be taken as the most positive potential measured.

Task 2 – Field-based data collection and analysis

As described in the Work Plan, early in Task 2, it became apparent that the amount of data from direct examinations was not going to be sufficient not only to achieve statistically significant conclusions, but it also lacked the variety to cover all possible combinations of CIS profile shapes.

Considering the challenges associated with accumulating the necessary real-life data for analysis, in order to maximize the use of the available funds allocated to Task 2, it was decided that it would be preferable to change the type of data used for the analysis. Therefore, the chosen approach was to use inline inspection data from actual pipelines. The ILI data indicated the external corrosion damage, which was superimposed on the CIS profiles obtained from the inspected pipelines

Sourced data: type, limitations and assumptions

One of the challenges encountered during data search was the scarcity of the information relevant to the goals of the project. The primary obstacle was the availability of the survey data (CIS) collected from the buried lines that also had sufficient number of coating and corrosion damage data. Since the External Corrosion Direct Assessment (ECDA) protocol is traditionally employed as an alternative assessment technique for underground pipelines that cannot easily be assessed by other means (such as inline inspection (ILI)), the coating and corrosion-related data could only be found in the direct examination (dig) reports. Given the substantial cost of digs, the number of excavated locations is limited to those necessary to comply with the ECDA process.

Therefore, although CIS surveys are common and the data is readily available, it is the scarcity of the dig reports that limits the amount of data that can be used for the analysis of the CIS profile patterns and associated corrosion and coating damage. For example, a two-mile segment evaluated by the co-funding agency using ECDA was found to contain multiple potential anomaly indications; of these, 10 were selected for dig inspections. While the number of digs from the standpoint of ECDA process is high, it insufficient for a statistical analysis. Further (and perhaps even more limiting) complication is that the digs are conducted in the locations that are of the primary interest to the pipeline operator (typically, areas out of compliance with the CP protection criteria); some of the less common ON/OFF potential combinations are frequently not expected to have any corrosion associated with them and, as such, would not be excavated as the costs of exploratory digs would be prohibitive.

In order to accomplish the project objectives, a decision was made to use a different source of data – inline inspections results from the pipelines surveyed by CIS. Due to the same reasons (difficult to find combinations of ILI-inspected lines with CIS), the ILI/CIS combination, while providing a larger array of data, suffered from the similar limitation with regard to the desired variety of CIS conditions that had corrosion anomalies (ILI calls). Some of these limitations are the result of the fact that most of the underground structures are adequately protected by cathodic protection and corrosion damage is mitigated, thus restricting the number of anomalies with coating damage but little or no corrosion attack (shallow attack below the limit that can be detected by ILI). From the practical standpoint, the latter limitation may not be regarded as important (low or no immediate risk to pipeline integrity), however, it affects the accuracy of the analysis.

The data used for the statistical analysis came from the total of 593 miles of pipelines with CIS and inline inspection data. The total number of ILI calls (corrosion anomalies) was 252. It was assumed that the ILI tool was accurate in making the determination about the size (area) of the corrosion damage (metal loss). In reality, the ILI tools are generally accurate 80% of the time to within 10% of the detected anomaly size. The minimal depth of corrosion detectable by an intelligent tool is typically about 10% with a 90% probability of detection; therefore, some superficial corrosion (and associated coating holidays) may have been overlooked by the pig and are subsequently undercounted in the analysis.

Methodology of Shape selection

Given the objective of the project, the CIS data was evaluated to determine the correlation between the CIS profile and corrosion damage. In addition to the ILI

data, the CIS profile was attempted to be linked to characteristics of the soil surrounding the pipe (soil data obtained from National Resource Conservation Service (NRCS)). The CIS and ILI data was first aligned and overlayed; next the CIS profile was analyzed for the distinct patterns to identify all possible ON/OFF potential combination (curve shapes).

Acquiring Data

Close interval survey, ILI inspection and soil data were acquired for six separate steel underground natural gas transmission pipelines from around the continental United States. The characteristics of the pipelines varied greatly by steel grade, wall thickness, and coating type. The diameters varied from 6” outside diameter (OD) pipe to 26” OD pipe, providing a balanced sample distribution.

The three types of data used in this investigation were acquired from three different outside sources. The CIS and ILI inspections were conducted by independent groups who performed the surveys according to established processes and guidelines. These data sets were finalized by the survey-conducting companies who then gave them to their client.

GPS data collected from the pipeline operator was used to identify the areas of land that are traversed by the pipeline. Soil properties for these areas were gathered from the NRCS soil database resulting in up to an 80 ft data resolution. This database contains soil information which is grouped into soil “polygons”. Each polygon contains up to six separate components, where the dominant component is identified. A component is a portion or area of the soil polygon; there can be up to six distinct areas reported for the same soil polygon.

Data for each soil horizon included aggregated or averaged data over the entire soil polygon (polygon data), general data for each component (component data), and specific data for the dominant component (dominant-component data).

Soil characteristics were chosen based on their expected effect on cathodic protection and pipe-to-soil potential readings. These characteristics included:

- Electrical conductivity (Number of cations absorbed)
- Salinity (Milliohms per centimeter)
- pH
- Amount of organic mater found in the soil (%)
- Amount of sand comprising the soil (%)
- Amount of silt comprising the soil (%)
- Amount of clay comprising the soil (%)

Data Alignment

Prior to identification of CIS shapes, CIS, ILI, and soils data were aligned to a common metric. The first step in this process is to identify tie points in both the CIS and ILI data sets that could be used to align these data sets to a list of pipeline features and GPS points, with known stationing, obtained from the pipeline operator. Once the list of tie points is compiled, the data sets are adjusted accordingly. The soils data did not require further alignment because they were obtained using known GPS points with known stationing. An example of the resulting overlaid data can be seen below in Figure 29.

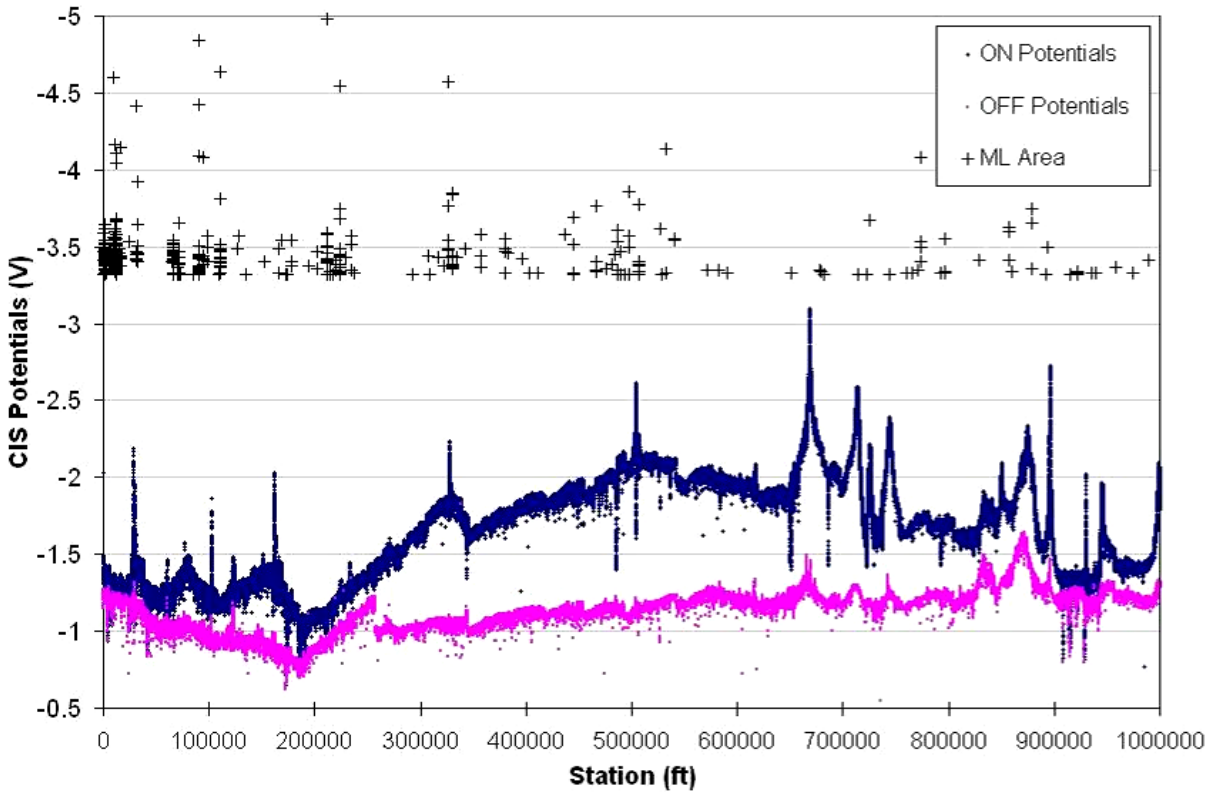

Figure 29. Overlaid CIS potentials and ILI metal loss data

Shape Selection

A catalogue of all possible CIS scenarios was developed and is reproduced again in Table 5 The two lines (top and bottom) making up each shape represent the CIS ON potential readings (top) and OFF potential readings (bottom). For example, Catalogue Number (CN) 1 represents the situation when the ON potentials remain relatively flat and the OFF potentials over the same area exhibit

a ‘dip’. It is understood that certain combinations (particularly CN8 and CN9 are not likely to be encountered as frequently as others (such as CN 5 or CN6).

Table 5. Possible CIS Shapes

Catalogue Number	1	2	3	4	5	6	7	8	9
On Potentials Off Potentials **Shape**									

The six pipeline segments used for this study correspond to a total length of 593 miles. For each line segment, the aligned CIS and external metal loss area from the ILI run was overlaid (plotted) in Microsoft Excel®. The entire line length was incrementally stepped through to identify the CIS shapes that corresponded with external metal loss area. Once a shape was identified as being associated with metal loss, specific information was recorded about the shape area.

The CIS stationing and potential readings were documented for the start, middle, and end of each shape for both the ON and OFF potential data. The start and stop points for each shape were chosen as the locations immediately before and after a shape. The distance between these points (the shape length), varied greatly and depended on the extent of the shape. The “middle” point was selected based on the shape (generally an apex) and did not necessarily correspond to the halfway point between the start and finish stationing.

For every selected shape, the attempt was made to capture the entire extent of the shape. This resulted in shapes of various sizes being selected. The smallest a shape could be was three consecutive potential data points in a row, while the length of the largest could be quite extensive. The CIS profile spacing between the two adjacent potential readings was different for the different pipelines, resulting in a minimum and maximum *shape length* of 5 and 600 feet, respectively. In addition to the shape length, the ‘depths/heights’ (the potential difference between the lowest and the highest values) also varied. However, as indicated in Table 1, the primary selection criterion for assigning the catalogue number to a shape was the potential-vs.-distance trend of ON/OFF potential. An example of the shapes belonging to the same catalogue number despite the differences in length and depth is shown below.

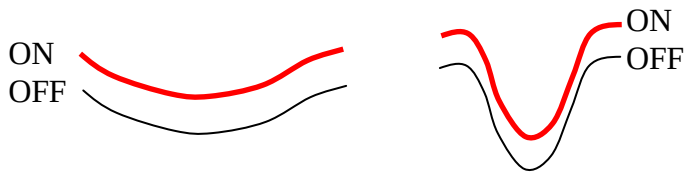

Figure 30. Example of two shapes belonging to the same catalogue number (CN 5).

Figure 31 to Figure 39 show examples for each of the shapes making up the catalogue. Identified on the plots are the extents of the shape.

Also recorded was the cumulative amount of external metal loss area in the section of the pipeline confined by the CIS shape (also demonstrated in Figure 31 to Figure 39). The recorded external metal loss features were identified by the ILI tool vendor as general corrosion, pitting, or axial or circumferential grooving. Metal loss depths varied from 1 to 88% of the wall thickness, though the average metal loss depth was 13%. The metal loss area of an individual anomaly varied from 0.123 in^2 to 193 in^2 with an average metal loss area of 3 in^2. Vertical lines denoted 1, 2, and 3 in the lower graphs in each Figure indicate the beginning, the middle, and the end stationing for each shape.

In addition, each identified shape was associated with the soil data characterizing the vicinity conditions. Soil data at both the pipe depth (assumed to be 36”) and average data from the pipe depth to the surface was obtained.

Task 3 – Computational modeling using field data

Correlation between CIS shapes and corrosion

From this investigation a total of 74 separate variables were identified for use in the statistical evaluation. Many of these variables represented mathematical combinations of the original data sets. Given that each catalogue number encompasses shapes of varying sizes (both laterally – chainage and vertically – potentials) and, further, the shapes are associated with different potential levels (e.g., the same shape can be found either above or below CP protection criterion of -850mV (CSE)), another, composite variables were created to capture these differences for the analysis. Thus, to account for the differences in the shapes with the same catalogue number (see Figure 30 for the illustration), the shape ‘area’ (the product of the shape length and shape depth/height) was introduced.

CN 1

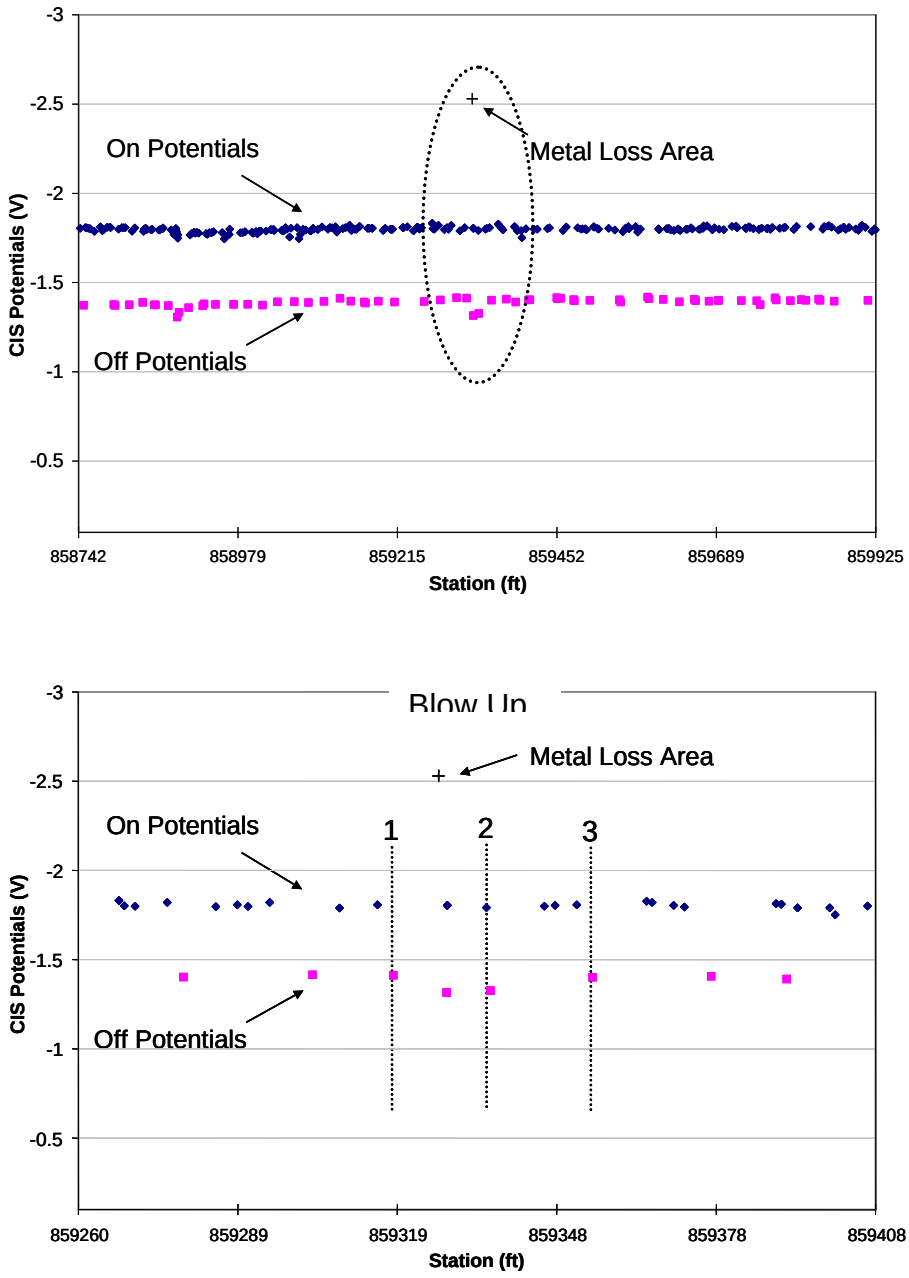

Figure 31. Shape CN1. Lower graph shows expanded view of the encircled area in the upper graph.

CN 2

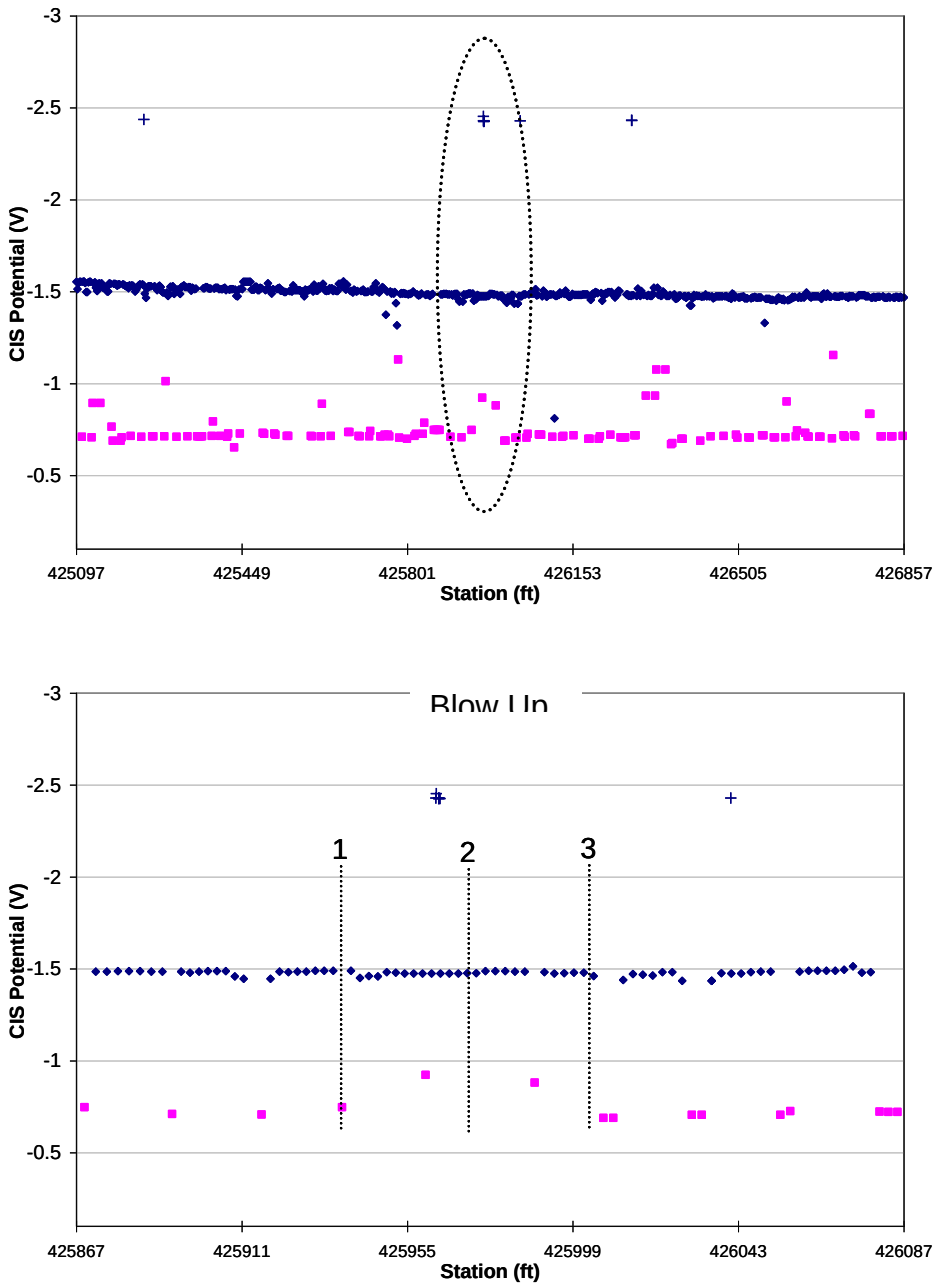

Figure 32. Shape CN2. Lower graph shows expanded view of the encircled area in the upper graph.

CN 3

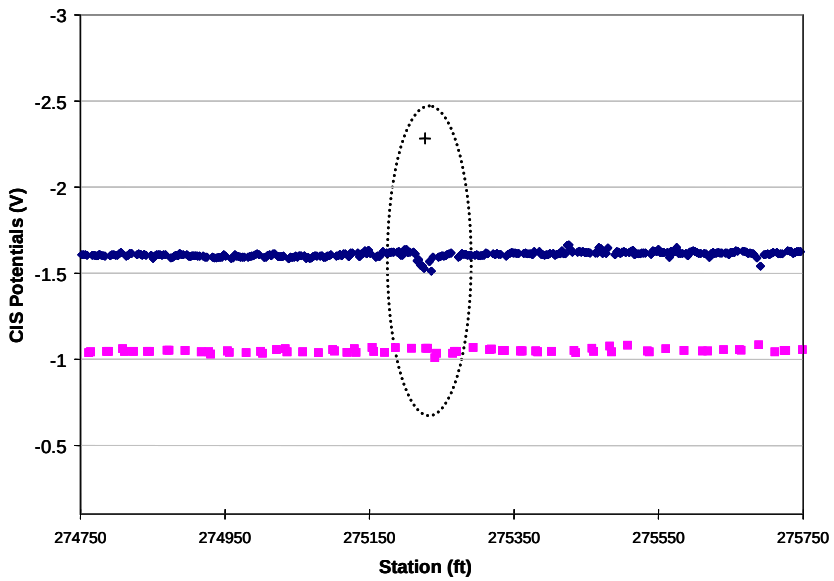

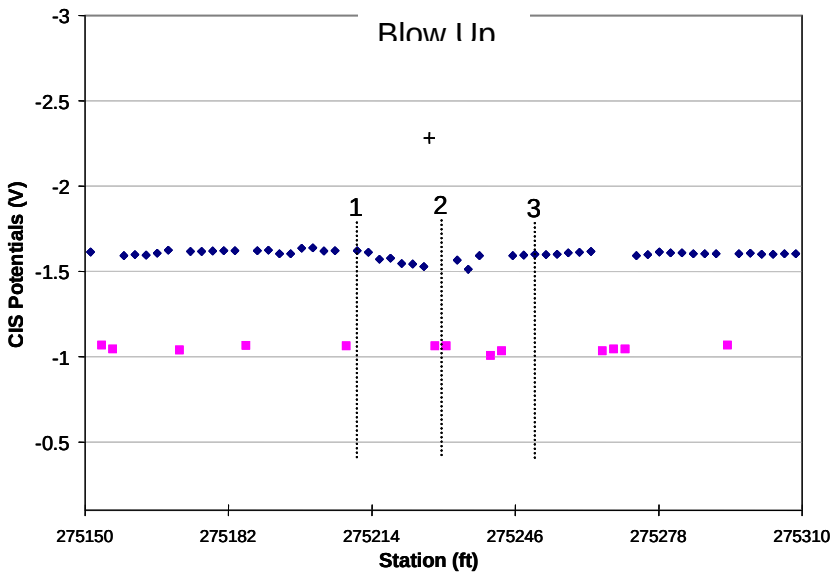

Figure 33. Shape CN3. Lower graph shows expanded view of the encircled area in the upper graph.

CN 4

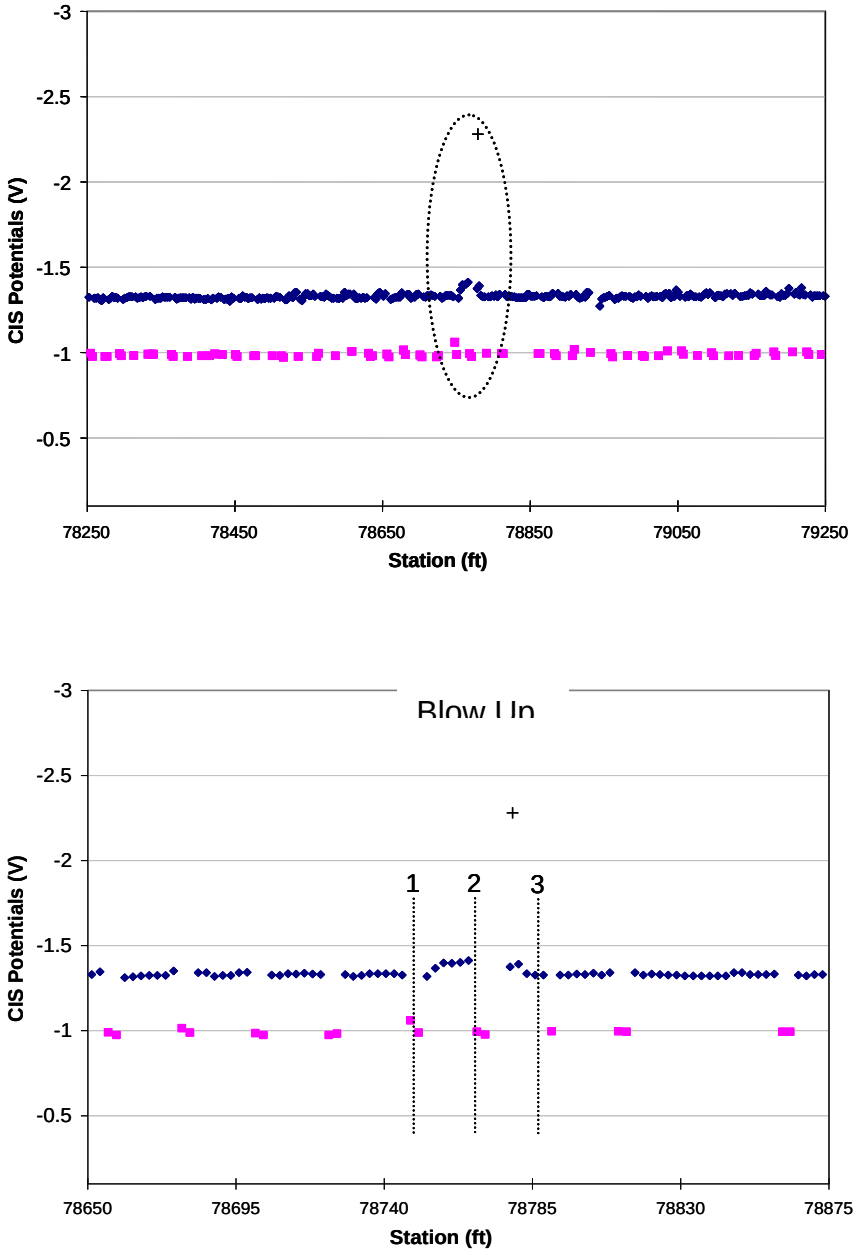

Figure 34. Shape CN4. Lower graph shows expanded view of the encircled area in the upper graph.

CN 5

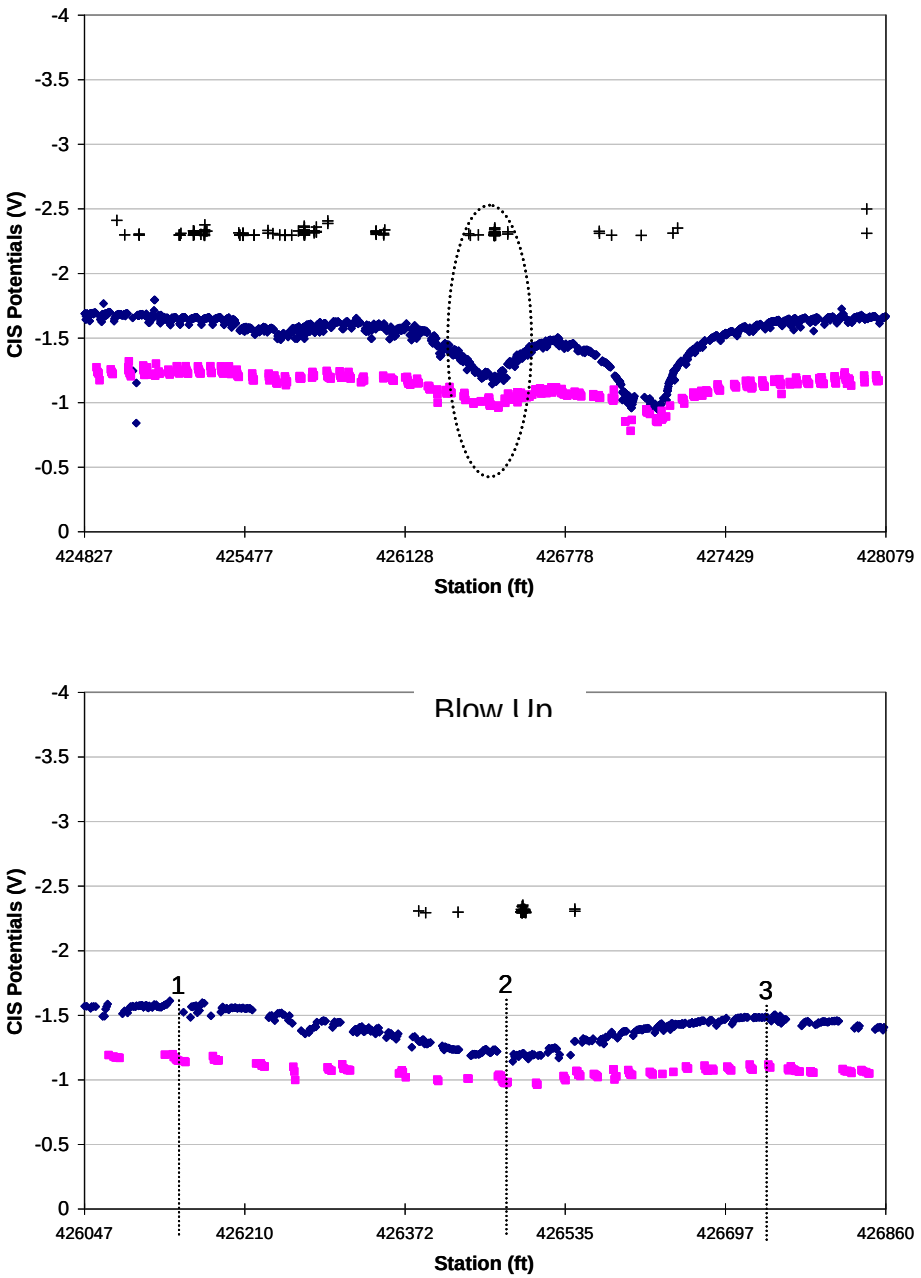

Figure 35. Shape CN5. Lower graph shows expanded view of the encircled area in the upper graph.

CN 6

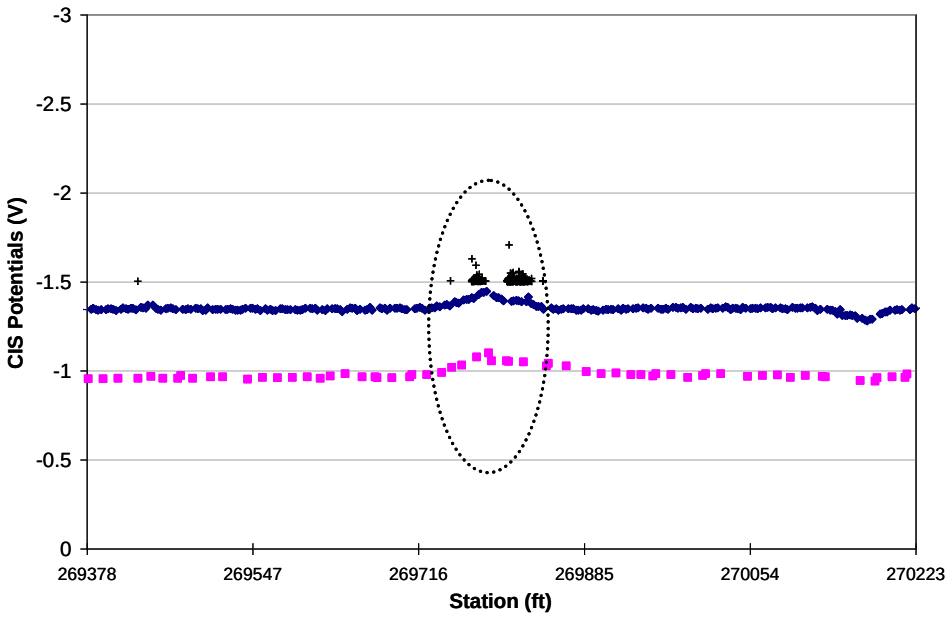

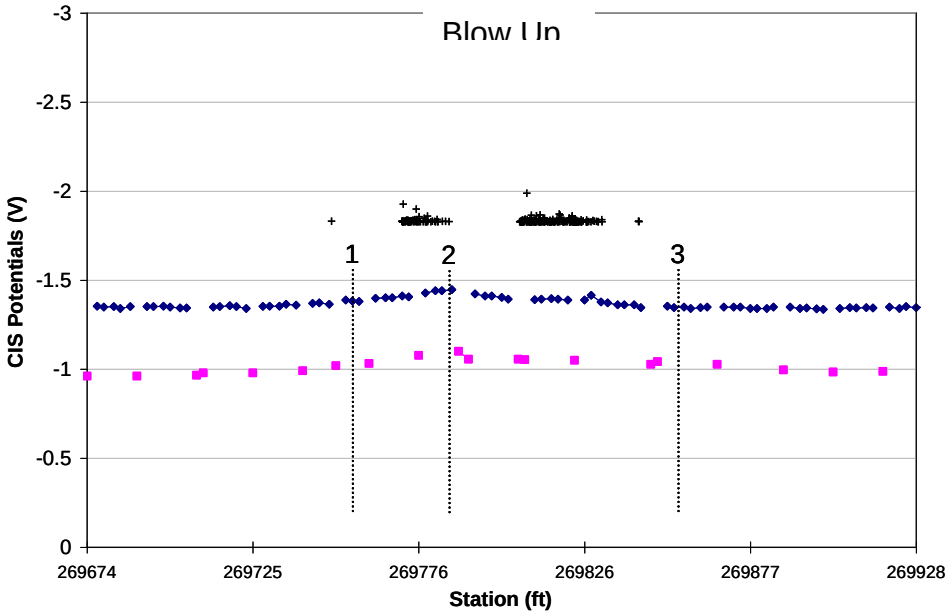

Figure 36. Shape CN6. Lower graph shows expanded view of the encircled area in the upper graph.

CN 7

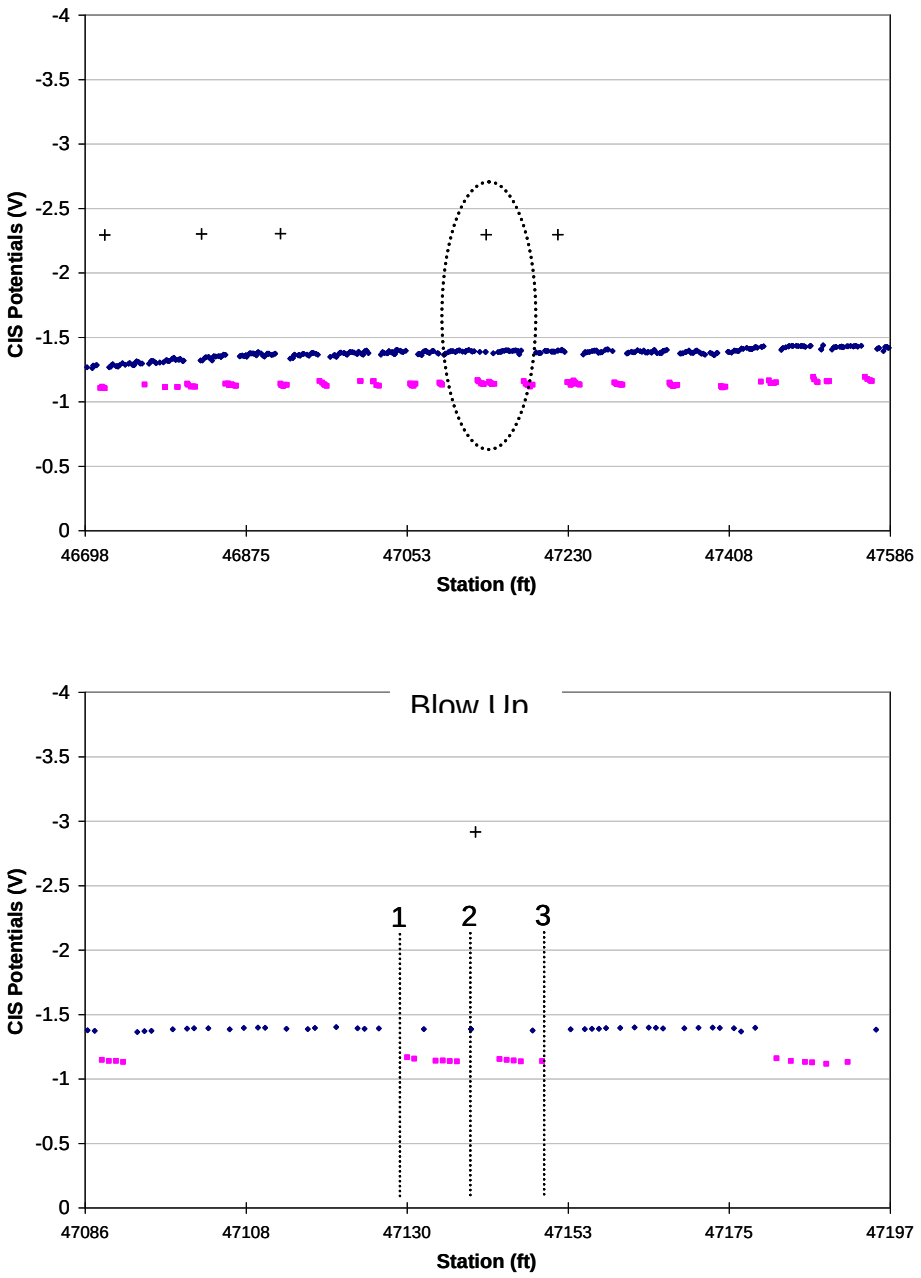

Figure 37. Shape CN7. Lower graph shows expanded view of the encircled area in the upper graph.

CN 8

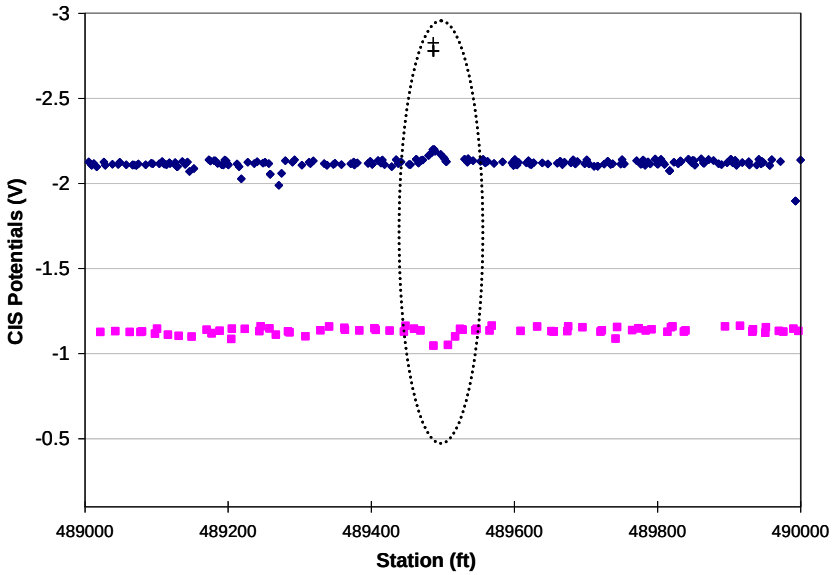

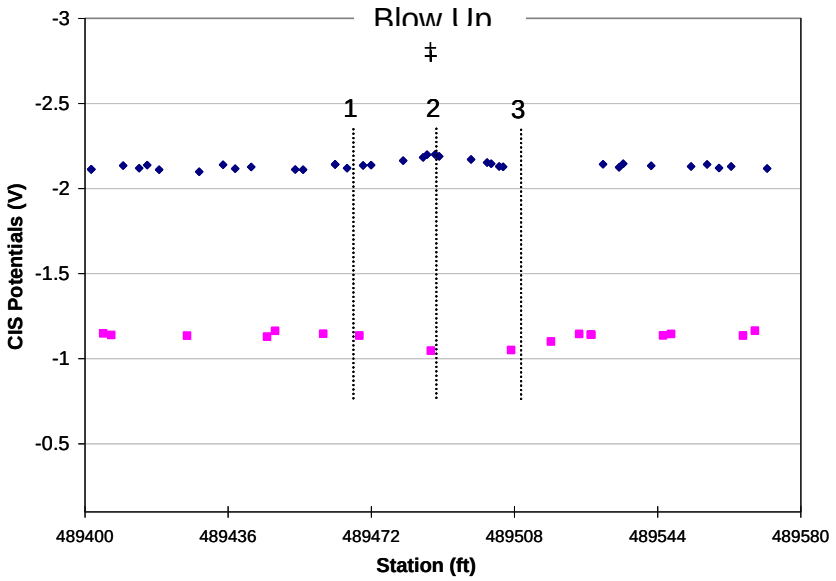

Figure 38. Shape CN8. Lower graph shows expanded view of the encircled area in the upper graph.

CN 9

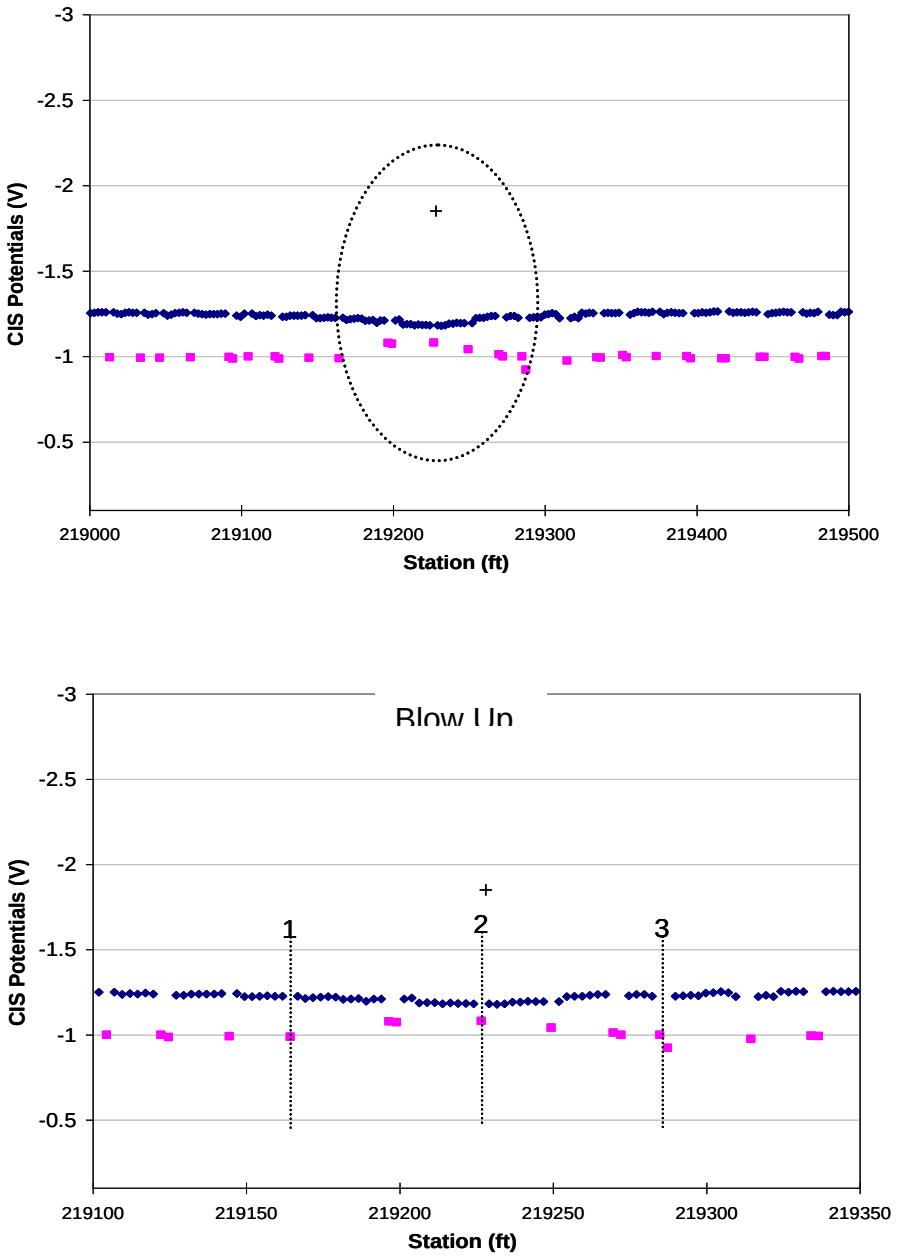

Figure 39. Shape CN9. Lower graph shows expanded view of the encircled area in the upper graph.

To capture the position of the shape with regard to the CP protection criterion, another variable was used – the product of the shape area and the least negative potential value associated with the shape. The case of two shapes in the same CN category but in different potential 'zones' is illustrated in Figure 40.

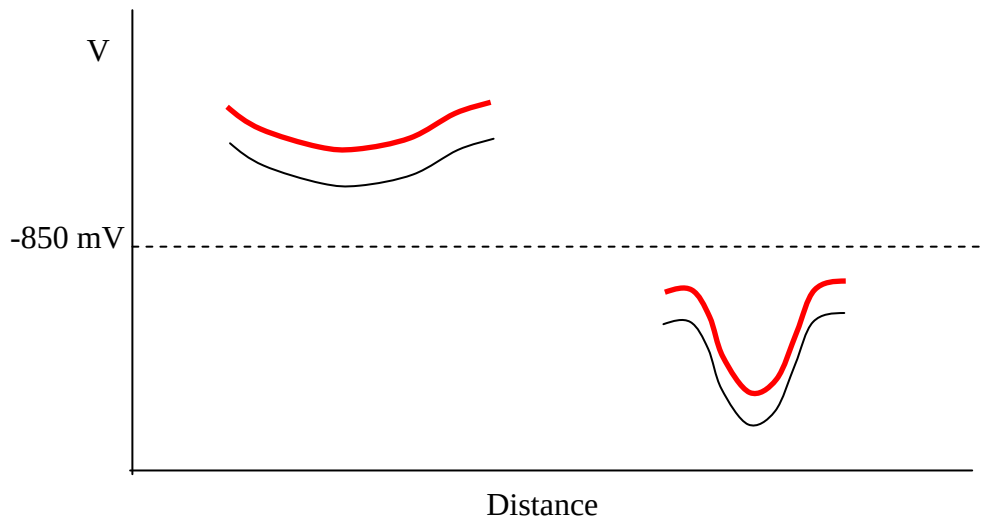

Figure 40. Two shapes belonging to the same catalogue number (CN5), but falling into two different potential 'zones' with respect to the -850mV CP protection criterion.

Considering that the product of the area and potential values involves three values, there may be incidences when the product of a × b × C is the same as a × B × c. The values of potentials were entered in V, and the values of distance were entered in feet.

A complete list of the variables and their definitions can be found in Table 6.

Table 6. List of variables identified in the investigation

	Variable Name	Description
1	First Point On (Chainage)	The chainage of the first (from left to right) on potential point selected
2	First Point On (Potential)	The pipe-to-soil potential reading of the first (from left to right) on potential point selected
3	Second Point On (Chainage)	The chainage of the second (from left to right) on potential point selected
4	Second Point On (Potential)	The pipe-to-soil potential reading of the second (from left to right) on potential point selected
5	Third Point On (Chainage)	The chainage of the third (from left to right) on potential point selected
6	Third Point On (Potential)	The pipe-to-soil potential reading of the third (from left to right) on potential point selected
7	First Point Off (Chainage)	The chainage of the first (from left to right) off potential point selected
8	First Point Off (Potential)	The pipe-to-soil potential reading of the first (from left to right) off potential point selected
9	Second Point Off (Chainage)	The chainage of the second (from left to right) off potential point selected
10	Second Point Off (Potential)	The pipe-to-soil potential reading of the second (from left to right) off potential point selected
11	Third Point Off (Chainage)	The chainage of the third (from left to right) off potential point selected
12	Third Point Off (Potential)	The pipe-to-soil potential reading of the third (from left to right) off potential point selected
13	Shape Length (ft)	Distance (in feet) between the first and last point chainages
14	Magnitude of 1st to 2nd Change (ON)	Difference (in mV) between the first and second points On potentials - absolute value
15	Magnitude of 2nd to 3rd Change (ON)	Difference (in mV) between the second and third points On potentials - absolute value
16	% Change for 1st to 2nd Change (ON)	Difference (in %) between the first and second points On potentials - absolute value
17	% Change for 2nd to 3rd Change (ON)	Difference (in %) between the second and third points On potentials - absolute value
18	First Point On (Potential)_Dev from 850(mv)	Difference (in mV) between the first point On potential reading and the 850 mV criterion
19	Second Point On (Potential)_Dev from 850(mv)	Difference (in mV) between the second point On potential reading and the 850 mV criterion
20	Third Point On (Potential)_Dev from 850(mv)	Difference (in mV) between the third point On potential reading and the 850 mV criterion
21	Slope of 1st to 2nd Change (ON)	Slope of the line connecting the first and second On potential points
22	ABS Slope of 1st to 2nd Change (ON)	Absolute Value of the slope of the line connecting the first and second On potential points
23	Slope of 2nd to 3rd Change (ON)	Slope of the line connecting the second and third On potential points
24	ABS Slope of 2nd to 3rd Change (ON)	Absolute Value of the slope of the line connecting the second and third On potential points
25	Magnitude of 1st to 2nd Change (OFF)	Difference (in mV) between the first and second points Off potentials - absolute value

	Variable Name	Description
26	Magnitude of 2nd to 3rd Change (OFF)	Difference (in mV) between the second and third points Off potentials - absolute value
27	% Change for 1st to 2nd Change (OFF)	Difference (in %) between the first and second points Off potentials - absolute value
28	% Change for 2nd to 3rd Change (OFF)	Difference (in %) between the second and third points Off potentials - absolute value
29	First Point Off (Potential)_Dev from 850(mv)	Difference (in mV) between the first point Off potential reading and the 850 mV criterion
30	Second Point Off (Potential)_Dev from 850(mv)	Difference (in mV) between the second point Off potential reading and the 850 mV criterion
31	Third Point Off (Potential)_Dev from 850(mv)	Difference (in mV) between the third point Off potential reading and the 850 mV criterion
32	Slope of 1st to 2nd Change (OFF)	Slope of the line connecting the first and second Off potential points
33	ABS Slope of 1st to 2nd Change (OFF)	Absolute Value of the slope of the line connecting the first and second Off potential points
34	Slope of 2nd to 3rd Change (OFF)	Slope of the line connecting the second and third Off potential points
35	ABS Slope of 2nd to 3rd Change (OFF)	Absolute Value of the slope of the line connecting the second and third Off potential points
36	Shape Area_Ons	The area of the triangle defined by the first, second, and third points selected for the On potentials
37	Shape Area_Offs	The area of the triangle defined by the first, second, and third points selected for the Off potentials
38	Least Negative Potential_Ons Absolute Value	The least negative On potential point selected - absolute value
	Least Negative Potential_Offs Absolute Value	The least negative Off potential point selected - absolute value
39	Area x Slope_Ons	The area identified for the On potential shape multiplied by the slope from the first and second On potential points
40	Area x Slope_Offs	The area identified for the Off potential shape multiplied by the slope from the first and second Off potential points
41	Area x Potential mag_Ons	The area identified for the On potential shape multiplied by the least negative On potential point selected
42	Area x Potential mag_Offs	The area identified for the Off potential shape multiplied by the least negative Off potential point selected
43	Slope x Potential mag_Ons	The slope from the first and second On potential points multiplied by the least negative On potential point selected
44	Slope x Potential mag_Offs	The slope from the first and second Off potential points multiplied by the least negative Off potential point selected
45	Area x Slope x Potential mag_Ons	The area identified for the On potential shape multiplied by the slope from the first and second On potential points and the least negative On potential point selected
46	Area x Slope x Potential mag_Offs	The area identified for the Off potential shape multiplied by the slope from the first and second Off potential points and the least negative Off potential point selected
47	Area x Slope_Direction x Potential mag_Ons	The area identified for the On potential shape multiplied by the direction of the slope (1 or -1) from the first and second On potential points and the least negative On potential point selected

	Variable Name	Description
48	Area x Slope_Direction x Potential mag_Offs	The area identified for the Off potential shape multiplied by the direction of the slope (1 or -1) from the first and second Off potential points and the least negative Off potential point selected
49	ln ML* Area_On	The natural log of the cumulative metal loss corresponding with the On potential shape multiplied by the area of the shape
50	ln ML *Area_Off	The natural log of the cumulative metal loss corresponding with the Off potential shape multiplied by the area of the shape
51	ln ML * Area * Slope *Potentials_On	The natural log of the cumulative metal loss corresponding with the shape multiplied by the area of the shape, the slope of the first and second points, and the least negative On potential value
52	ln ML * Area * Slope *Potentials_Off	The natural log of the cumulative metal loss corresponding with the shape multiplied by the area of the shape, the slope of the first and second points, and the least negative Off potential value
53	ln ML / Total Shape Area	The natural log of the cumulative metal loss divided by the combined area of the two shapes (On and Off potentials)
54	ML / Total Shape Area	The cumulative metal loss divided by the combined area of the two shapes (On and Off potentials)
55	Total Shape Area * min dist from 850* max slope	The combined area of the two shapes (On and Off potentials) multiplied by the minimum distance that either of the shapes are from the 850 mV criterion and the maximum slope value from either shape (On or Off potentials)
56	Scaled Metal Loss	The cumulative metal loss multiplied by: the combined shape areas (On and Off potentials), the minimum distance that either of the shapes are from the 850 mV criterion, and the maximum slope value from either shape (On or Off potentials)
57	LNScaledML	The natural log of the cumulative metal loss multiplied by: the combined shape areas (On and Off potentials), the minimum distance that either of the shapes are from the 850 mV criterion, and the maximum slope value from either shape (On or Off potentials)
58	Scaled Metal Loss * Least negative potential	The cumulative metal loss multiplied by: the combined shape areas (On and Off potentials), the minimum distance that either of the shapes are from the 850 mV criterion - squared, and the maximum slope value from either shape (On or Off potentials)
59	Approximate Associated ML Area [sq.in.]	The cumulative metal loss corresponding to the location of the shape (On and Off potentials)

Table 7 below lists the soil-related variables used to characterize the conditions in the proximity of each of the shapes associated with the metal loss and selected for statistical processing.

Table 7. Soil variables characterizing conditions in the vicinity of metal loss anomalies.

60	Electrical Conductivity (Number of cations absorbed) at pipe	The electrical conductivity measurement taken at the pipe depth (assumed to be 36")
61	Electrical Conductivity (Number of cations absorbed) ave	The average of the electrical conductivity measurements taken from the pipe depth to the surface
62	Salinity (Milimhos per centimeter) at pipe	The soil salinity measurement taken at the pipe depth (assumed to be 36")
63	Salinity (Milimhos per centimeter) ave	The average of the soil salinity measurements taken from the pipe depth to the surface
64	pH at pipe	The soil pH measurement taken at the pipe depth (assumed to be 36")
65	pH ave	The average of the soil pH measurements taken from the pipe depth to the surface
66	Organic Material Content (%) at pipe	The amount (in %) of organic material found at the pipe depth (assumed to be 36")
67	Organic Material Content (%) ave	The average amount (in %) of organic material found from the pipe depth to the surface
68	Sand (%) @pipe	The amount (in %) of sand making up the soil found at the pipe depth (assumed to be 36")
69	Sand (%) ave	The average amount (in %) of sand making up the soil found from the pipe depth to the surface
70	Silt(%) @pipe	The amount (in %) of silt making up the soil found at the pipe depth (assumed to be 36")
71	Silt(%) ave	The average amount (in %) of silt making up the soil found from the pipe depth to the surface
72	Clay(%) at pipe	The amount (in %) of clay making up the soil found at the pipe depth (assumed to be 36")
73	Clay(%) ave	The average amount (in %) of clay making up the soil found from the pipe depth to the surface

After the original incremental evaluation of each pipeline section, the pipeline CIS profiles were once again incrementally stepped through, this time to identify areas containing the catalogued CIS shapes that were not associated with metal loss area. This was necessary to determine what percentage of each of the catalogued shapes was associated with the metal loss, as the initial processing only took into account the shapes linked to the external corrosion damage.

For the purpose of the second incremental evaluation, only 15% of each line was sampled to limit the effort that would be required to identify every shape throughout the 593 miles of pipeline. The 15% was made up of sections of varying line length and was spread out over the entire length of the line in attempt

to obtain a representative sample. The number of occurrences for each of the CNs for the sampled regions was then extrapolated to 100% of the line lengths. The number of shapes found with and without corresponding metal loss can be seen below.

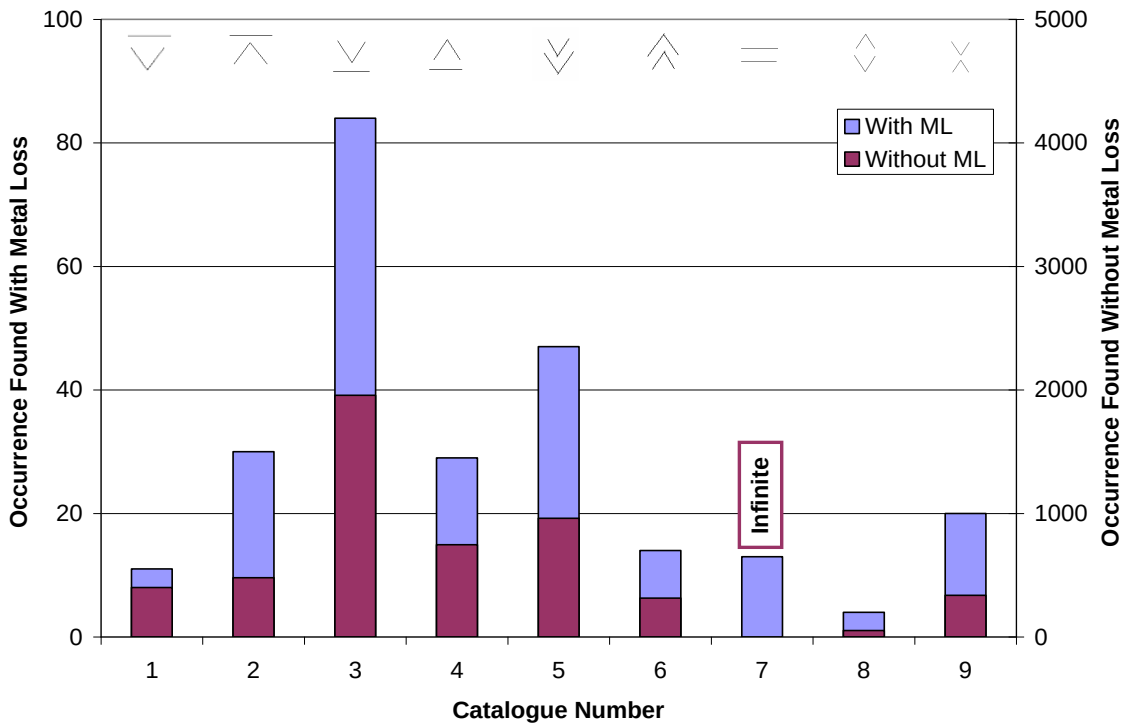

Figure 41. Occurrence of CIS shapes with and without metal loss. Catalogue shapes are shown on the top of the graph.

As can be seen from Figure 41, shapes CN3 and CN5 were the most common ones with and without metal loss (excluding shape seven which has an infinite amount of occurrences). The total number of locations/CN shapes associated with external corrosion was 252 (approximately 4.80% of the total identified shapes using the extrapolation).

The graph in Figure 42 shows the average damage area associated with each of the CN shapes; included also is the standard deviation of the corroded area for each of the shapes. As seen from the graph, there is a considerable scatter in the observed external damage, as the standard deviation value is 2 to 5 greater than the average.

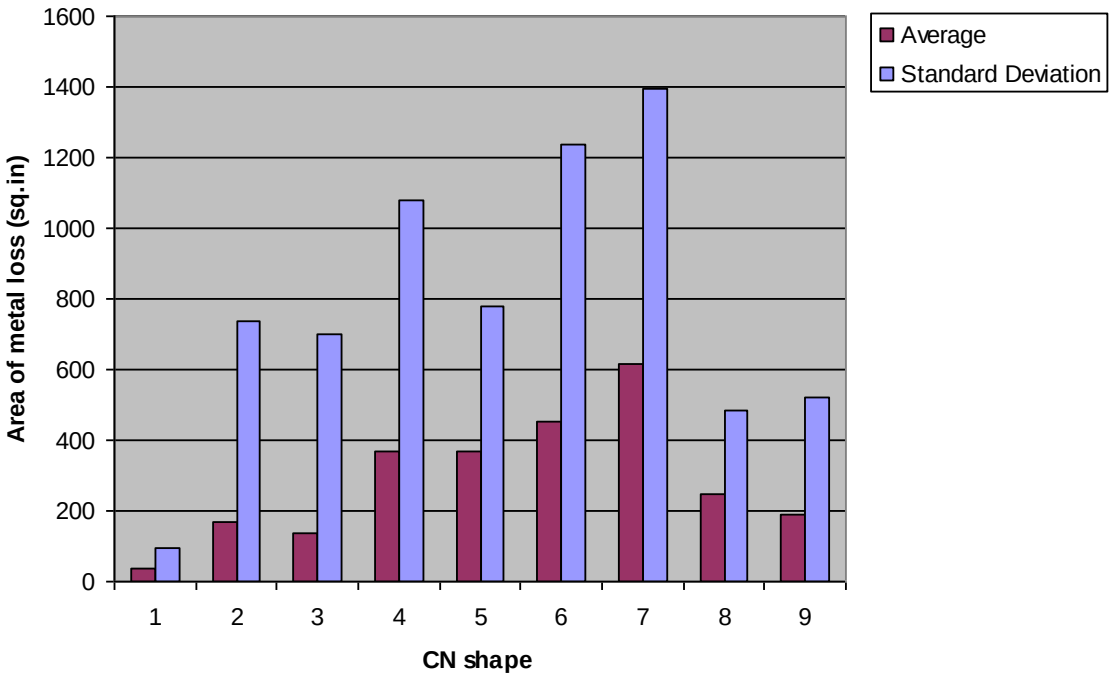

Figure 42. Average external damage area and standard deviation for each CN shape.

The graphs in Figure 41 and Figure 42 point out the difficulty in discerning any obvious correlations between the CN shapes and corrosion. The shape of the CIS profile is determined (as shown in the modeling analysis) by the damage area, its circumferential position, the depth of cover, and soil properties. For example, CN7 in Figure 42 shows the largest average area of metal loss; however, the data in Figure 41 suggests that the number of occurrences is low and therefore, the average area is composed of few, but large anomalies. The low number of occurrences, coupled with the high dispersion of the data presents a considerable challenge for deducing reliable trends.

One exception to the above is the association of the metal loss with the lack of compliance with the CP acceptance criterion on -850mV (CSE). The data in Figure 43 separates the metal loss occurrences with regard to the protection criterion. As expected, irrespective to the CN shape (with the exception of CN1 and CN2), the anomalies that did not receive sufficient protection exhibit larger damage areas than those that were adequately protected.

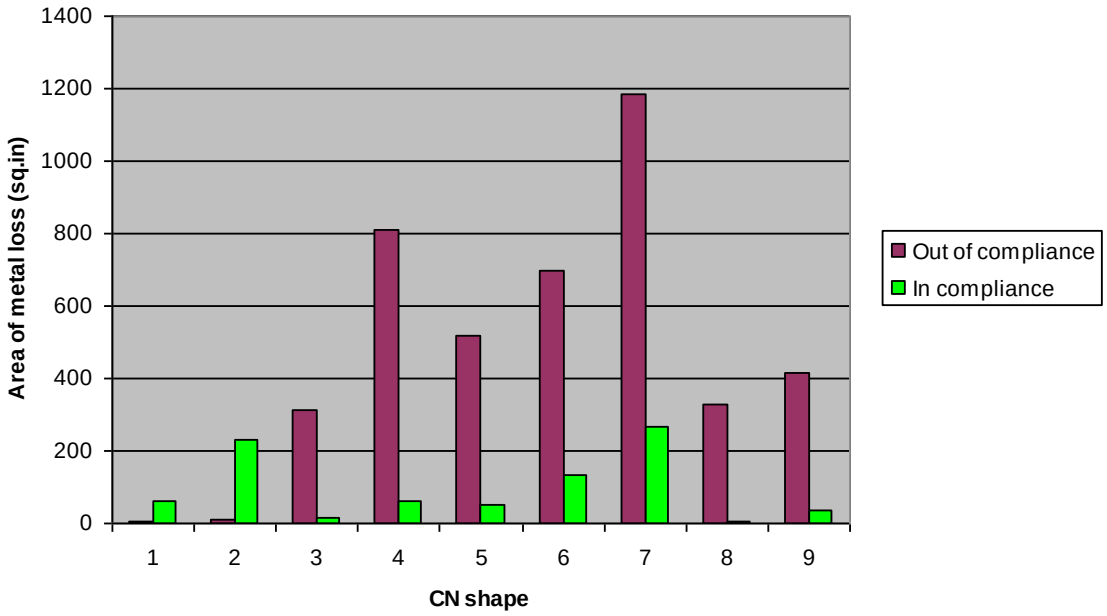

Figure 43. Average external damage area for each CN shape – separated by compliance with the -850mV CP criterion.

Correlation between metal loss and CIS shape parameters

Once the shapes have been identified, catalogued, and primary and secondary variables defined, the data was analyzed to determine whether a link existed between CN shapes and external corrosion damage (or any of the 73 variables listed in Table 6 and Table 7).

Metal loss as well as other measures of corrosion loss had highly skewed non-symmetric distributions such as the one seen in Figure 45. It is often difficult to predict such skewed values. In addition to looking at multiple metrics (variations of metal loss), a natural logarithm transformation was employed to make the resulting distribution more symmetric and often easier to predict. See Figure 46 for such an example. The natural log transformation greatly improved predictability in all cases. The goal is to use the catalogue shapes and their characteristics to be able to predict where corrosion damage is most likely to have occurred. The establishment of ties between the catalogue shapes and corrosion will aid ECDA in the future.

The natural logarithm of the scaled metal loss (LNScaledML, variable 57) was found to be the best corrosion metal loss-related variable in terms of both differentiating between the nine CN shapes and in terms of the development of a predictive model for corrosion metal loss. Scaled metal loss is computed by

multiplying the cumulative metal loss by the combined shape areas (ON and OFF potentials), the minimum distance that either of the shapes are from the 850 mV criterion, and the maximum slope value from either shape (ON or OFF potentials) An example of such calculation is shown below in Figure 44.

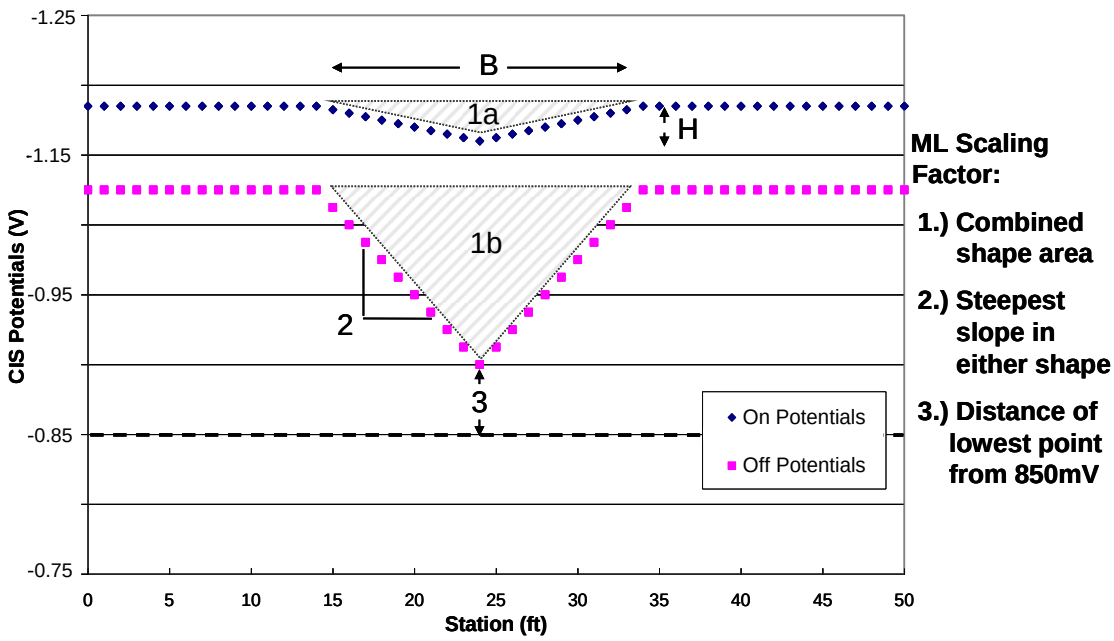

Combined Shape Area:

$$Shape1a = \frac{1}{2}BH = \frac{1}{2}20\,ft * 0.025V = 0.25$$

$$Shape1b = \frac{1}{2}BH = \frac{1}{2}20\,ft * 0.225V = 2.25$$

Steepest Slope in Either Shape:

$$Slope = \frac{0.225V}{20\,ft} = 0.01125$$

Distance of Lowest Point From 850mV:

$$Distance = Absolute\left(-0.90 - (-.85)\right) = 0.05$$

Metal Loss Scaling Factor:

$$(Shape1a + Shape1b) * Slope * Distance = (0.25 + 2.25)x0.01125x0.05 = 0.0014$$

Figure 44. Example of calculating Scaled Metal Loss variable for shape CN5.

The resulting natural log-transformed variable, LNScaledML, is the main basis of the analysis in this section.

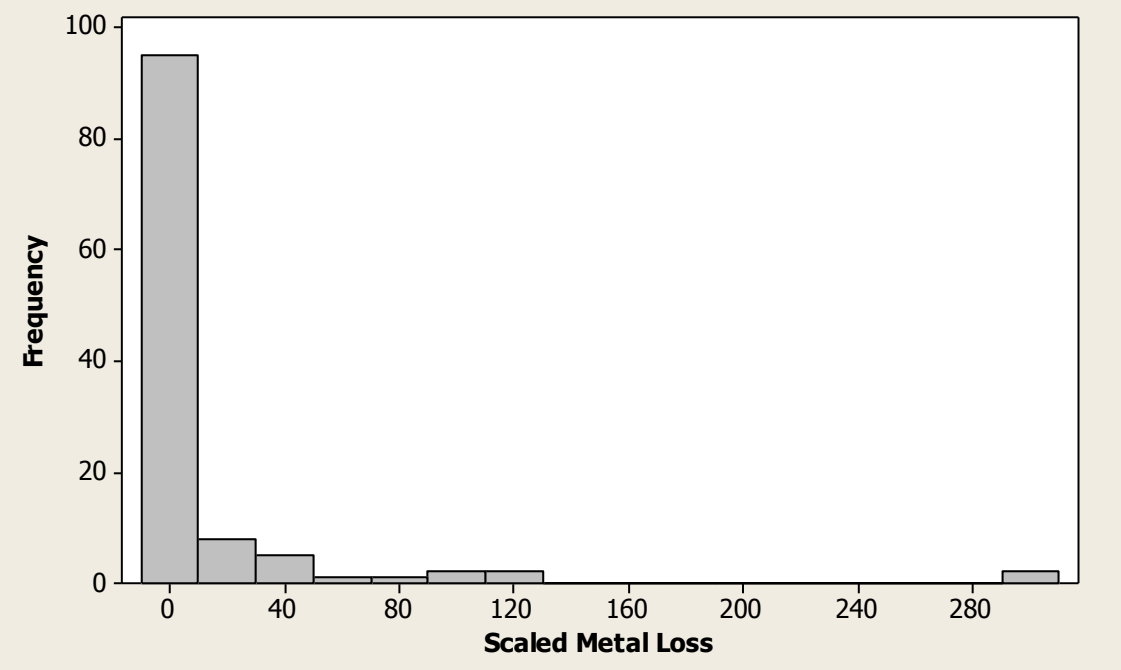

Figure 45. Scaled Metal Loss Histogram.

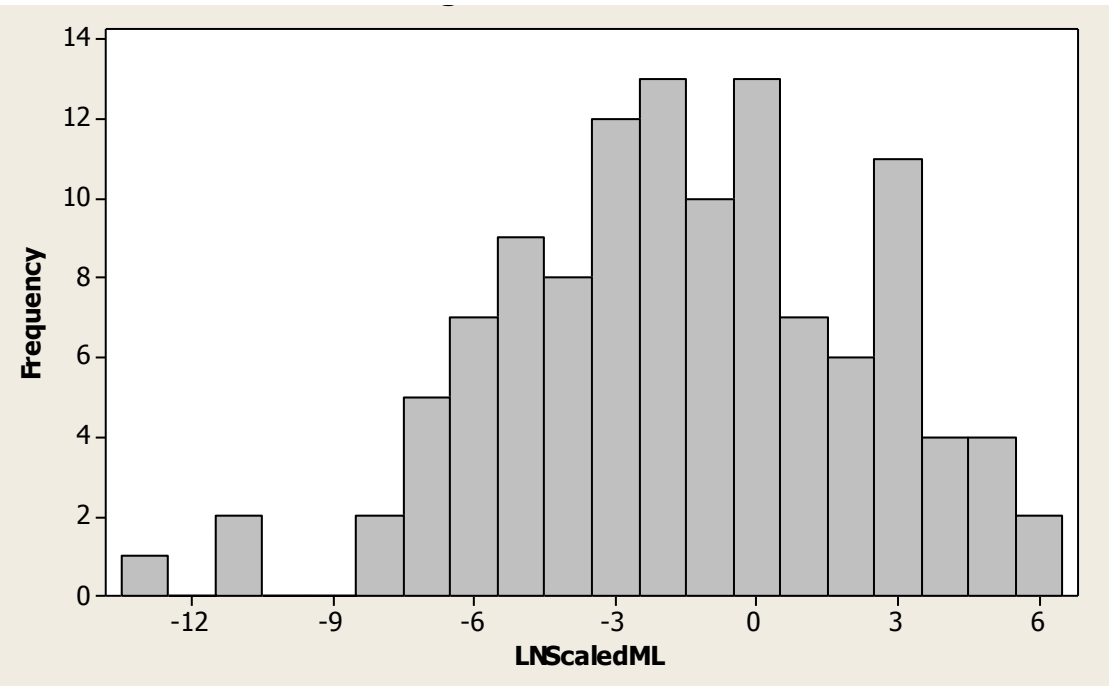

Figure 46. Natural logarithm-transformed Scaled Metal Loss Histogram.

The initial analysis that follows uses the full 252 observation data set. In this analysis, the initial step was to identify whether a correlation exists between metal loss and any of the other 70+ variables. As noted earlier, the natural logarithm of the scaled metal loss (LNScaledML) provided the best link. In what follows are a variety of statistical analyses on the full 252 observation data set showing the key

results obtained. These analyses strongly show that the nine catalogue shapes and the associated measurements can serve as potential predictors of metal loss.

A statistical technique called “Analysis of Variance (ANOVA)” was used to see if statistically significant differences in the scaled average metal loss could be found among the nine catalogue shapes. A resulting p-value less that 0.05 is statistically significant at the 95% confidence level. Similarly, a p-value less than 0.01 means that the finding is significant at the 99% confidence level.

The ANOVA table below (Table 8) provides the rounded p-Value of 0.000 indicating that metal loss is highly dependent on the catalogue shapes. In the chart following the table, there is data showing 95% confidence intervals for each of the scaled metal loss means vs. CN shapes. For example catalogue shape CN5 has 47 observations with an average of 0.214 for LNScaledML and a standard deviation of 3.166. The graphed confidence interval for its mean is seen to the far right of many of the other catalogue shapes (highlighted in red), thus implying that this shape has more metal loss associated with it than many of the other shapes.

Table 8. One-way ANOVA: LNScaledML versus Catalogue Number (full data set, n = 252)

Source	DF	SS	MS	F	P
Catalogue Number	8	787.16	98.40	9.86	0.000
Error	243	2425.62	9.98		
Total	251	3212.79			
S = 3.159 R-Sq = 24.50% R-Sq(adj) = 22.02%					

```
                                Individual 95% Confidence Intervals For
                                Mean Based on Pooled StDev
CN Sh  N    Mean  StDev  ---+---------+---------+---------+-----
1      11  -3.309  2.036             (-------*------)
2      30  -2.960  2.647                  (---*----)
3      84  -4.043  2.879               (--*--)
4      29  -3.751  4.434              (----*----)
5      47   0.214  3.166                                (---*--)
6      14  -2.839  3.710                (------*-----)
7      13  -6.428  3.893  (------*------)
8       4  -2.374  2.346            (------------*-----------)
9      20  -1.563  2.341                      (-----*----)
                          ---+---------+---------+---------+------
                           -7.5      -5.0      -2.5       0.0
```

The second case below (Table 9) focuses on the 116 observation data set that included the incidences of CN shapes associated with metal loss and CP potentials that did not meet the -850 mV criterion. These 116 observations have more pronounced corrosion as would be expected. The corresponding ANOVA table has the same basic findings as the full dataset ANOVA above, i.e., highly statistically significant differences between the average corrosion metal loss based on catalogue number. These findings show the potential usefulness of the catalogue shapes in aiding the direct assessment of corrosion.

It can be seen below that, once again, shape CN5 has higher metal loss associated with it. Also as before, CN7 has the lowest average associated metal loss. By evaluating the CIS profile (and hence identifying shapes), one can make inferences regarding the probability of greater or lower metal loss. In general (and as shown in the subsequent t-test), if the shapes linked to the higher probability of metal loss also fall in the area of potentials not meeting the -850 mV criterion, are expected to have significantly more metal loss.

Table 9. One-way ANOVA: LNScaledML versus Catalogue Number (only data not meeting -850mV criterion, n = 116)

Source	DF	SS	MS	F	P
Catalogue Number	8	539.8	67.5	6.63	0.000
Error	107	1088.6	10.2		
Total	115	1628.4			
S = 3.190 R-Sq = 33.15% R-Sq(adj) = 28.15%					

```
                                Individual 95% Confidence Intervals For
                                Mean Based on Pooled StDev

CN Shp  N    Mean  StDev  -------+---------+---------+---------+-
1       4  -3.187  2.051           (--------*--------)
2       9  -4.141  2.629           (-----*-----)
3      35  -2.733  2.963                  (--*--)
4      12  -1.290  3.684                    (----*-----)
5      32   1.299  2.957                               (--*--)
6       8  -1.704  4.178                  (-----*------)
7       5  -6.806  5.298  (--------*-------)
8       3  -2.485  2.860           (----------*---------)
9       8  -0.034  2.700                       (-----*-----)
                         --------+---------+---------+---------+-
                               -7.0      -3.5       0.0       3.5
```

Regression analysis correlating metal loss to CIS and soil characteristics

The two sample t-test below shows that the average LNScaledML is significantly higher for the observations that did not meet the -850mV criterion (Group A) vs. the observations that did (Group B). The analysis uses the full 252 incident set.

The p-Value below of 0.000 shows that there is a highly statistically significant increase in average metal when the -850mV criterion is not met.

Next, the analysis attempts to answer the question whether it is possible to predict the magnitude of metal loss in cases of the CIS profile shapes falling in the potential range more positive than -850mV criterion. The results suggest that such prediction can be possible for this particular subset (Group A). In other words, LNScaledML is modeled below for all catalogue shapes using regression and results in accounting for roughly 2/3's (66.5%) of the variation in the data when the CP protection criterion has not been met.

Two-Sample T-Test and CI: LNScaledML, A/B

```
Two-sample T for LNScaledML
A/B    N   Mean  StDev  SE Mean
A    116  -1.51   3.76     0.35
B    136  -4.06   2.95     0.25
Difference = mu (A) - mu (B)
Estimate for difference:  2.55419
95% CI for difference:  (1.70387, 3.40452)
T-Test of difference = 0 (vs not =): T-Value = 5.92
P-Value = 0.000  DF = 216
```

The regression equation below (Table 10) has all parameters statistically significant at the 95% confidence level, which includes both the CIS and soil-related characteristics (9 variables of the 72 listed in Table 6). The regression

accounts for 66.5% of the variability in the metal loss variable LNScaledML. The predicted LNScaledML = 5.019 -10.7* Least Negative Potential_Offs Absolute Value + … - 3.5* Third Point On (Potential). This equation should be further verified in subsequent studies; however, it does show promise accounting for about 66.5% of the variability in metal loss when the CP is insufficient.

Table 10. Variables and their coefficients for regression equation.

Parameter	Regression Coefficient
Intercept	5.019
Least Negative Off Potential (Absolute Value)	-10.7
Area × Off Potential magnitude	0.252
Electrical Conductivity (Number of cations absorbed) at pipe	0.92
Electrical Conductivity (Number of cations absorbed) average	-0.95
Sand (%) at pipe	0.346
Sand (%) average	-0.319
Second Point (On Potential)	5.8
Area × Slope Direction × Potential	-0.052
Third Point (On Potential)	-3.5

Table 11 below expands Table 10 by showing the associated t statistic, the absolute value of the t statistic, and the p-value for each variable in the regression model. The larger the t statistic is in absolute value, the more important that variable is in the regression model. In a similar vein the p-value measures the observed level of significance. The smaller the p-value is, the more significant the variable in the regression model. While none of the p-values below are truly 0.0, most round to 0. A p-value < 0.01 implies that the variable is statistically significant at the 99% confidence level as are all nine of the variables below.

Table 11. Statistical analysis of regression model.

	Coeff	t	abs(t)	p-value
Constant	5.019			
Least Negative Off Potential (Absolute Value)	-10.7	-4.56	4.56	0
Area x Off Potential magnitude	0.252	4.66	4.66	0
Electrical Conductivity (Number of cations absorbed) @pipe	0.92	6.96	6.96	0
Electrical Conductivity (Number of cations absorbed) ave	-0.95	-6.34	6.34	0
Sand (%) at pipe	0.346	5.59	5.59	0
Sand (%) average	-0.319	-5.06	5.06	0
Second Point On (Potential)	5.8	4.42	4.42	0
Area × Slope Direction × ON Potential magnitude	-0.052	-3.28	3.28	0.001
Third Point On (Potential)	-3.5	-2.76	2.76	0.007

Table 12 sorts these statistically significant variables in descending order of the absolute value of the t statistic. This puts the variables in order of their importance to the regression equation. Electrical conductivity and sand are in the regression equation twice – once based on their value at the pipe and once based on their overall average. Examining the corresponding regression coefficients for these two pairs, it is seen that the coefficients are similar in magnitude but opposite in sign. Thus there is somewhat of a cancellation effect that may be further investigated in the future and is touched on again below.

Table 12. Regression variables in order of importance.

Variable	Abs(t)
Electrical Conductivity (Number of cations absorbed) at pipe	6.96
Electrical Conductivity (Number of cations absorbed) average	6.34
Sand (%) at pipe	5.59
Sand (%) average	5.06
Area x Off Potential magnitude	4.66
Least Negative Off Potential (Absolute Value)	4.56
Second Point (On Potential)	4.42
Area × Slope Direction × ON Potential magnitude	3.28
Third Point (On Potential)	2.76

Table 13 performs a sensitivity analysis on these regression parameters. The regression equation was used to establish a baseline at which each variable was set to its mean. Then, for a given variable, the % Change column is the percentage change from the base case when going from one standard deviation

above the variable's mean (first evaluation) to one standard deviation *below* the mean (second evaluation) while holding all other variables at their respective means. Thus, the percentage change evaluated the regression equation twice for each variable. The ratio of the first evaluation minus the second evaluation divided by the base case regression is the % Change in the last column below.

As can be seen below, the two soil variables (electrical conductivity, sand %) have the largest sensitivities though as mentioned before these are in pairs at the pipe and the average. Thus there appears to be a cancellation effect for these soil variables (see further discussion on the next page).

Table 13. Sensitivity analysis of regression variables.

Variable	Mean	StDev	% Change for ±1 standard deviation change
Least Negative Off Potential (Absolute Value)	0.6863	0.1227	162%
Area × Off Potential magnitude	3.107	4.323	-134%
Electrical Conductivity (Number of cations absorbed) at pipe	14.562	9.768	-1109%
Electrical Conductivity (Number of cations absorbed) average	12.343	8.041	942%
Sand (%) at pipe	43.39	25.25	-1078%
Sand (%) average	46.94	23.82	937%
Second Point (On Potential)	-0.871	0.2395	-171%
Area x Slope Direction × ON Potential magnitude	7.17	17.97	115%
Third Point (On Potential)	-1.039	0.245	106%

Another way to examine the impact of the soil parameters electrical conductivity and sand % is to perform separate regression analyses for soil and CP-related variables. In the first only the 4 soil parameters (electrical conductivity and soil % both at the pipe and averaged) are used to predict metal loss. In the second only the other 5 regression variables are used.

Recall that the *full* regression equation accounted for 66.5% of the metal loss variability. Separation into two regressions does not result in two numbers that add to 66.5%; however, it provides a relative indication of how much predictive ability these two groupings have. The first regression using only the four soil related parameters accounts for 25.2% of the metal loss variability while the second regression using the CP-related variables accounts for 46.4% of the metal loss variability. Thus when the four soil parameter pairings are taken into

consideration, their impact while important is not as significant as that of the CP-related five variables.

Still, such apparent contradiction between seemingly related terms requires further consideration, particularly because the soil-related variables appear to cancel each other. In addition, soil resistance featured prominently in the numerical simulation model. The effect of electrical conductivity, an inverse of resistance, was found to be "self-cancelling" in the CIS analysis – the conductivity at the pipe level directly correlated with corrosion, while 'bulk' soil conductivity was inversely proportional to corrosion damage. However, to resolve the perceived contradiction, maybe the effects of the conductivity (bulk vs. at-pipe) could be better understood if considered separately.

The higher conductivity *at-pipe* is linked by the analysis to greater (likelihood of) corrosion – which would be expected, as soils with low resistivity are typically considered to be more corrosive. On the other hand, *bulk* soil conductivity would be directly proportional to the soil ability to pass cathodic protection current to the buried pipe. The regression analysis confirms it – and the higher bulk conductivity is indeed *inversely* correlated with the corrosion damage. In this sense, if a section of the pipe has dryer, less conductive bulk soil, but is surrounded by conductive backfill, then it is likely to corrode more because sufficient CP current may not reach it.

If one adopts this argument, the initially perplexing effects of sand can be better understood using the 'bulk vs. 'local' logic. Higher sand content at pipe does not necessarily mean higher bulk sand content (consider sand backfill, e.g.); however, higher bulk content is likely to translate into a higher at-pipe (local) sand content.

A higher sand percentage at pipe was positively correlated with corrosion. A higher fraction of sand in soil next to a holiday would be expected to result in higher oxygen content, and, consequently, higher corrosion rate due to higher diffusion-limited cathodic reaction current. Higher sand content would also cause locally high resistance and possibly lead to lower CP protection.

However, *higher* bulk sand content was linked to *lower* corrosion. While such soil may be more aerated, it is less likely to hold as much water as a heavier soil. As the cathodic reaction in soil involves oxygen *and* water, lower moisture content in bulk soil, and thus lower at-pipe moisture can be the reaction-limiting step (rather than oxygen availability) in areas with high sand content.

The results, when considered being semi-quantitative, are consistent with the expectations. Potential terms listed in Table 10 containing individual variables

follow the same pattern. Thus, the logarithm of the metal loss is directly proportional to the least negative OFF potential associated with any particular shape on the CIS profile. The greater the absolute value of the CN shape OFF potential is, the more negative the logarithm value, and the smaller the accumulated weight loss. Similarly, the more positive the second ON potential of the CIS shape is, the less negative is the logarithm value, and the greater the corrosion damage at the CN shape location.

The composite terms, by virtue of their being a product of several variables, are more complicated to interpret. As noted before, a × B × c can occasionally yield the same value as a × b × C. One of the terms that include CN shape "area" (change in potential multiplied by the distance over which this change took place) also includes the "slope direction term". Therefore, if the potentials become more positive, the slope is positive, and the term, when factoring in the sign of the regression coefficient, is positive as well – and would point to a larger (greater likelihood of) corrosion damage. Another term containing shape area follows the same logic – the greater (more negative) the least positive OFF potential is (which defines the position of the CIS shape on the y-axis), the smaller the corrosion damage.

Conclusions

What has the field data analysis shown? Despite the apparent simplicity typically ascribed to the interpretation of the CIS profiles, the regression analyses reveal that the reality is considerably more complicated. The graphs in Figure 41 and Figure 42 point out the difficulty in discerning any obvious correlations between the CN shapes and corrosion. The shape of the CIS profile is determined (as shown in the modeling analysis) by the damage area, its circumferential position, the depth of cover, and soil properties. For example, CN7 in Figure 42 shows the largest average area of metal loss; however, the data in Figure 41 suggests that the number of occurrences is low and therefore, the average area is composed of few, but large anomalies.

Some shapes were more commonly encountered than others (CN 7, flat ON and OFF potentials were the most common, as expected). No single shape on the CIS profile was free from corrosion damage associated with it, which again underscores the lack of absolutism in the CIS profile interpretations – i.e., there are always exceptions to the rule. Beyond that, as can be seen from Figure 41, shapes CN3 and CN5 were the most frequent ones – whether with or without metal loss. These two shapes are the ones that have a familiar 'dip' on the profile – one with the concomitant dip in the OFF potential, the other one without.

As noted earlier, there are differences in the number of corrosion anomaly occurrences for each shape; comparing Figure 43 to Figure 41 indicates that, perhaps, shapes CN3 and CN5 were linked to smaller-sized and more frequent anomalies, than shape CN7, which had a greater total area but fewer incidents of damage (more extended damage per each anomaly).

While it would be desirable to be able to make definitive inferences of whether corrosion damage can be linked to a CIS shape, the limitations of the dataset (the number of observations and the geographical similarities in the source of data) make it unadvisable. Still, the analysis strongly suggests that some CIS profile shapes were found to be more likely to be associated with corrosion if the CP criterion has not been met. Indeed, as shown in Figure 43, if the -850mV OFF-potential criterion is not observed, the total extent of corrosion damage associated with a particular CN shape was more likely to be greater, regardless of the profile shape.

While this finding could be regarded as obvious, one should realize that this observation has been reached through independent analysis of the CP data; in other words, the conclusion fulfills an important role of validating the existing CP assessment practices, particularly, the ECDA process which invariably uses CIS as one of the assessment tools.

Further, the regression analysis holds promise with regard of making broad estimates of the extent of corrosion using the CIS profile. More extensive evaluations are mandatory, as the CIS profile (as demonstrated by the modeling and known from field practice) is a function of the soil characteristics. Thus, the observation with regard to the electrical conductivity/sand content at the pipeline depth and average for the soil cover is puzzling in that the two pairs of variables seem to cancel each other out.

The sample of 252 observations is large enough to show promise; however, how typical the data used in the analysis is of pipelines in general requires further investigation. One deficiency in the current study is the inability to state if what has been found is universal or just isolated to the pipeline segments evaluated. To address this, further work will be needed for both verification and testing generality.

Correlation between numeric analysis and field data

It is interesting to correlate the results of the numerical simulation and field-based data analysis. These approaches were quite different in that the former was a ‘forward’ model (looking from the pipe ‘up’ to the grade level) and the latter was in

essence, a “reverse” analysis (looking from the grade level ‘down’ at the pipe). In broad terms, the results of the two analyses are in concert. The numerical simulation indicated that the parameters that determine the at-grade ON potential distribution were linked to soil properties, defect size, and OFF potentials. The results showed that corrosion damage was more likely at the more positive ON potentials, as the defect size was likely to be greater.

The field data analysis points in the same direction. More positive potentials are linked to greater corrosion; the compound terms that include the CIS profile shape area act in the same manner as the numerical simulation term of potential difference between the anomaly OFF potential and the OFF potential of the adjacent coated pipe. Soil resistivity (conductivity) was also an important factor; however, its effects can be better understood in terms of corrosion process rather than the influence on the measured IR drop.

Task 4 – Guidelines for interpretation of CIS for ECDA

Upon completion of the laboratory and field components of the proposed research effort, the findings were summarized into a set of guidelines for the pipeline operators. The guidelines, the primary deliverable of the project, outline the observed trends and provide narrative for assisting in making decisions regarding interpretation of the CIS profiles and prioritizing anomalies regarding the threats to pipeline integrity. The guidelines were prepared in the format suitable for inclusion in the NACE International RP0502. The guidelines are included in Appendix A.

GENERAL CONCLUSIONS

The literature search results have validated the initial assessment that the primary focus of the project - to determine whether certain correlations between the CIS profile shapes and corrosion conditions at the pipe/soil interface can be possible – has addressed an existing knowledge gap. The findings were consistent with the expectations in that even among the publications that address the issue of the CIS profile interpretation (the ones selected for the review), there is no discussion about the implications of the differences in the CIS profile shapes. There seems to be no consideration given to whether any of the CIS shapes can be further interpreted to address such issues as coating defect size or the likelihood of corrosion – at least not beyond the commonly recognized concurrent drop (to more positive values) in potential on ON and OFF potential charts in the vicinity of the coating holiday on a buried pipe.

Numerical model adequately described most of the first order effects between defect geometry, soil related parameters, and CP potentials. On the basis of the model-generated values, a regression analysis-derived relationship of the pipe/soil characteristics and ON potentials was established. The regression equation indicates that the impedance (soil resistivity and defect geometry) dominates the relationship, with the defect size being an important factor in determining the ON potential value for a given OFF potential.

Experimental work was in concert with numerical modeling of potential distribution at the pipe and grade levels. It showed that resistance-based factors are the major drivers that determine the relationship between the ON and OFF potentials. This observation is consistent with the corrosion monitoring practice of taking close interval surveys; the difference between ON and OFF potentials is defined as IR-drop, with the R being the composite term encompassing the geometry and soil-related impedances.

However, the relationship between the at-grade potential measurements and the actual at-pipeline depth conditions is complex. On a real-life “macro” system, such as a buried pipeline, the modeling assumption that the holidays represent isolated breaches in an otherwise perfect external coating is not going to be universally applicable. There are variations of soil chemistries and soil particle sizes, which can be considerable even over a short distance along the pipe; these differences can affect not only the impedance characteristics of soil, but polarization behavior of the steel exposed through holidays.

Further, the presence of multiple adjacent holidays or electrically conductive areas of the (aging) coating, as demonstrated by the experimental modeling, may produce a ‘composite’ ON/OFF CIS potential value, which, under certain circumstances, can obscure the actual CP potential of the least polarized holiday. The experimental and numerical modeling underscored the often underappreciated inherent difficulty of interpreting CIS profiles; every point on the CIS shape (typically) represents not a single defect, but an array of adjacent coating holidays of various sizes.

Given the complexity of such a relationship and the inevitably simplifying assumptions necessarily employed by any model, it is not entirely surprising that the results of the analysis are inconsistent in some aspects. Depth of cover and soil resistivity both affect the difference in ON and OFF potentials, and this can be explained in terms of the IR drop. The orientation of the defect does not seem to have an effect. One must consider further the nature of the IR drop between grade and pipe surface.

Potential gradient associated with the coating holiday is highly localized. The effect is greater in the high resistance soils. Therefore, it is not reasonable to assume a simple mathematical relationship amongst depth of cover, soil resistivity and potential difference. In effect, the IR-drop calculations cannot assume a linear relation, and any conclusions drawn from a simple inspection of the data must be made with caution. The IR-drop arguments are inherently valid, but do not describe the *complete relationship* of the various parameters that affect the ON and OFF potentials. Therefore, numerical modeling, which focuses on individual defects, can not be expected to fully reflect the complexity of real-life conditions on a buried pipeline. In this regard, the numerical modeling results would be best understood in terms of trend analysis, rather than the means of providing absolute, precise correlations between at-grade potential measurements and coating holidays.

With regard to the CIS shapes, analyses showed that for some of the less-explainable shapes, such as CN1-2 or CN3-4, the change in the OFF potential to more negative values with the ON potential remaining the same may be indicative of coating condition equivalent to a series of defects of increasing sizes. Conversely, if the OFF potentials remain the same and the ON potentials increase, the worst of the coating conditions occur at the most positive of the ON potentials. In that sense, the results are in agreement with the intuitively expected – the lower the IR drop (the separation between ON and OFF lines), the larger the defect, and the more positive the combined ON and OFF potential values (it is

after all, more difficult to protect larger holidays). In other words, it is very likely that, if other conditions are fixed, the coating holiday is located at the spot of the most positive local potentials making up the CIS shape – which is traditionally assumed when analyzing CIS profiles.

The regression equation could be used to further refine the field data, as CIS will provide ON, OFF and coating potentials. The potentials at the holiday (OFF) and the pipe outside of the anomaly regions would have to be determined by recognizing variation in the OFF potentials on the CIS plot. The OFF potential associated with a defect is expected to be more positive than the OFF potential associated with intact coating. The coating potential used for the above calculations would be taken as the "baseline", the more negative of the OFF potentials measured along a given length of pipe. The OFF potential associated with a defect would be taken as the most positive potential measured.

The results produced by the research undertaken in this project demonstrate that despite the apparent simplicity typically ascribed to the interpretation of the CIS profiles, the regression analyses reveal that the reality is considerably more complicated. The shape of the CIS profile is determined (as shown in the modeling analysis) by the damage area, its circumferential position, the depth of cover, and soil properties. Some shapes were more commonly encountered than others (CN 7, flat ON and OFF potentials were the most common, as expected). No single shape on the CIS profile was free from corrosion damage associated with it, which again underscores the lack of absolutism in the CIS profile interpretations – i.e., there are always exceptions to the rule. Beyond that, shapes CN3 and CN5 were the most frequent ones – whether with or without metal loss. These two shapes are the ones that have a familiar 'dip' on the profile – one with the concomitant dip in the OFF potential, the other one without.

While it would be desirable to be able to make definitive inferences of whether corrosion damage can be linked to a CIS shape, the limitations of the dataset (the number of observations and the geographical similarities in the source of data) make it problematic. That being said, some general observations can be made:

- The area of corrosion damage tended to be largest where the CN shape was flat for both ON and OFF potentials.
- The number of corrosion metal loss sites was greatest for the CN shape with an ON potential dip and a flat OFF potential

- The area of corrosion damage was found to be larger for most CN shapes when the OFF potentials were not in compliance in the CP protection criterion
- Very few observations of corrosion were associated with dips in the OFF potential where the ON potential was flat, and what corrosion defects were found under these circumstances tended to be relatively small; interestingly these locations were generally still classified as being in compliance
- Similarly, few observations of corrosion and small corrosion defect sizes were associated with peaks in the OFF potential where the ON potential was flat
- There does not appear to be a correlation between the number of corrosion indications for a given CN shape and the corrosion size; that is, just because corrosion is frequently found does not mean that it is necessarily extensive

Though it is uncertain if these observations are truly general in nature or a consequence of the data set analyzed, they do point to a few additional interesting inferences, some expected and some unusual. The analysis strongly suggests that some CIS profile shapes were found to be more likely to be associated with corrosion if the CP criterion has not been met. If the -850mV OFF-potential criterion is not observed, the total extent of corrosion damage associated with a particular CN shape was more likely to be greater, regardless of the profile shape.

The observation that the extent of corrosion damage tended to be larger when the potential readings were out of compliance was not unexpected. On the other hand, the observation that the third largest average area of corrosion was associated with the peak in the ON potentials and flat OFF potentials is unusual given that the assumption would be that the high ON potential was due to IR effects.

While some of the findings could be regarded as obvious, one should realize that this observation has been reached through independent analysis of the CP data; in other words, the conclusion fulfills an important role of validating the existing CP assessment practices, particularly, the ECDA process which invariably uses CIS as one of the assessment tools.

Further, the regression analysis holds promise with regard of making broad estimates of the extent of corrosion using the CIS profile. More extensive

evaluations are mandatory, as the CIS profile (as demonstrated by the modeling and known from field practice) is a function of the soil characteristics. Thus, the observation with regard to the electrical conductivity/sand content at the pipeline depth and average for the soil cover is puzzling in that the two pairs of variables seem to cancel each other out.

The sample of 252 observations is large enough to show promise; however, how typical the data used in the analysis is of pipelines in general requires further investigation. One deficiency in the current study is the inability to state if what has been found is universal or just isolated to the pipeline segments evaluated. To address this, further work will be needed for both verification and testing generality.

APPENDIX A

GUIDELINES FOR CIS

The guidelines in this appendix are intended to summarize the conclusions of the subject project in a way that can be incorporated in technical standards. The relevant standards are 1) NACE SP0207-2007 titled *Standard Practice: Performing Close-Interval Potential Surveys and DC Surface Potential Gradient Surveys on Buried or Submerged Metallic Pipelines*, and 2) NACE SP0502-2002 title *Standard Practice: Pipeline External Corrosion Direct Assessment Methodology*.

NACE SP0207 presents procedures for performing close interval surveys (CIS) but contains no guidance on interpretation of data. The standard states

> *1.2.4 This standard includes procedures to perform these types of surveys along a buried or submerged pipeline. The standard acknowledges that all potential measurements contain error, and includes some guidance to minimize the error in each measurement. The standard does not address interpretation of survey data. A qualified person must determine whether the data contain an acceptable amount of error and can be used to evaluate the level of cathodic protection.*

NACE SP0502 presents the process of external corrosion direct assessment (ECDA) including recommendations on prioritizing indications by CIS, which is almost always the first ECDA tool. Table 3 lists an example severity classification for CIS:

- Minor indications are those with 1) small dips and 2) on and off potentials above CP criteria (e.g., -850mV vs. $Cu/CuSO_4$ or 100mV polarization as specified by NACE SP0169).
- Moderate indications are those with medium dips or off potentials below CP criteria.
- Severe indications are those with 1) large dips or 2) on and off potentials below CP criteria.

The results of the subject project support the recommendation that guidance on interpreting CIS data can be added to NACE SP0207 and that the example severity classification in NACE SP0502 can be modified with improved criteria

- Minor indications are those with any change in on or off potential (i.e. dip in the downward or upward direction).

- Moderate indications are those with off-potential not meeting protection criteria or dips in the on potential.
- Severe indications are those with off-potential not meeting protection criteria and dips in the on potential.

The primary basis for the revised guidelines is that >80% of corrosion locations in the subject study were at locations not meeting CP criteria, >90% of corrosion locations were at changes in on or off potential, >80% were at on potential changes, and >60% were at dips in the on potential.

One of the most useful aspects to the revised criteria is that on-potentials can be used to identify minor and moderate indications. This outcome might allow operators that cannot interrupt all sources of cathodic protection to gain benefit from CIS without the complication of addressing IR-drop effects.